DRILLING OF HYBRID REINFORCED MAGNESIUM MATRIX COMPOSITES

2018
DOCTORAL THESIS
THE INSTITUTE OF NATURAL AND APPLIED SCIENCES
DEPARTMENT OF MANUFACTURING ENGINEERING

Mustafa M. ABDULGADIR

DRILLING OF HYBRID REINFORCED MAGNESIUM MATRIX COMPOSITES

A THESIS SUBMITTED TO
THE INSTITUTE OF NATURAL AND APPLIED SCIENCES OF
KARABUK UNIVERSITY

BY

Mustafa M. ABDULGADIR

IN PARTIAL FULFILLMENT OF THE REQUIREMENTS FOR
THE DEGREE OF DOCTOR OF PHILOSOPHY IN
DEPARTMENT OF
MANUFACTURING ENGINEERING

KARABÜK
November 2018

I certify in my opinion that the thesis which submitted by Mustafa M. ABDULGADIR entitled "DRILLING OF HYBRID REINFORCED MAGNESIUM MATRIX COMPOSITES" is fully sufficient in value and quality as a degree of Doctor of Philosophy thesis.

Prof. Dr. Bilge DEMİR .....
Thesis Advisor, Department of Mechanical Engineering

This thesis is accepted by the examining committee with a unanimous vote in the Department of Manufacturing Engineering as a Doctor of Philosophy thesis. 16/11/2018

Examining Committee Members (Institutions)	Signature
Chairman: Prof. Dr. Adem ÇİÇEK (AYBÜ)	.....
Member : Prof. Dr. Bilge DEMİR (KBÜ)	.....
Member : Doç. Dr. Hakan GÜRÜN (GÜ)	.....
Member : Dr. Öğr. Üyesi. Mehmet BOY (KBÜ)	.....
Member : Dr. Öğr. Üyesi. Gökhan SUR (KBÜ)	.....

..... / ..... / 2018

The Administrative Board of the Graduate School of Natural and Applied Sciences, Karabük University approves the degree of Doctor of Philosophy by the thesis submitted.

Prof. Dr. Filiz ERSÖZ .....
Head of Graduate School of Natural and Applied Sciences

"I declare that all information in this thesis is collected and presented in agreement with academic and ethical principles, and I refer to all those that are not derived from this work in accordance with the requirements of these regulations and principles."

Mustafa M. ABDULGADIR

ABSTRACT

Doctor of Philosophy Thesis

DRILLING OF HYBRID REINFORCED MAGNESIUM MATRIX COMPOSITES

Mustafa M. ABDULGADIR

Karabük University
The Institute of Natural and Applied Sciences
The Department of Manufacturing Engineering

Thesis Advisor:
Prof. Dr. Bilge DEMİR
November 2018, 175 pages

In this thesis research, a systematic drilling experimental study has been accomplished, with the aim of achieve an extra inclusive realization of the merits of Mg-MMCs machining aspects. This thesis research was motivated by growing demands of miniaturized components in various industrial applications. Mg-MMCs turn into one of the best alternatives because of its lightweight, strength, and elevated creep and wear resistance. The material system examined in this thesis research is Mg-MMCs which has been reinforced with nano-sized of the graphene nanoplatelets (GNPs) and micro-sized of the silicon carbide (SiC) particles. The machinability of two categories of Mg-MCs; (Mg/0.25wt%GNPs) and the hybrid Mg-MCs (Mg/10wt%SiC/0.25wt%GNPs) which are fabricated via the powder metallurgy procedure were investigated during dry drilling process. The microstructure, the cutting parameters influence, cutting forces, torque, machined surface topography, delamination, cutting tool failure and wear mechanisms were grouped

and optimized for fully realization of the process mechanisms and to eliminate the undesirable effects.

The Taguchi approach and regression analysis were applied with the aim of evaluate the machinability of the composite materials. The experiments were done with the uncoated, PVD (TiN) and the CVD (AlTiN) coated carbide bits at three different cutting speeds namely :(30, 40 and 50 m/min), along with three different feed rates namely: (0.10, 0.15 and 0.20 mm/rev) under dry-machining conditions. The analysis of the variance (ANOVA) was utilized to assert the outcome of the process parameters on the torque, thrust force, surface roughness and delamination factor. The homogenous distribution of SiC_P and GNPs into the Mg matrix was confirmed and the microstructure was free of macro defects. The experimental outcome point out that the thrust force, torque, surface roughness and the delamination formation were extremely reliant on the feed rate and cutting speed; and the higher cutting speed combine with lower feed rate was preferable in the drilling of Mg-MMCs. The predicted values derivate through the utilization of quadratic regression models and the measured values were very close to each other.

Key Words **:** Drilling, hybrid Mg-MMCs, PVD/CVD coating, thrust force, torque, surface roughness, delamination, parameters optimization.

Science Code : 914.1.090

ÖZET

Doktora Tezi

HİBRİT TAKVİYELİ MAGNEZYUM MATRİSLİ KOMPOZİTLERİN DELİNEBİLİRLİĞİ

Mustafa M. ABDULGADIR

Karabük Üniversitesi
Fen Bilimleri Enstitüsü
İmalat Mühendisliği Anabilim Dalı

Tez Danışmanı:
Prof. Dr. Bilge DEMİR
Kasım 2018, 175 sayfa

Bu tez çalışmasında, magnezyum matrisli, karbür ve nanografen katkılı/katkısız metal hibrit (Mg-MMCs) kompozit malzemelerin farklı işleme parametreleri ve matkap uçları kullanılarak delme ile işlemelerinin deneysel, istatiksel ve Taguchi metodu ile incelenmeleri detaylı olarak gerçekleştirilmiştir. Bu tez çalışmasının motivasyonu; çeşitli endüstriyel uygulamalarda minyaturize edilmiş yapı bileşenlerine olan talebin büyük bir hızla artarak büyümesidir. Mg-MMC'ler yüksek sürünme direnci, yüksek aşınma direnci yüksek dayanım düşük ağırlıkları sebebiyle mükemmelliğe aday bir malzemedir. Bu tezdeki araştırmaya esas incelenen malzeme grup ve kombinasyonu; nanografen katkısı (GNPs) ve mikro-boyutlu silikon karbür (SiC) partiküllerinden oluşmaktadır. Delme işlenebilirlik deney numuneleri Mg-MCs; (Mg/0.25GNPs) ve hibrid Mg-MCs (Mg/10SiC/0.25GNPs) olmak üzere iki grup olarak klasik toz metalürjisi (T/M) yöntemi ile üretilmiştir. Mikroyapı, kesme parametreleri, kesme kuvvetleri, tork, işlenmiş yüzey topografyası, deleminasyon,

kesme takımı hasarları ve aşınma mekanizmaları; işlenebilirliğini tam olarak anlaşılması ve arzu edilyen olumsuz etkilerin minimize edilmesi için gruplandı ve optimizasyon yapıldı.

Taguchi yaklaşımı ve regresyon analizi, kompozit/hibrid kompozit malzemelerin işlenebilirliğinin anlaşılması için uygulandı. Deneysel çalışmalar (delme işleme) kaplamasız PVD (TiN) ve CVD (AlTiN) nitrür kaplamalı matkap uçlarıve üç farklı kesme kesme hızı (30, 40 and 50 m/dk), yanında üç farklı ilerleme hızı (0.10, 0.15 ve 0.20 mm/dev) ve kuru işleme şartlarında yapılmıştır.Varyans analizleri ANOVA yöntemi ile kesme parametreleri çıktılarının kesme kuvvetleri, yüzey prüzlülüğü ve deleminasyon üzerindeki etkisinin belirlenmesi için kullanıldı. SiC_P ve GNP' nin Mg metal matris içerisinde homojen dağılımlı gösterdiği tespit edildi ve metalurjik yapı makro hatalar içermiyordu. Deneysel çalışmalar, kesme kuvvetleri, tork, yüzey pürüzlülüğü ve deleminasyon oluşumu üzerinde ilerleme hızı, kesme hızı ve düşürülmüş ilerleme hızı ile yüksek kesme hızına tam bağlı olarak Mg-MMC'ler tercih edilebilir bir pozisyondaydı. Kuatratik regrasyon analiz modelinden türetilerek açıklanan değerler ve deneysel ölçülen değerler birbirleri ile yüksek bir uyum göterdi. Sonuç olarak literatürde geniş ve detaylı olarak yer almayan Mg-MMC'lerinişlenebilirliği teorik ve deneysel olarak ortaya konularak alanda literatüre önemli bir katkı sağlanmıştır.

Anahtar Kelimeler : Matkap, hibrid Mg-MMCs, PVD/CVD kaplamalı, kesme kuvvetleri, tork, işlenmiş yüzey topografyası, deleminasyon, parametreler optimizasyonu.

Bilim Kodu **:** 914.1.090

ACKNOWLEDGMENT

First, I would like to extend my sincere appreciation to my advisor Prof. Dr. Bilge DEMİR. His supervision, patience, encouragement and support have guided and allowed me to go throughout the most complicated steps during stages of this thesis research. I am sincerely influenced and greatly motivated by his passion, devotion, obligation and endurance.

I would also like to express thanks to Dr. Mehmet BOY and Dr. Gökhan SUR for helping on my examination and advisory board and for providing me with some great sufficient guidance.

It has been a privilege and I was lucky to work with my colleagues in KARABÜK and GAZI Universities, especially Mr. Muhammet EMRE TURAN, Dr. Gultekin UZUN and Mr. Bahattin YILMAZ, who assisted me in several ways.

Lastly, my heartfelt gratefulness goes to my family. Their ultimate love and wonderful support have always encouraged me to attain better and to envision living a full life of striving, succeeding, and excelling through excellence.

CONTENTS

Page

Page

Page

Page

Page

Page

LIST OF FIGURES

Page

Page

Page

Page

Page

Page

Page

LIST OF TABLES

Page

Page

SYMBOLS AND ABBREVITIONS INDEX

SYMBOLS

i : inclination angle

V_C : cutting speed

b : cutting width

h : cutting depth

F_t : tangential force

F_f : feed force

F_r : radial force

l_{st} : chip sticking region

l_{sl} : chip sliding region

W : out corner wear

V_B : flank wear

M_W : margin wear

K_M : crater wear

C_T : chisel edge wear I

C_M : chisel edge wear II

P_T : lips chipping wear I

P_M : lips chipping wear II

$2w$: chisel width

f : feed rate

t_c : chip thickness

r : instantaneous radius

F_{th} : thrust force

A_C : chisel edge instantaneous indentation area

dF_n : cutting force in normal direction

dF_t : cutting force in tangential direction

K_n : specific cutting pressure in normal direction

K_t : specific cutting pressure in tangential direction

R : drill radius

D : drill diameter

SD : drill shank diameter

L : drill overall length

R_a : surface roughness

f_d : delamination factor

D_o : nominal hole diameter

D_{max} : maximum delaminated diameter

N : Newton

C_T : cutting tool type

T : torque

ABBREVITIONS

MMCs : metal matrix composites
Mg-MCs : magnesium metal matrix composites
BUE : built up edge
BH : Brinell hardness
Al : aluminum
Ti : titanium
Mg : magnesium
SiC : silicon carbide
TiC : titanium carbide
B_4C : boron carbide
Al_2O_3 : aluminum oxide
CNT : carbon nanotubes
GNPs : graphene nanoplatelets
PVD : physical vapor deposition
CVD : chemical vapor deposition
PCD : polycrystalline diamond
CBN : cubic boron nitride
TiN : titanium nitride
AlTiN : aluminum titanium nitride
CNC : computer numerical control
HV : Vickers hardness
SEM : scanning electron microscopy
EDS : energy dispersive spectroscopy
S/N : signal to noise ratio
ANOVA : analysis of variance
DF : degree of freedom
SS : sum of squares
MS : mean square

CHAPTER 1

INTRODUCTION

1.1. PREFACE

Composites consist of a grouping of two or more elements (phases) that have dissimilar mechanical and chemical characteristics, which could do not attained by any one of them. The prime phase is the matrix, which offers the dispersal the loads, safeguards the composite's formation, and provides the final outward outer shell of the composite structure. The other phase is the composite reinforcement elements offer better mechanical properties intended for the composite and enhance the matrix in the desired direction.

Superb mechanical properties make the composites valuable for a widespread range of applications such as; chemical purposes, automotive production, aerospace applications. The high (strength-to-weight) ratio, elevated specific strength, high limit of fatigue strength, elevated elasticity limit, wear resistance are the most expected apparent in the above areas of applications. Composite materials meet most of these requirements.

Among composite materials, metal matrix composites (MMCs) are the most universally functional and utilized materials in several employments as a result of the superb mechanical and thermal properties. Other than the new employments in the automotive, chemical, energy, defense and biotech industries, most MMCs are also advanced for the aerospace industry. Although, composite materials are commonly fabricated in near net shape, then machining procedure are utilized to attain the wanted profile and dimensions of the produce pieces.

The process that involves the utilization of different factors and tools to take out the unwanted material is known as a machining process. The machining of MMCs is a hard task as compared to machining of traditional metals. In the machining process, the MMCs behave inhomogeneous and anisotropic, but the various reinforcing elements, matrix material properties, and the volume friction also affect this. Tough and abrasive reinforcements in MMCs have hardness characteristics almost alike to that of the tools that are utilized. During the cutting process, these hard reinforcements wipe alongside the cutting edge and it severely increases the edge wear. In addition, the complication of the chip formation method during MMCs machining further increases the complication of the cutting process. These obstacles come from the interface between tools, matrix material and the reinforcement elements. Therefore, dealing with machining of MMCs is a challenging process consideration.

Drilling process remains the most important applied machining processes for a variety of applications, including automotive, aircraft and aerospace, mold, medical and electronic equipment industries, through the process involves the formation of holes for different categories of materials [1-5]. Drilling process is the most frequently used process for the purposes of fastening and joining of composite materials. The drilling is applied for a great quantity of MMCs components, which are made for the aviation and the automotive industries. The major difficulty in machining of MMC is the extensive tool damage, which leads to an extravagant manufacturing process or formulate the process impractical.

Intended for MMCs, initially could be considered as challenging for industrialized engineers and researchers, MMCs can be machined using conventional cutting processes for instance turning, drilling, milling, etc. The machinability of MMCs is harshly affected by reinforcement (sort and quantity), and matrix properties [5-13].

Additionally to tool wear, one key characteristic is the surface integrity of the machined MMCs surfaces. In any case, the delamination and the fractured are virtually unavoidable in MMCs drilling. Drilling MMCs poses many troubles for the

industrialized sectors, such as high drilling forces, wear, delamination, surface finish quality and burr.

Magnesium matrix composites (Mg-MCs) has numerous of advantages greater than magnesium metal, for instance elevated strength, elevated modulus of elasticity, excellent creep properties and superb wear resistance at high temperatures [14-24]. The required performance is achieved throughout a cautious assortment of the size and type of reinforcing particles to be used.

The most frequently used reinforcements with Mg matrix are silicon carbide (SiC), aluminium oxide (Al_2O_3), titanium carbide (TiC), boron carbide (B_4C), carbon nano-tubes (CNTs) and more recently graphene nano-platelets (GNPs) [13,15,16,18,19,22,23,25].

The machining characteristics of graphene-reinforced Mg-based hybrid nanocomposites have not yet been wholly documented. Researchers have in general endeavored to scrutinize the microstructure and mechanical properties of this newfangled metal matrix composite. This thesis research focuses on the assessment of the machinability of these materials in cases of microstructure, the influence of cutting parameters, cutting forces, machined surface integrity, delamination, cutting tool failure and wears mechanisms in order to fully comprehension of the process mechanisms and with the mean to eliminate the undesirable effects.

1.2. THE NEEDS OF METAL MATRIX COMPOSITES DRILLING INVESTIGATION

MMCs are a novel category of advanced materials, with superior stiffness, strength and lower density than the equivalent metals. Due to these properties, MMCs are gaining more applications in the aerospace, automotive, petrochemical, wind turbine blade manufacturing etc. Drilling is the majority widely used with MMCs manufacturing processes for fastening purposes. The anisotropic character of MMCs makes it complicated to drill compared to monolithic metals. Problems such as high thrust forces, surface delamination, insufficient surface finish and internal cracks are

common. These issues do not only affect the quality of service of the MMCs, but are occasionally enough to seriously affect its intended use.

It has been found that these defects of the MMC during drilling can be reduced by controlling the drill bit geometry and process parameters. A. Taskesen et al. [26] point out that; the cutting process parameters, the optimal level of weight percent fraction of the reinforcement, and the category of tool coating can be combined to reduce harm to the machining surfaces. J. Paulo Davim [27] found throughout his experiments that the feed rate and cutting speed have a large influence on the cutting pressure and surface roughness. T. Rajmohan et al. [28] used three different drill types, with diverse geometries and coated layers, and found that the PCD drills performed better than the other drills in the improvement of surface finish.

1.3. MOTIVATION

The advances in the industrial and engineering technologies motivate the utilization of MMCs in a broad variety of applications and industries which making the manufacturing processes more cost efficient. Graphene reinforced Mg-based hybrid nanocomposites by providing an outstanding and highly customizable mechanical property. However, their processing technology is still in its infancy stage, with many limitations in shape and structure formation, all of which make the design and manufacture of these materials more difficult and costly. Extensive research and development are currently under way to overcome the constraints and difficulties at all phases of production. Our work aims to contribute to the synthesis and machining (drilling) of these materials.

Since MMCs made parts are often integrated into mechanical assemblies, drilling is the most common process in the manufacture planning of these parts. Drilling occurs mainly throughout the finishing stages of the manufacturing process to form a fixed feature. Drilling of MMCs and metal drilling have dissimilar substantial laws (the formation of brittle chip rather than plastic deformation), which is why the current industrial practice has not been wholly comprehended and optimized.

In drilling of MMCs, several of the major issues highlighted, such as high thrust force, surface finish damage, delamination defects and tool wear need for more examination and optimization. The stratification of the general hole quality is a key feature of the MMCs drilling process as it may result in failure to the utilization process. The overmuch tool wear over the drilling of MMCs, makes it very expensive, and because that a limited number of holes can be drilled in an exacting drill bit.

The core differentiation between metallic and MMCs components is their structure: in the metals is isotropic and is anisotropic for the MMCs materials; this means that for a metallic materials every part of the structures work in a like mode under the cutting loads. The MMCs structure will have a local reply from the same load, resulting in faults in the interior structure of the remaining workpiece material.

In this thesis research, a systematic drilling investigational experiments were accomplished, for more understanding the merits of Mg-MC machining aspects. The material system studied in this research is Magnesium Matrix Composites (Mg-MCs) reinforced with nano-sized of graphene nanoplatelets (GNPs) and micro-sized of silicon carbide (SiC) particles. The motivation for this research is the escalating demands for the lightweight components with superior mechanical properties in a variety of industries and applications. Mg-MCs begin to be one of the best alternatives due to its lightweight, high strength, high creep and wear resistance.

Moreover, the superior strength and abrasive assets of the reinforcements present major challenges for performing the drilling process ideally. Thrust forces, torques, surface topography, surface roughness and delamination are characterized for optimal understanding and comprehension of the machining mechanism during drilling of the two categories of Mg-MCs (Mg/0.25wt.%GNPs) and hybrid Mg-MCs (Mg/10wt.%SiC/0.25wt.%GNPs) fabricated throughout the use of the powder metallurgy procedure.

CHAPTER 2

DRILLING PROCESS: BACKGROUND AND THEORY

2.1. MACHINING PROCESS

Machining process is the taking away of needless materials from the workpiece in the form of chip to attain the desired size, shape and supreme finish of the finished product. To comprehend this process mechanism, it is essential to understand the two categories of cutting process, orthogonal and oblique cutting. The main difference among the orthogonal and oblique cutting models is the cutting edge orientation relative to the cutting track, associated with the zero inclination angle (i) in orthogonal cutting mode. The orthogonal cutting mode is relatively simple, as shown in Figure 2.1 (a). The cutting process in orthogonal mode can be illustrated in the plane enclosing the tool cutting edge movement vector and the finished surface normal's. Geometrical and kinematic conversion models regularly utilized to orthogonal cutting processes to assess the extra complex three-dimensional oblique cutting mechanics. Orthogonal cutting is alike to a shape process with a straight rim whose movement is perpendicular to the cutting speed (V_C). The chip having a cutting width (b) and a cutting depth (h) is cut off from the working material.

At the orthogonal cutting, it is presumed that the cutting is homogeneous all along the cutting edges. Therefore, it is a strain deformation progression in two-dimensional plane with no side dispersal of the material. Hence, the cutting forces are performed just in the directions of the velocity and uncut chip depth that are called tangential force (F_t) and feed force (F_f). However, in the oblique cutting process, the cutting edge is sloping at an inclination angle (i) and an additional force acts in the radial track (F_r). There are three deformation locales during the cutting process, as illustrated in Figure 2.2 of the orthogonal cutting cross section approach.

When the cutting edge of the tool comes into the material, the material facing the cutting edge is sheared into the chip over the primary shear locale.

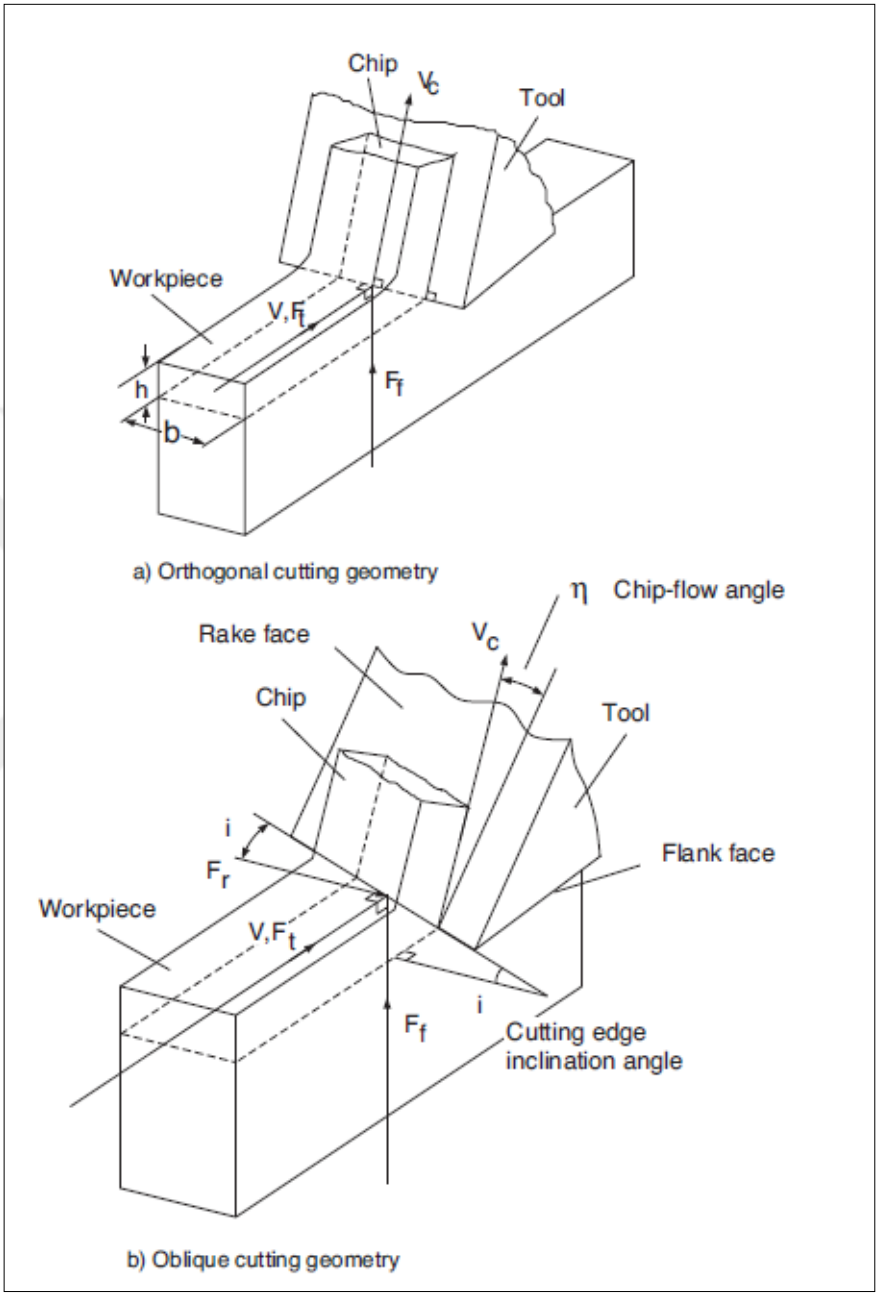

Figure 2.1. The orthogonal and the oblique cutting patterns geometries [29].

Just the once the material is cut off, the chip is partially deformed and stir alongside the rake face of the tool, which is recognized as the secondary deformation zone. The friction region, which the tool flank side wipes the machined surface, is identified as the tertiary zone.

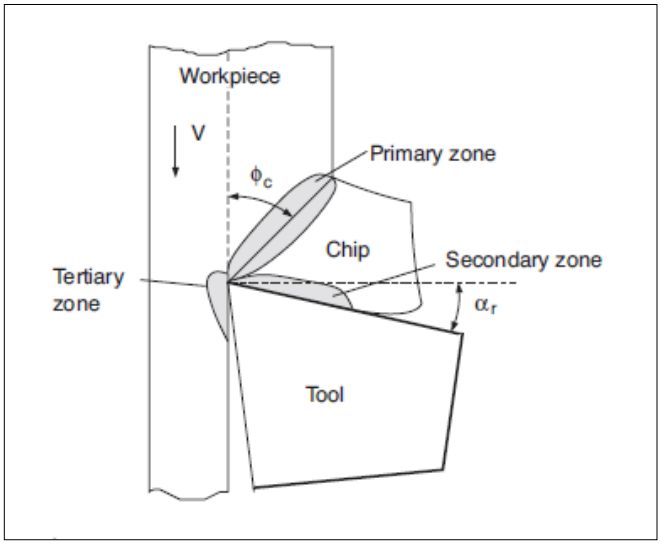

Figure 2.2. Cutting areas during cutting process [29].

The chip at the beginning, sticks to the rake plane of the cutting tool, as shown in Figure 2.3. This is labeled as the chip-sticking region (l_{st}). At the sticking region, the frictional stress is around the equal of the yield shear stress of the working material that the produced chips go over the material attached to the rake face of the tool. The chip finishes sticking and begins to sliding on the tool rake face (l_{sl}), and the sliding friction coefficient is constant during sliding length [30].

The chip leaves the tool and loses the touch with the cutting tool rake face. The interval of the pertain region relies on the cutting speed, cutting tool geometry, and the material properties.

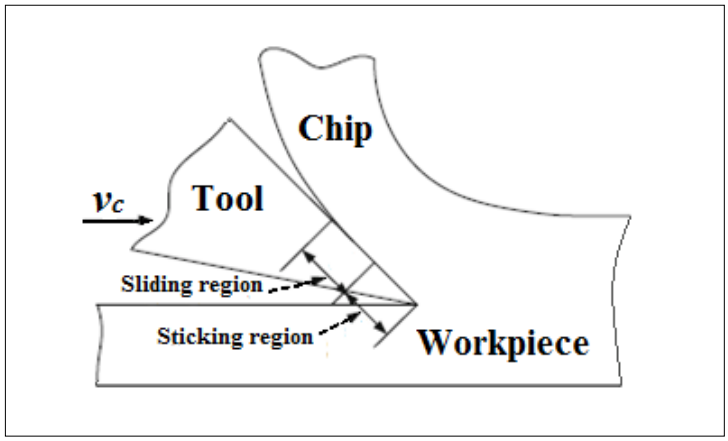

Figure 2.3. Sliding friction and sticking friction regions.

2.2. DRILLING AS A MACHINING PROCESS

Drilling is considered and acknowledged as one of the most relevant processes for machining. Drilling is the process of forming circular holes in a bulk material or expanding existing holes using a rotary multi-tooth cutting tool called a drill bits or drills. A variety of cutting tools are accessible for drilling processes, however twist drills are the essentially common utilized. Drill bits are endangered rotary tools consisting of single or multiple cutting lips and one or multiple flutes to discharge the chip and as a coolant canals delivery.

2.2.1. Drills Classification and Terminology

There are varieties of types of drills. Twist drills are the mainly commonly utilized drill bits. Currently, being applied and generally rated as the most effective drill bits for all drilling tools. The geometric features of a commonly used twist drill are shown in Figure 2.4. The following is a list of key terms for twist drills and illustrated in Figure 2.4.

1. Drill: Drills are end-cutting instrument used for holes making. They have one or several cutting edges and flutes that allow fluid to come into and the chip to be outlet. The drill tool includes of the shank, body, and drill point.

2. The Shank: The shank is the piece which holding and motivating the drill. It can be whichever straight or tapered. A drill with a little diameter typically has a straight shank. Large drill bits have shanks ground among a tang or a taper to guarantee an accurate alignment and a reliable drive.

3. The Tang: The tang is the plane-end of the drill shank that fits directly and exactly into the drive slot of the drill holder on the instrument spindle shaft.

4. The Body: The piece of the drill expands and broadens from the shank to the drill point and it includes the flutes. The twist drill body has two twisting flutes (grooves) which are cut into the drill body.

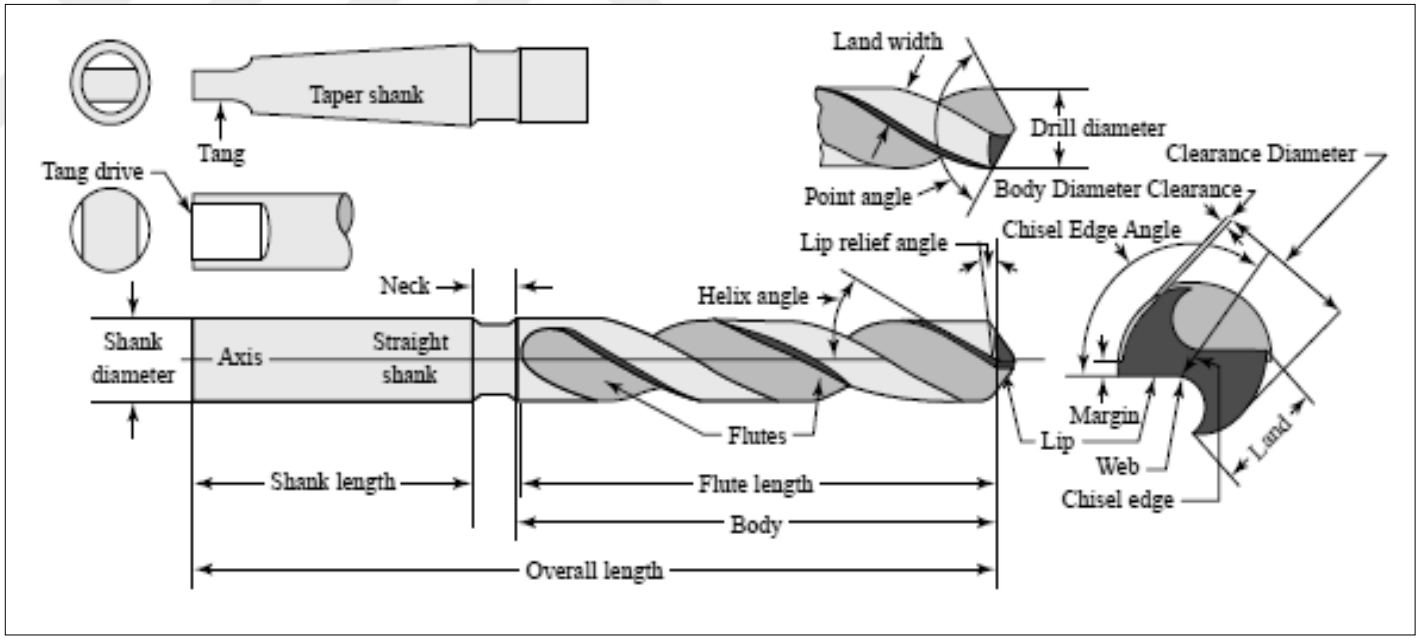

Figure 2.4. The geometry of a typical twist drill [31].

5. The Drill Point: The cutting end of the drill is the drill point. The all-cutting procedures are situated on the point of drill. The geometries of the drill point are determined with the cutting lip, chisel edge and lip clearance as shown in Figure 2.5. The lips or cutting edges lengthen from the chisel rim to the margin and they are the pieces of the drill point, which creates the cutting action. The chisel edge is the left over segment among the grooves (flutes). It is supposed to be as small as possible. The lip clearance is provided by grinding the heel below the cutting edge. With no this clearance, the drill bit could not be able to be in motion forward through the workpiece.

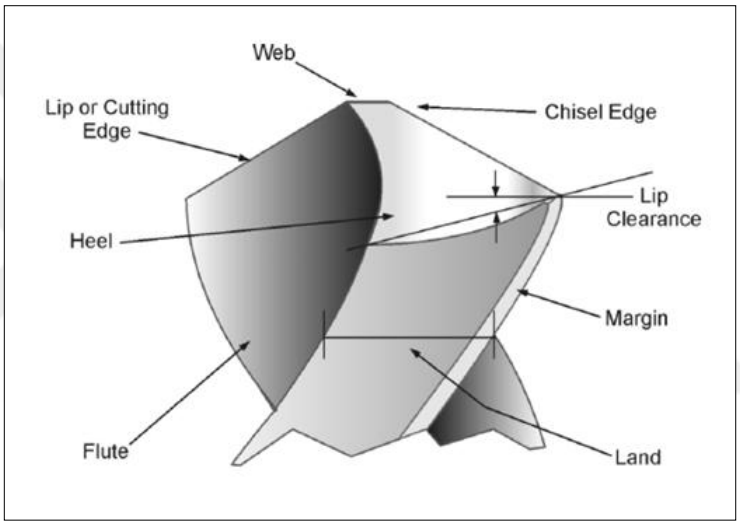

Figure 2.5. Drill point [32].

6. The Flutes: Furrows (groove) that are made or formed in the drill body which allowing coolant fluids oncoming to the drill point, chips and workpiece surfaces. The flute length is measured from the drill point to the overflow end of the flute. The straight flutes are used in a number of cases.

7. The Land: This region is the leftovers exterior of the drill body later than the flutes sections are cut, and it known as the drill body part that located between the flutes. To offer a clearance, the land is cut back from the outside drill thickness. The land provisions much torsional strengths during drilling process. Reduced land width increases chip space and reduces strength.

8. The Margin: The slim raised wedge all along the length of the flutes is the margin. The diameter of the drill bit is measured on the cross of the margin. However, the body of the drill is cut to make available free space at the back of the margins. Margin clearance would help to avoids extreme friction and abrasion.

9. The Web: The web is the central piece of the drill body attached to the lands and determined by the thickness intended across the base of the flutes. However, this assists to overturn the drill bit torsion strength.

10. The Chisel Edge: It is the edge land all along the web on the drill point, and the chisel edge joins the cutting lips. Chisel edge is not cut; it takes away the workpiece material by penetrating and moving through.

11. The Lips (cutting edges): Lips are the major cutting edge of the drill; cutting edges expand from the drill center to the outer diameter. They expand from the chisel point to the periphery of the drill bit. With mainly of typical drills, the cutting edge forms a straight line, and for various special and high-performance drills, curved cutting lips may be utilized.

12. The Axis: The axis is the central line of the drill body. It takes place over the web and perpendicular to the diameter plane.

13. The Body Diameter Clearance: The elevation commencing the margin to the land level is referred to as the body diameter clearance.

14. The Web Thickness: The web thickness is the nominal distance on the web. The web thickness increases occasionally when moving up along the body from the drill point, but it typically is grounded downward with a sharpness to decrease the edge size of the chisel. However, this process is identified as 'web tinning'.

15. The Helix Angle: The angle located among the leading edge and the drill's axis is renowned as the helix angle. This angle is formed between the line crossways the drill axis and the edge of the land. Helix angle is the key parameter for controlling the shape of the cutting geometry section along the cutting edges (lips) area. Drills with different helix angles are found in various operating needs. The helix angle is generally divided into three main categories:

16. Low (slow) spiral, this is between 12° to 22° helix angles and is used for materials that formed broken chips such as brass, bronze or cast iron.

17. The normal (regular) spiral: from 28° to 32°, generally utilized for general purposes and used for an extensive collection of drilling purposes.

18. The fast spiral, this is between 34° to 38° helix angles and is utilized for high helix general purpose and deep hole parabolic drills for soft iron and nonferrous materials that producing chewy chips. The helix angle provides quickly discharges of the chip at very high rotating speeds.

19. The Point Angle: The angle located between the lips (cutting edges) is renowned as the point angle. It is diverged for various types of the workpiece materials. High Point Angle (Flatter point) is expressed as follows: suitable for the hardest and most durable materials, stronger cutting edge, the known shorter cutting lip produces a seemingly narrower chip, and the point angle higher than 130° is utilized for hardened and very tough materials. Low point angle (Sharper Point): for soft materials, and point angles lower than 118° is commonly utilized for soft non-ferrous and non-metallic materials.

20. The Lip Relief Angle: A very alike to the classic relief angle seen in the other tools is the lip relief angle. However, it is measured at the perimeter. It relies on the diameter magnitude of the drill and the toughness or rather the hardness of the working material. For drills with bigger diameters and more durable

materials, the lip relief is often reduced to 8°. Drills for soft material and small diameters constantly have a high relief angle recognized as up to 24°.

21. Chisel Edge Angle: Which is the angle formed between the chisel edge and the cutting lip, its magnitude is generally between 125° and 135°.

2.2.2. The Geometry Effectiveness on Drill Performance

Drilling process performance is influenced by the difference in the drill geometric variables. However, they affect thrust force, torque, tool life and drilled surface quality as the following:

1. The Point Angle: While the point angle increases, the thrust force magnitude increases and the torque value decreases slightly. The large point angle (greater than 118°) discharges a less significant amount of cut material from the workpiece, which in turn reduces the burr formation through the drilling. It has sharper and more fragile cutting corners that often wear out because of the greater degree of thrust applied. Smaller point angles (less than 118°) permit additional material to be ejected and removed from the workpiece, but with a more stabilized cutting edge. For each one of workpieces material there is an most advantageous point angle at the best value with drilling thrust, wear and burning [3,32].

2. Helix Angle: It has a major impact on the drilling forces and torque. By increasing the helix angle, it diminishes the thrust force and torque. The increment of the helix angle declines the cutting edge and tends to limit the drill life. Select of the most advantageous value of helix angle for the material to be drilled is the solution to attain the superior drilling conditions. According to S. Ema [3], the torque decreases significantly as the helix angle increases.

3. Rake Angle: The cutting tool can be with positive, neutral or negative rake angle. Active rake cutting edges dominance chip flow to decrease the cutting forces, power consumption, improves surface finish quality but decline the

cutting edge. The narrow and sensitive side of the cutting edges of a positively raked tool shortens the drill life. Negative rake is the worst geometric feature amongst drilling of composite materials, resulting in production maximum heat, poor hole surface, and poor quality chip. If the chip formed during cutting is pushed to the front of the cutting edge, it is typically pressed into the pack, and eventually cuts off the flute (groove) and then harmfully affects the drilling process.

4. Web Thickness: For the reason that of increasing the web thickness, it enhances the cutting edge, but it is recognized to be dependable for raising the thrust force pointlessly [3]. The thrust force created by thicker webs can be significantly reduced by various thin techniques that increase the effective length of the cutting edge and reduce the proportional load per entity length of the cutting edge. These factors reduce the total force and increase the drill life. Therefore, reducing web thickness is a vital design characteristic to reduce drilling forces.

5. Chisel Edge Length: A common increase in the chisel edge angle technically decreases the drilling force values but the torque remains as same.

2.2.3. The Cutting Conditions Effectiveness on Drilling Performance

Drilling parameters such as cutting speed and feed rate are considerable factors that can influence the performance and well-organized of the drilling process. The effective tool life is not restricted by the higher limit of the cutting speed, although is restricted by the risk of MMCs thermal harm. This is for the reason that the drilling temperature goes above the softening high temperature of the matrix material [5,8,9,11].

The most advantageous cutting speed must be high sufficient to attain efficiently cutting process with minimal heat riskiness. The higher the feed rate, the greater the force required to penetrate the workpiece. Slower feed rate results a concentricity of the heat and an increment in the operation’s time.

2.2.4. Tool Wear in Drilling Process

Heat generated, pressure, friction and stress distributions are the most important factors cause of drill wear. Drill wear could be diversified into the following types of wear; outer corner (w), flank (V_B), margin wear (M_w), crater wear (K_M), the two categories of chisel edge wear (C_T and C_M), lips chipping wear (P_T and P_M) and built up edge formation wear (BUE) has been also observed in drilling processes [33]. Figure 2.6 shows the categories of wear described above.

Wearing begins at the cutting edge's corners and is distributed all along the cutting edge and even the chisel and along the margin of the drill. Flank wear is recognized and acknowledged as one of the criteria for measuring drill performance [6,12,14]. Flank wear occurs for the reason of the friction among the workpiece and the contact region of the clearance face.

The built up edge formation wear (BUE) were produced due to the speedy deformation of the working material flow at the tool faces during the secondary deformation and due to the work hardening caused by convergence. Drilling operations can generate BUE's over the drill lips, chisel edges, the margin and outer corners. The damaged drill with important flank wear, chisel edge wear, and crater wear can be utilized for drilling while its outer corner and margin remnants in good situation.

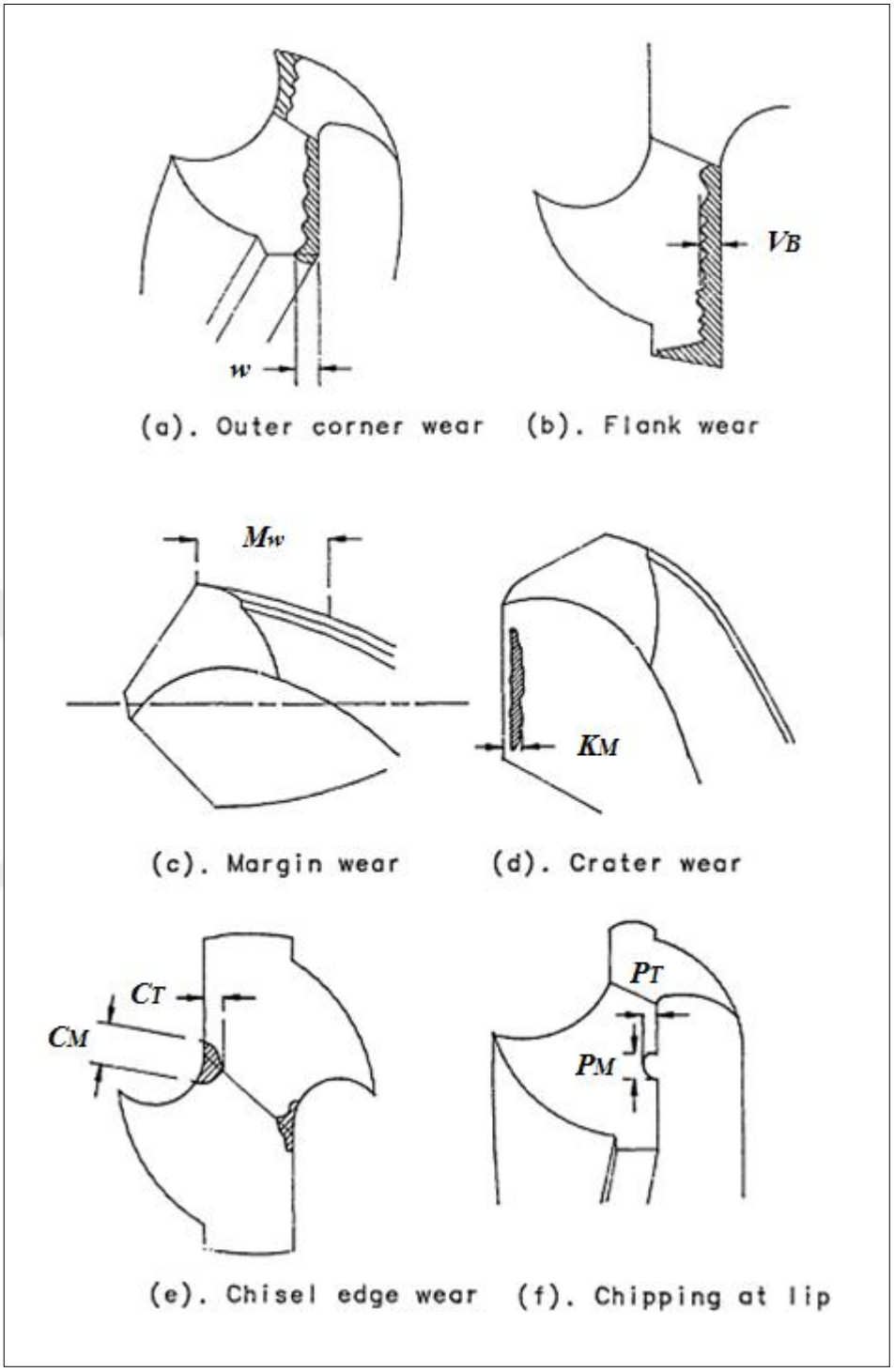

Figure 2.6. The drill wear catagories [33].

2.3. DRILLING PROCESS MECHANICS

The forces observable throughout the drilling action are the thrust force applied by the rotary drill to the working workpiece and the torque provided by the spindle to

uphold the drill rotates. The drill point causes the thrust force and torque in the typical drilling process. As shown in Figures 2.7 and 2.8, the drill point is the key cutting sector and consists of the chisel edge (web) and the lips (cutting edges). Drilling operation is considered as the oblique cutting procedure by dual lips or more, which has varied angles of inclination along the cutting edges. Additionally to the thrust force and torque, the drill is subjected to lateral cutting forces due to the asymmetric lips or the drill's axis deviations. The lateral vibration greatly affects the excellence of the finished surface. The cutting achievement all along the drill lips is different from other machining operations. However, due to various rake angles and inclines (inclination), there is a divergence in cutting achievement in different radius of the cutting edge. Nonetheless, the metal removal through the chisel edge is not a vital attribute of the process because it is a small fraction of the wholly drilling operation, although it has problems with various geometries and constraints.

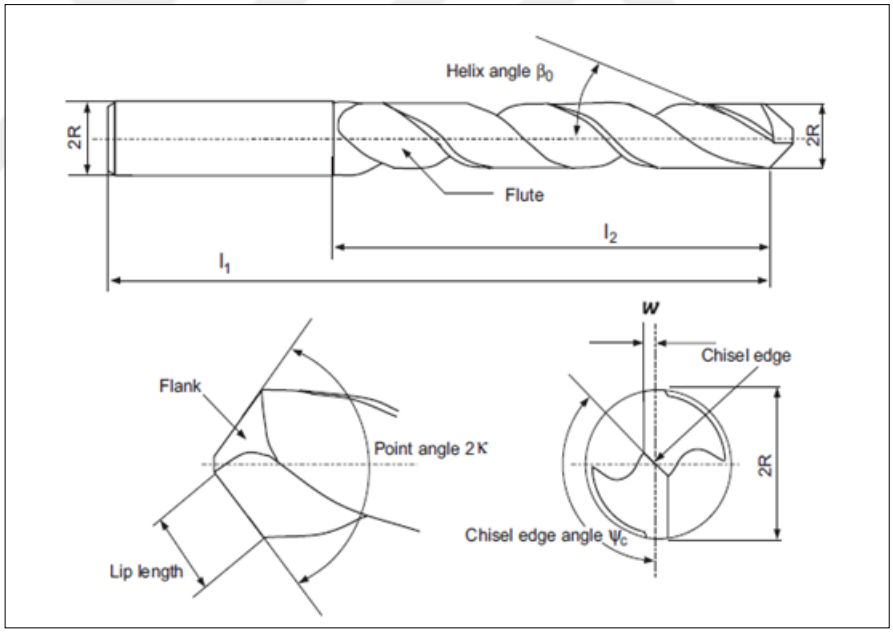

Figure 2.7. The basic geometry of the twist Drill [29].

Figure 2.7 presents a model of a twist drill. The base of the twist drill has a chisel edge and the two helical cutting lips having a point angle ($2K$), and the helix angle intersects with is (β_0). Helical grooves (flutes) do not cut; they are utilized to take away the chip from the drilled hole. The chisel has a width of ($2w$) and an edge angle of (ψ_c). Due to the chisel edge, the cutting lips deviates from the drill bit center.

When the drill bit is cut into the material at a feed rate of (*f*) [*mm/rev*], the lip enlarges the hole by taking away the material with a steady chip thickness (t_c). In order to evaluate the mechanics procedures of the drilling process, the thrust force required to move forward the drill bit into the working workpiece and the torque functional to the drill bit through the revolving spindle are required. For chisel and cutting lip regions, the drilling mechanism must be analyzed individually.

2.3.1. The Geometry of Drill Point

The recognized point of the drill comprises of the cutting edges, the rake and the clearance faces. However, drills have two cutting edges: the cutting lips and chisel edge. The cutting lips are spaced out (off-center), parallel and narrowly linked to the edge of the chisel. The point angle ($2K$) is defined as the angle between the cutting lips of the drill, as revealed in Figure 2.7. The characteristic stretch among the cutting lips is defined as web thickness ($2w$), as publicized in Figure 2.8. The angle occurrences between the cutting lip and the chisel edge is defined as the chisel edge angle (ψ_c). However, the web is thinnest at the ending of the drill and still larger in the drill's body.

Since the cutting lips have not intersection with the drill central, as an outcome the instantaneous radius (r) is recognized in relative relation to the inclination angle ($i(r)$) as illustrated in Equation 2.1.

$$i(r) = sin^{-1}\left(\frac{w}{r\ sin(K)}\right) \tag{2.1}$$

However, the helix angle (β_0) is specified with the drill diameter, and the helix angle magnitude varies by reason of the alterations in the radius. The magnitude of the instantaneous helix angle ($\beta(r)$) can be set as given in equation 2.2.

$$\beta(r) = tan^{-1}\left(\frac{2r\ tan(\beta_0)}{D}\right) \tag{2.2}$$

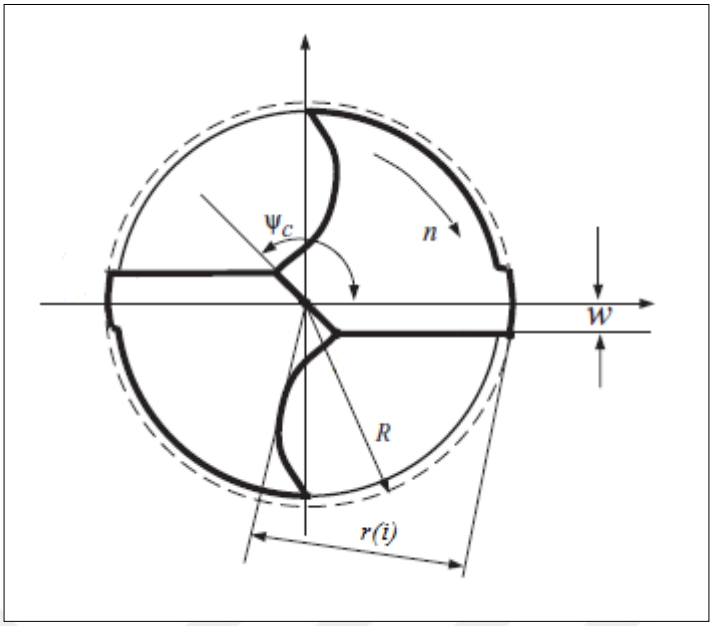

Figure 2.8. The top view of drill point {adapted from [29]}.

As can be seen in Equation 2.3 [34], the inclination angle and helix angle are utilized to find out the normal rake angle ($\alpha_n(r)$) alongside the cutting lips.

$$\alpha_n(r) = \tan^{-1}(tan\beta_0(r)cosi(r)) \tag{2.3}$$

2.3.2. Chisel Edge Section

The chisel edge is not cut, but disperses the material laterally throughout the indentation mechanism. Rather than utilizing of cutting laws, the indentation mechanics must be utilized. When the process is simplified to a hardness assessment, based on this the thrust force acting on the chisel edge could be symbolize as follows:

$$Thrust\ force(I) = F_{th} = A_c\ (HB) \tag{2.4}$$

Where *HB* is the hardness of Brinell of the working workpiece material, and A_c is the chisel edge's instantaneous indentation area. The A_c was assessed as the dispersal of the length of the chisel ($2w/sin(\pi-\psi_c)$) and the length of the disperse material

contacting with the lip (*f/(2sinK*)). Given that the chisel on both sides, there is a contact area for indentation as:

$$A_c = \frac{2wf}{sin(\pi - \psi_c)\, cos(\text{K})} \tag{2.5}$$

2.3.3. Cutting Lips Region

Cutting lips cut the working workpiece throughout the oblique mode. The chisel edge of the drill provides the constancy for the drill point and reduces the drilling vibration. The cutting lips equalize from the drill center but are parallel to the plane including the center line of the drill as revealed in Figure 2.9.

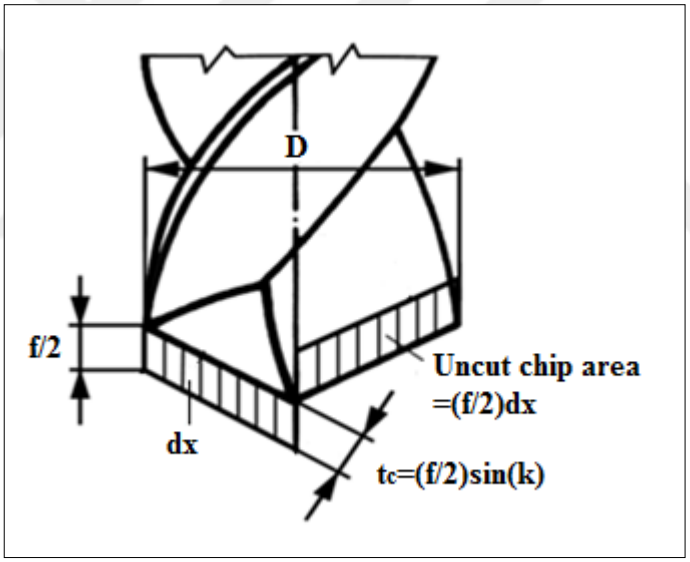

Figure 2.9. Drill pressure areas {adapted from [4]}.

The influential forces performing on the cutting edge of a rotary drill could be decomposed into normal, tangential and radial components as illustrates in Figure 2.10. It could be supposed that the drill cutting thickness segmented into slices. The fundamental cutting forces in the normal trend (dF_n) and the tangential trend (dF_t) acting on each segment are expressed in the Equations in 2.6 and 2.7 by multiplying the specific cutting pressure in the normal (K_n) and the tangential (K_t) directions by the uncut chip area (*f/2*).

$$dF_n(r) = K_n(r)\left(\frac{f}{2}\right)dx = K_n(r)\left(\frac{f}{2}\right)\cos i(r)\,Rdr \tag{2.6}$$

$$dF_t(r) = K_t(r)\left(\frac{f}{2}\right)dx = K_t(r)\left(\frac{f}{2}\right)\cos i(r)\,Rdr \tag{2.7}$$

The chip widths (*dx*) are measured alongside of the cutting lips projected on the plane normal to the center line of the drill. It can be also described by radial direct normalized using the inclination angle ($i(r)$) as shown in Equation 2.8.

$$dx = \cos i(\rho r)\,Rdr \tag{2.8}$$

The totality thrust force and torque created by the dual cutting lips is displayed and explained as follows:

$$Thrust\ force\ (II) = F_n(r)\sin(k)$$
$$= \int_0^r 2dF_n(r)\sin(k) = \int_0^r 2K_n(r)\left(\frac{f}{2}\right)\sin(k)\cos i(r)\ R\ dr \tag{2.9}$$

$$Torque\ (II) = \int_0^r 2F_t(r)Rdr = \int_0^r 2K_t(r)\left(\frac{f}{2}\right)R^2\ r\ \cos i(r)dr \tag{2.10}$$

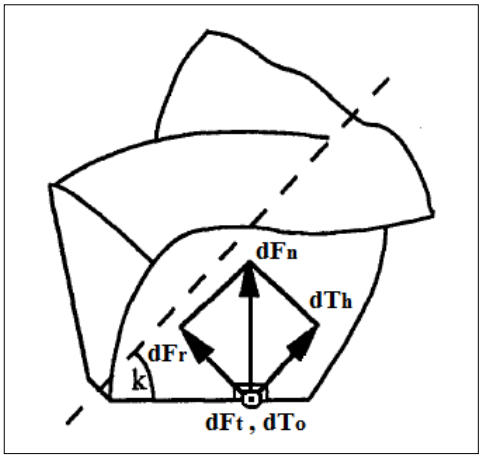

Figure 2.10. The directions of the elemental forces acting on the cutting lips {adapted from [34]}.

The totality thrust force applied on the drill is the summation of the chisel and cutting lips forces as presented in Equation 2.11.

$$Thrust\ force = Thrust\ force(I) + Thrust\ force(II) \quad (2.11)$$

The torque produced by the chisel could be neglected.

2.4. IMPORTANT ASPECTS IN METAL MATRIX COMPOSITES DRILLING

Undoubtedly, the strength and physical property of MMCs materials are enhanced attributable to the presence of reinforcing particles. However, high-energy requirements, hasty wear and related surface roughness degradation during metal matrix composite (MMCs) machining are major negative aspects of the presence of the reinforcement particles. Therefore, the application of MMCs is still restricted in some areas. For that reason, understanding the results of reinforcement on the chip formation and the machinability characteristics is critical for assortment of the proper tooling equipments and machining conditions. This would be minimizing of the processing costs and advancement the MMCs to higher-level of applications.

The various features of the reinforcement particles, such as nature, shape, size, volume percentage and distribution, are dependable on the mechanical behavior of the MMCs, which is also the affect of the cutting forces and tool wear mechanisms. Some of these process indicators are still not easy to predict as a result of the character that the reinforcement take part in throughout the chip formation and the manner in which particles are removed or cut.

Drilling is an important for processing the MMCs components. Many fasteners are utilized to securely attach the MMCs to the constructions and make the entire structure behave like a stiff body. Drilling of the MMCs is dissimilar in several ways from the metals drilling. MMCs are very hard, abrasive, rapidly damage the pointed tools, and worn tools can tear filaments and damage the drilled surfaces of the MMCs.

The extensive researches have been performed in the drilling of MMCs to improve tool life and optimize cutting conditions for diverse drills types (in geometries and materials). The generally utilized drills in these studies comprise of: PCD drill bits, high speed steel (HSS), diamond coated HSS and coated carbides (TiAlN and TiN) [5,8,10,26,27,28,35-42]. One of the high-cost factors is identified in the MMCs drilling processes is the drill bits charge.

During the drilling of MMCs, the tighter holes tolerances are required. This requirement is needed to avoid the locally crush or delamination of the composite materials when the fastener is inserted. For MMCs, tighter tolerance of the hole required a reduced amount of drilling feeds than the metal drilling and then takes longer duration. This increases drilling outlays and affects productivity. The MMCs are predominantly harsh on the drill bits, and this increasing the drill wear rate.

During the drilling of MMCs, peaks and drops in the variation of the thrust force are become noticeable, this associated to the interacting among the tool edge and the reinforcement particles [43].

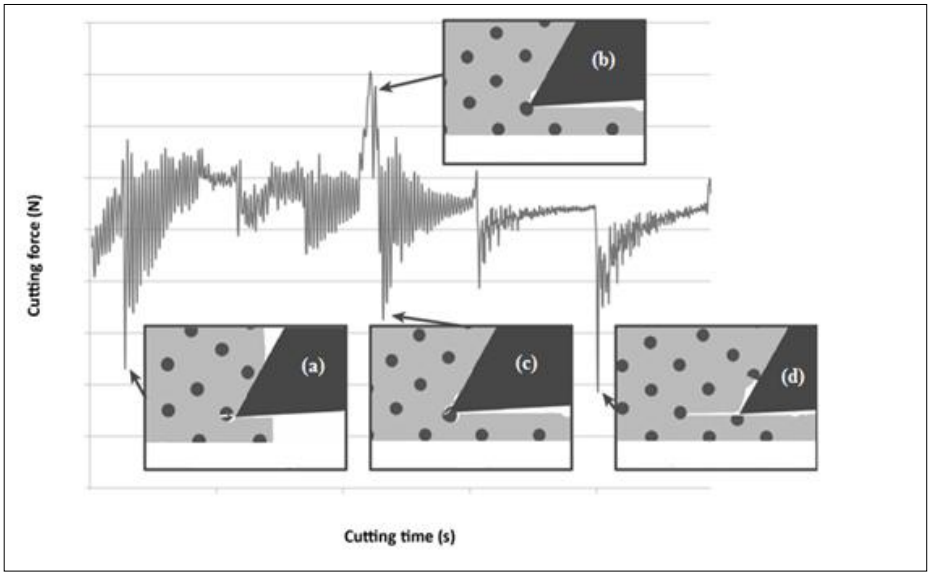

Figure 2.11. Cutting forces variation during machining of MMCs materials [43].

Figure 2.11 illustrates the interaction manners among the tool edge and the reinforcing particles as follows: (a) a diminution in the force by reason of particle

fracture and separation; (b) an increment in the force by reason of particle extrusion without cracking; (c) quick drop in the force by reason of the fracture in the particle, and (d) decrease in the force by reason of particle fracture and crack expansion in the matrix material. As could be clearly seen in the figure, the initiation and growth of particle cracks could lead to diminish the forces. However, the interaction of the cutting edge with the particles before the initiation of cracking leads to a raise in the forces.

CHAPTER 3

MAGNESIUM METAL MATRIX COMPOSITES

3.1. INTRODUCTION

Retrospectively, throughout the years, in attendance has been a elevated demand for light weight structural materials, particularly in the fast growing industries; automotive, aerospace and chemical industries [17,44-48]. Currently, alloys of Al, Ti, and Mg have increased the importance in these applications because of their outstanding properties and comparative advantages, which are; its light-weightiness, good machinability, its dimensional stability, and its low power consumption during the machining processes. Although, Mg alloys have various attractive properties, they, however, do not totally meet up to the whole requirement in the application processes, where the components are supposed to resist high mechanical-thermal stresses under tribological conditions. This situation therefore, creates the opportunity and the need for to advance and develop their properties in order to actualize full potential in their industrial applications. In the case of these advantages, MMCs are viewed to consist of magnificent potentials in the various industrial and commercial sectors, which include automotive, aviation, biomedical, sporting equipments, and consumer electronics.

The magnesium matrix composites (Mg-MCs) are the kind of MMCs by which one of the constituents is Mg or its alloy are reinforced with the particles of SiC, TiC, B_4C, Al_2O_3, CNT and presently with GNPs [15,19,21,22,48,49]. There are now, however, numerous approaches by which Mg matrix composites can be fabricated. The favorable approach of producing Mg matrix composite are; the powder metallurgy, the stir-casting process, the squeeze- casting, the In-situ process, the spray forming, and the pressure-less infiltration techniques.

Hence it is identified that ; Mg and its alloys are the lightest structural metallic materials that have the highest form and specific strength, it therefore means that magnesium are based on metal matrix composites which can attract a desirable amount of interest due to their attractive mechanical properties over monolithic alloys.

Magnesium matrix composites in the recent years received attentions by reason of the manipulate of their attractive material for aerospace, automobile applications, attributable to their low density and highly specific element. The high growing demand for the light-weighted and high performance materials is predicted to be able to inspire the demand for Mg matrix composites.

3.2. MAGNESIUM METAL MATRIX COMPOSITES CHARACTERISTICS

Mg matrix composite (Mg-MC) has three essential features that ascertains its fundamentals: the matrix (Mg), the reinforcement, and the matrix-reinforcement interface.

3.2.1. Matrix

It has known that the Mg is the most light structural metal. Mg alloys are affirmed to be; 33% lighter than that’s of Al, 61% lighter than Ti and 77% that is lighter than the stainless steel that make them potential nominee as alternate material for these metals. In the terms of availability, Mg is the sixth most abundant element in the earth's crust that comprises of around 2%. The magnesium possesses a several number of other merits that includes an excellent castability, high damping capacity, good electromagnetic shielding, and easy machinability of all the structural metals and less energy requirement in the production of magnesium. The limitation of Mg, however, includes the lower elastic modulus and low ductility, reduced creep and abrasion resistance and elevated corrosion. These limitations have been frustrated by the advancements of the new magnesium alloys and the by the adding of the reinforcement to produce magnesium composites.

Matrix is the continuous part (phase) and its properties are extemporized by shifting it into a composite with the presenting of a proper reinforcement. The assortment of the matrix and the reinforcement could greatly rely on the end utilization and the amenability for the function of production. Numerous Mg alloys schemes have been applied as the matrix.

3.2.2. Reinforcement

The secondary part (phase) of the composite is recognized as the reinforcement phase in the MMCs. By reason of its elevated stiffness and elevated strength, it is the core and major load-bearing member in the composite. The reinforcement is mostly ceramics in the shape of whiskers, fibers, and particles. The characteristics of the reinforcement are very vital and relevant in the controlling of the properties of MMCs, while the interaction with the matrix could modify the composite microstructure, characteristics, and performances.

Currently, nano-sized reinforcements SiC, Al_2O_3, B_4C, etc. with size lesser than 50 nm are been utilized. The CNT and GNPs are also potential reinforcements. The main merit and benefit of utilizing and applying nano-reinforcements is that the development and betterment in properties can be achieved at a much-more lower volume fractions which is; (less than 2%), as opposed to the micron-scale particle reinforced Mg-MCs which has higher-volume fractions which is; (more than 10%) are required. However, in order to formulate nanocomposites with advanced mechanical properties, good dispersion of the nano-reinforcement phase within the matrix is needed, which is strongly controlled and managed through the choice of a compatible production technique.

3.2.3. Interface

The interface amid the matrix and the reinforcing phase engage in recreation through a crucial role in the functioning of composite materials. The major characters of the interface are the chemical reaction and the strong of bonding. Porosity creates an impact in the interfacial reactions between the matrix and the reinforcing phases.

The interface has a numeral of physical and mechanical properties, which are outstanding and are not from either the reinforcements or the matrix. By reason that the interface between the matrix and the reinforcement, is thermodynamically unstable, and it exerts an influential level of presence on the total performance of the composite. The interface leads to a broad level of discontinuity in material parameters like the modulus of elasticity and the thermal coefficient. Quite closely, a chemical capacity of discontinuity could result to an inter-diffusion zone. This could create some preferential sites for any segregation and precipitation.

The uniform extend and sharing of the reinforcements in the Mg matrix is fundamental for obtaining a high strengthening effect due to the uneven allocation that can result to the early failure in both reinforcement/free and reinforcement/rich locales. However, the reinforcement/free locales appear to be more weak than the reinforcement/rich locales. In the location of relevant segregation or agglomeration of normally very brittle hard particles, fragile bonds are composed in the material that always results to the decline and decrease in mechanical properties.

3.3. FABRICATION METHODS OF MAGNESIUM MATRIX COMPOSITES

The fundamental difficulty and challenges faced in the processing of the MMCs is the homogeneously distribution of the reinforcement to accomplish a defect-free microstructure.

3.3.1. Conventional Fabrication Techniques

3.3.1.1. Stir Casting Technique

Throughout the stir casting procedure, the reinforcing phase (powder form usually) are distributed amongst the molten Mg through mechanical stirring. A common stir casting procedure in the orderly steps of Mg matrix composite is presented and illustrated in Figure 3.1.

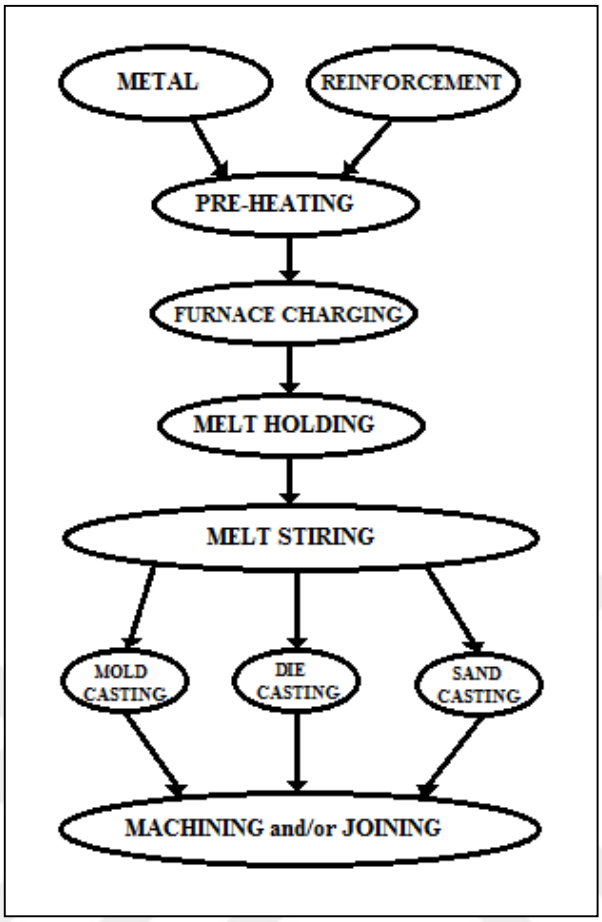

Figure 3.1. The stir casting process steps for Mg-MCs.

The heating system and the fundamental of this process are referred to as the mechanical stirring. The outcome molten Mg, with ceramic particles, is therefore utilized for the die-casting, the permanent mold casting, or sand-casting. The cast composite are extruded to decrease and limit porosity, to tenderize the microstructure, and to homogenize the allocation of the reinforcement. Magnesium composites with numerous matrix compositions, such as; SiC/WE43 [20], SiC/Mg-5Nb [21], TiC/SiC/pure Mg [23,24], Al_2O_3/ZX51[48], $Mg_2B_2O_5$/AZ31B [50], and SiC/AZ91 [51,52], are formed through the utilization of this approach technique. The schematic diagram of the stir casting procedure is illustrated and presented in Figure 3.2.

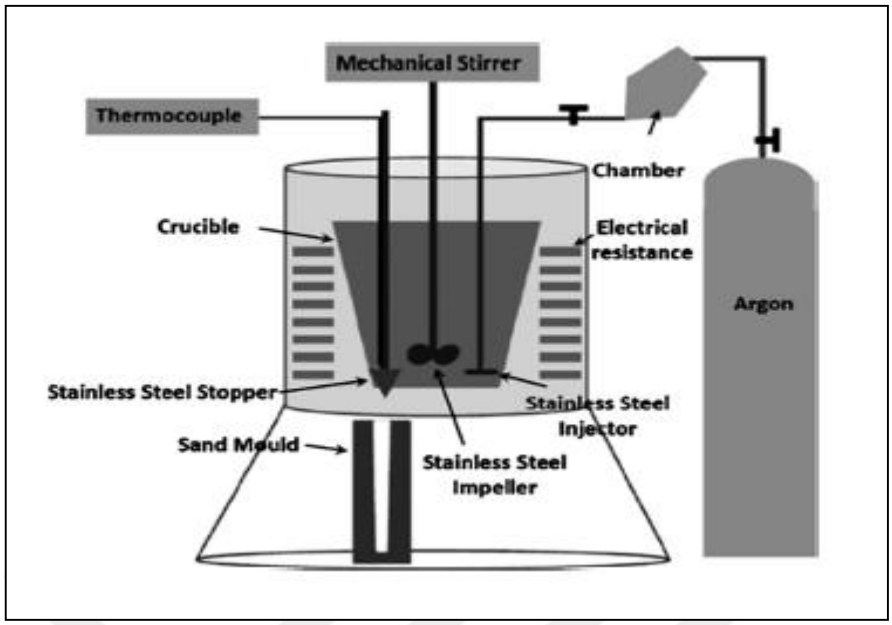

Figure 3.2. The stir casting (vortex) process [53].

The allocation of the particles in the molten matrix relies on the geometries of the mechanical stirrer, the stirring parameters, the situation of the mechanical stirrer in the melt, the melting heat, and the actions of the particles integrated.

The main benefits of stir casting are its utilization of the wide quantity fabrication. In the midst of the entire, well-established MMCs production techniques, the stir casting is more affordable and more resourceful for mass production [54]. Owing to this, stir casting has recently been the most preferred and most common commercial technique for the fabrication of aluminum-based composites. Moreover, no commercial application of the stir casting has been presented about the Mg-MCs.

3.3.1.2. Powder Metallurgy Process

The varieties of Mg-MCs are fabricated by the use of the powder metallurgy procedure such as; GNPs/pure Mg [16,19], SiC/GNPs/pure Mg [45]. The principal steps for fabricating parts through the powder metallurgy procedure are outlined and presented as enlisted below:

1. The production stages and process of powders,

2. The mixing or blending Process,
3. The compacting process,
4. The sintering process.

Powder metallurgy procedure is utilized as an approach to fabricate particulate or shorten the fiber-reinforced composites. Technically, this has to do with; the cold pressing and the sintering, or hot pressing in order to fabricate fundamentally the particles or the whisker reinforced MMCs.

The matrix and the reinforcement powders are, however, blended in order to produce the homogeneous distribution process. This blending stage is accompanied with the cold pressing which is utilized to fabricate the green blocks. The cold pressed green blocks are therefore scanned in containers and degassed in order to eliminate all the absorbed moisture from the particle surfaces. Furthermore, the composite is then hot pressed, uniaxially or isostatically, in order to be fully applied as a dense composite and extruded, as illustrated and presented right below in Figure 3.3.

Powder production

Beginning amid the first step of the powder metallurgy procedure it involves the mixing of the powders of matrix and where the reinforcements are in the weight proportions through the application of the ball mill through high energy or planetary ball mill.

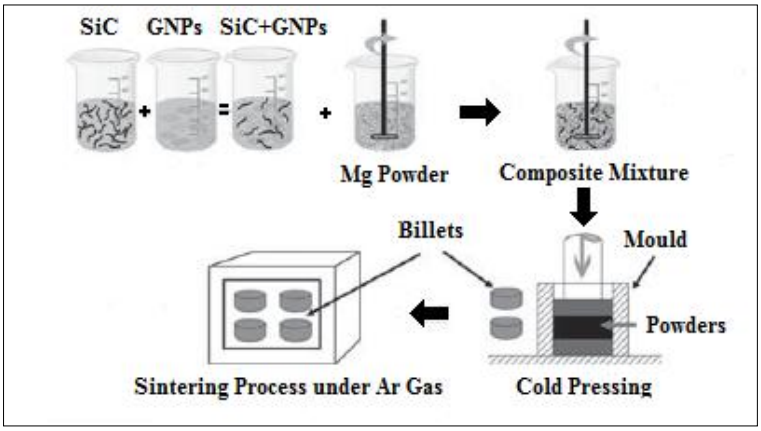

Figure 3.3. Sketch diagram of powder metallurgy procedure for hybrid Mg-MCs.

Compaction

In the subsequently stage the powder metallurgy recognized as the dominant consolidation process comprises of pressing in a stiff mold, which consists of a die punches and possibly mandrels. The popularly compacting methods are axial and isostatic pressing. In axial compacting, the metal powder is compacted amongst the punch faces and the die walls. Through the application of this method where geometrical tolerance can be achieved. This makes it clear to assert that, the axial powder pressing is a resourceful way of pressing metal powders in the mass production.

Sintering

Respectively the third stage of the procedure of powder metallurgy is identified as the heating of the mixed powders to a point of temperatures below the melting temperature bonds with its particles mixed; this situation is coined as sintering. This process involves consists and has to do with the melting point of the main and fundamental ingredient. In few occurrences, a minor ingredient can form a liquid phase at the sintering point temperature; situations like that can be identified as the liquid phase sintering. Sintering of the compact, this consists of both strength and integrity.

Respectively, following the sintering process, the secondary processes are implemented:

1. The machining process,
2. The polishing process,
3. The surfacing process.

The entire operations are carried out in the form of sintered composite materials just with the aim to accomplish the target of a finished product. The powder metallurgy technique comprises of 4 processes as listed earlier (above). The powder metallurgy steps are illustrated and presented further in details below in Figure 3.4.

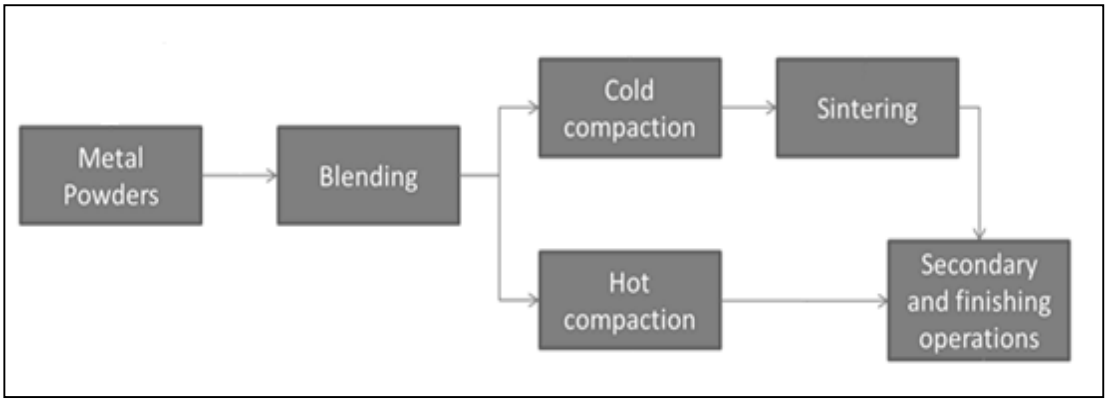

Figure 3.4. The powder metallurgy route steps.

Beneficially, the powder metallurgy technique consists of the capability of integrate a moderately elevated volume fraction of reinforcement. Furthermore, this technique needs specifically, alloy powders that are commonly more overpriced as opposed to the bulk material, and which entitles a complex process while the material are being fabricated.

3.3.1.3. Semi Powder Metallurgy Method

The pure Mg and its composites have been produced using the semi-powder metallurgy technique and means, which was accompanied with a hot extrusion technique. Figure 3.5 presents an easy solution resulting from the strategic approach referred to as the semi-powder metallurgy technique, which was applied as a borrowed means to mix the composite powders. Many of varieties of Mg-MCs have been fabricated with the semi powder metallurgy process like; GNPs/Al/pure Mg [17,18,25], CNTs/GNPs/pure Mg [22], CNTs/AZ61 [55], CNTs/AZ91 [56]. In the semi powder metallurgy procedure, the materials are however, mixed through the application of some liquid solvent via a mechanical agitator.

M. Rashad et al. [25] applied the semi powder metallurgy approach to produce Mg/1wt.%Al/1wt.%Sn alloy reinforced with the relatively low content of graphene nanoplatelets (GNPs). The Mg, Al (1 wt %) and Sn (1 wt %) powders were mixed simultaneously in ethanol solvent through the application of mechanical agitator.

Right when the GNPs were divided as ultra sonicated in ethanol for 1 hr. GNPs solutions were then included as drop wise into the above powder slurry in ethanol.

The mixing process lasted for about an hour with the purpose of attains the uniform mixture. The mechanically agitated mixture was then filtered and vacuum dried up at a temperature level of 70 °C with the aim to achieve the composite powder. The composite powders were then compacted in a stainless steel mold at a room temperature under; 580 MPa pressure to get the green billets. Thereafter, the compacting, the green billets were sintered in the furnace at a temperature level of 630 C° for two hours (2hr) under an argon gas atmosphere.

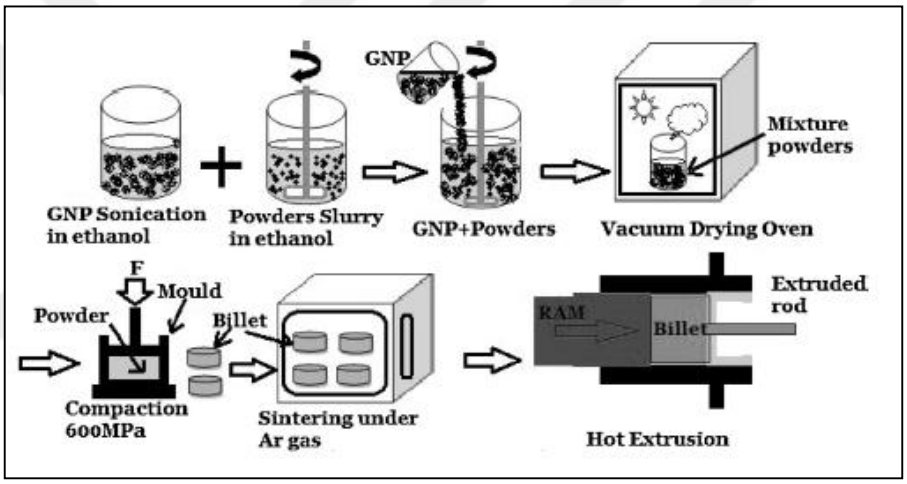

Figure 3.5. Scatch diagram of the semi powder metallurgy procedure for producing Mg/GNPs composite [25].

3.3.1.4. Squeeze Casting Method

Figure 3.6 illustrates the procedure of the squeeze casting of the Mg-MCs [47]. The period and process of the squeeze casting, the reinforcements (whether through the powders or fibers/whiskers) are generally, created into a specific form and positioned into a casting mold. The molten Mg alloy is thereafter, discharged into the mold and solidified under a specific elevated pressure. While compared amid stir casting, squeeze casting constantly has the benefits of permitting the integration of higher volume fractions (up to 40–50%) of reinforcement into the Mg alloys [54].

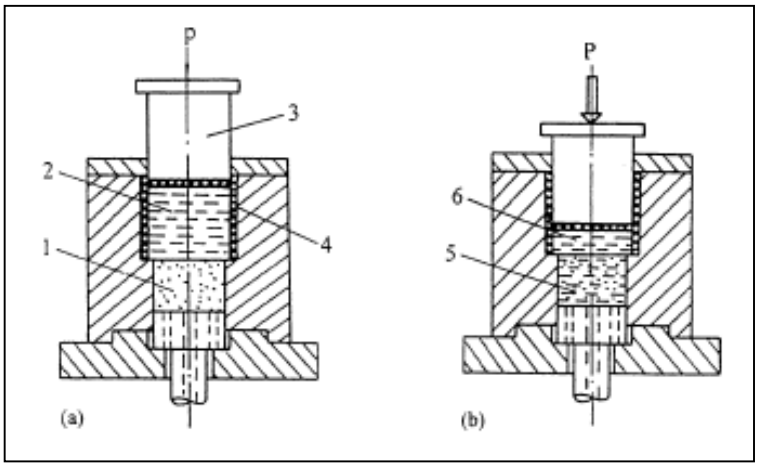

Figure 3.6. Scatch of the two step squeeze casting procedure: (1) the whiskers preform; (2) the melton matrix; (3) the punch; (4) the heater; (5) the whisker and melt mixture; (6) the melt excess [47].

Many Mg-MCs like; Kaowool alumina fiber/AZ91, Alborex aluminum borate whiskers/AZ91, Saffil alumina fibers/AZ91 [46], SiC/ZK51A [47], Al_2O_3 particles/Al_2O_3 fibers/AM60 [54], SiC/Al_2O_3/B_4C/AZ91 [57], have been made-up throughout the submission of this form of technology.

The level of pressure utilized is the primary variable, which further affects the microstructure then the mechanical properties of the casting composite. With the high pressure, various outstanding situations occurring in the process of the molten solidifying. The solidifying temperature of the alloy relies on: the magnitude of the applied pressure, the differences in its liquid, solid specific volumes, and the solidification of the latent heat [46,54]. The second stage effects of the high pressure is in the increased cooling rate because of the heat moved from that point which results from the closer contact between the mold walls and the solidifying melt. The usage of the high pressure also presents the effectiveness of the compensation for the solidification and contraction. The outcome material obtains and leads to accomplishments of prettier grains and a higher density, which results to a more-greater strength and importantly to a more improved ductility of the castings. The high pressure also gets rid of risers and feeders that are required in a conventional gravity casting and then it increases casting yield [46]. Conclusively, squeeze casting is referred to as a near-shape process, which has little or no requirement for subsequent machining.

Whereas, in the Mg-MCs, however, the pressure for squeeze casting has to be strategically and purposefully directed as a result to the fact that; an enormously, high pressure has the possibility to generate a turbulent flow of molten magnesium, thereby resulting to gas entrapment and magnesium oxidation.

3.3.2. Other Fabrication Techniques

Additionally, the four synthesis approaches explain above, that; a number of other techniques that has been examined for the fabrication of Mg-MCs, consist of the mechanical alloying process, the pressure-less infiltration process, the in-situ production process, the gas injection process, and the spray forming route.

3.3.2.1. Mechanical Alloying Process

Mechanical alloying is recognized as the procedure through which the raw powders are mixed with high energy milling balls, either included or not included with additives, in an inert environment. Throughout the mixing procedure, the powders are moved and then the cold-welding and fractures were occurred until the final composition of the extremely fine powders which corresponds and marches up to that of the preliminary charge. In concurrence amid the refining of powders, a quantity of solid status chemical reactions have the propensity to get place, ignited by the high mixing energy [58].

The mechanical alloying processes has been examined and analyzed for production of Mg-MCs [59]. While milling, the particles are refined when or not the reactions are occurring, relying on the powder system that are chosen. After the elevated energy mixing, the powders are generally, consolidated through a hot pressing or through a hot extrusion. Once there are any solid-state reactions, they have the tendency to occur during this stage. The solid-state reactions also may take place as the same-time as the milling process ongoing.

3.3.2.2. Pressure-less Infiltration Process

The fabrication of Mg-MCs via a pressure-less infiltration that is, however, relatively new when compared to the pressure infiltration (squeeze-casting). While the infiltration route is ongoing, the molten alloys flows throughout the canals of the reinforcement bed or it preform under the capillary action.

An Mg-SiC composite has been achieved while utilizing this approach [60]. Figure 3.7 illustrates the experimental setup for the pressure-less infiltration experiment. The SiC particles and infiltration agent SiO_2 powders have already been mixed and positioned in an alumina crucible, then later positioned in a steel crucible. An additional alumina crucible, which consists of pure magnesium, was, however set alongside the infiltration alumina crucible with the purpose of screen the temperature through the infiltration route. Once the structure was heated, the pure magnesium slab, which had been set right on the crest of the powder mixture.

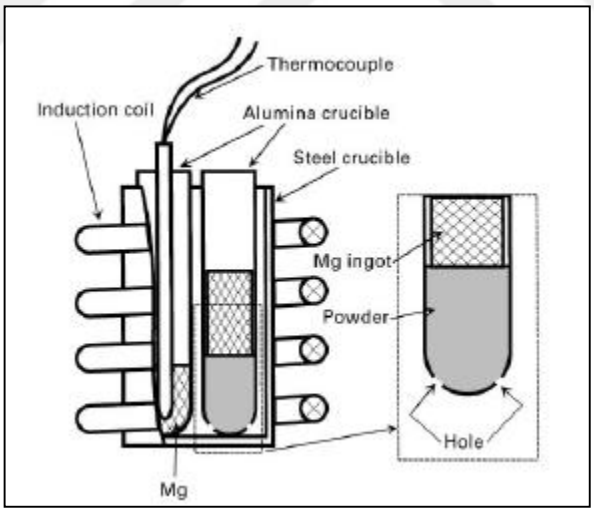

Figure 3.7. The experimental arrangement of the Mg infiltration in SiC and SiO_2 mixture [60].

The mechanism for the pressure-less infiltration is, however, referred to as the elevated heat generated at the infiltration front which often times results from the reactions between magnesium and SiO_2 [60].

3.3.2.3. In-Situ Synthesis Process

Whereas unlike the other fabrication techniques of the composites, the in-situ synthesis method is known to be the process, through which the reinforcement is formed in the matrix via directed metallurgical reactions. While fabricating, one of the reacting fundamentals is a basic molten matrix alloy. The other reacting fundamentals are exteriorly added with either the fine powders or the gaseous phases. This type of interiorly, produced reinforcement has various attractive characteristics.

Considerably, the thermo-dynamics of the anticipated reaction is the requirement for the process to be suitable and function able. Technically, fast reaction kinetics is, however, needed with the aim of make the fabrication procedure more functional. Moreover, in the case of Mg-MCs, this approach is still asserted as new.

3.3.2.4. Spray Forming Method

The Spray forming procedure is recognized as a process through-which an atomized stream of molten material droplets is controlled and built against a substrate with the purpose of build up bulk metallic materials. In the case of; a MMCs, the reinforcing particles are inserted into the stream of the atomized matrix.

A number of researches on the fabrication of Mg-MCs that applied the spray forming approach have evaluated and analyzed the relationships between the spray processing factors, the microstructure, and the mechanical characteristics of the Mg-MCs. The process factors were revealed to exert to have created an impact on the microstructure and characteristics of a SiC particle with size between 8–12 μm reinforced QE22 alloy [61]. Moreover, for the reason of the high cooling rate, the sprayed composite technically, presents the micro-structural behaviors that are traditionally of rapid solidification processes like; fine grains, porosity, and without brittle phases at the SiC/matrix interface. The smallest size of the sprayed SiC particles is even smaller than 1 μm.

3.3.3. Secondary Processing

The secondary processing stage of Mg-MCs like; extrusion and rolling, results to the fragment of particle (or whisker) agglomerates, the decrease and limitation of porosity, and an improved particles-to-particles bonding, all of that tend to advance the mechanical characteristics of the composites. During the produce of the composite sheet (when is needed), the rolling after the extrusion, due to the fact that; compressive stresses are lesser in the rolling route than in the extrusion, furthermore, edge cracking becomes a complex problem with these materials.

Some powder metal parts might, however, be utilized in the sintered state when in some other similar, situations extra secondary operations have to be carried–out in order to get the suitable surface completion of a closer tolerance etc. The secondary processes in most cases comprises of these enlisted types:

1. The annealing process,
2. The machining and polishing processes,
3. The rolling, forging or drawing processes,
4. The surface treatments to shield against corrosion process,
5. Alternatively, at the times when; infiltration is required in order to provide an increment in the strength, hardness, and in the density that can be obtainable via straight sintering.

3.4. THE MECHANICAL CHARACTERISTICS OF Mg-MCs

The development and advancements of such mechanical characteristics in a form of tensile strength, elastic modulus, creep resistance, and fatigue resistance, is commonly, the core attraction of composite materials. Hence, the entire advantages of these levels of development in the mechanical characteristics are derived from the composites that have to be weighed aligned with the diminish in other properties and not missing-out the included cost.

3.4.1. Ductility

The supposedly hard part of the secondary phases in Mg-MCs consists of two-fold effect. To beginning, once these phases are given through the Mg-MCs they can decrease through their ductility via a prevention of plastic deformation. Whereas, the particles can be further created with a grain refining effect that develops the level of ductility.

The inclusion of Ti particles to monolithic Mg results to the raise in the strength and ductility [19]. As the improved strength of Mg-10Ti alloy is, however, acknowledged to be a mismatch in the coefficient of thermal expansions and elastic modulus, through dislocation generation and the load relocate from the matrix to the reinforcement. A. Kandil [51] has proven that the adding of SiC particles to the matrix leads to a rise in the hardness value and the tensile strength as opposite to the not reinforced alloy (AZ91). Moreover, the elongation is examined to be lesser in the composites, while it decreases through the increasing of the capacity of the fraction of SiC in particulate. The net effect of the tough particles is always, as in order to diminish the ductility.

The increment in the volume percentage of Al_2O_3p advances the hardness and the yielding strength (with both in the tension and in the compression). Conversely, the tensile strength, the compressive strength, and the ductility are decreased when enlarge the Al_2O_3p content; accordingly, the toughness also reduces [48]. Moreover, there is a possibility that a mixture of the excellent strength, the ductility, and the creep resistance maybe achieved, with the adding of secondary hard phases.

3.4.2. Elastic Modulus and Tensile Strength

The strengthening of particle, the work hardening, the load transfer, and the grains refinement of the matrix by the reinforcement phases are the fundamental strengthening mechanisms in Mg-MCs. Work hardening occurs once and during whilst the composite is strained. If the bonding amongst the matrix and the

reinforcement is, however, strong a sufficient amount, the utilized stress maybe transferred from the soft matrix to the tough particle phase.

M. Rashad et al. [22] conclusively, asserted; that the magnesium composite reinforced with GNPs (Mg–1Al–0.6GNPs) showcases a level of improvement in tensile and compressive strength with a drastic decrease in the failure strain, which may be referred to the fast aggregation of GNPs in the matrix. The insertion of GNPs to Mg-10Ti alloy results to the rise in yield strength and the ductility. This level of development maybe accredited to high the specific surface region and the adhesion of GNPs and the two dimensional forms of the GNPs [19]. The high compatibility among the thermal and the mechanical substances and the good wet capability between the matrix alloys and the secondary phase technically, results to a highly combined deformation and a strong interface amid the composite matrix and its reinforcement. Consequently, the crack initiation in such composites, which derives from the matrix as opposed to the secondary phase and interface. The yield stress and tensile strength of AZ61 matrix material reinforced with CNTs were advanced and compared to pristine AZ61 [55]. The SiCw/ZK51A composite created by the two-step squeeze- casting possesses a very high altitude of elastic modulus and a high level of mechanical strength while comparing with the unreinforced matrix alloy [47].

3.4.3. Creep Behavior

A magnesium alloys have low creep resistance, particularly at elevated temperatures levels. The high creep rate of Mg alloys mostly leads from grain boundary slide and dislocation slip. Thereby, the obstructing of grain boundary slide and the dislocation of the slip through the precipitation of the tough phases at the grain boundary, or therein the grain, this is considered as the fundamental advance to the improvement of elevated temperature Mg alloys.

The materials reinforced with fibers and particles accordingly showcases the different creep outcomes even through the utilization of the same matrix. The insertion of SiC particles into AZ91 alloy also advances its creep resistance.

Whereas, when comparing with the enhancement in the creep resistance that occurs in consequence of the addition of Al_2O_3 short fibers, the SiC particles rarely creates a decent development [62]. The other characteristics of reinforcements, like; the size, the volume fraction, the profile, and the interfacial bond of the reinforcement with the matrix have also been revealed critically important and relevant to the creep outcome of a composites.

3.5. MICROSTRUCTURE OF Mg-MMCs

The relevant and vital characteristics in the microstructure of a Mg-MCs materials that is achieved from the interaction from the matrix and the reinforcement is mostly involves the type, the size, and the division of the secondary reinforcing phases, the matrix grain size, the matrix and the secondary phase interfacial behaviors, and the microstructural defects. The mechanical characteristics of the Mg-MCs materials are greatly impacted through these factors:

3.5.1. Types of Reinforcement

There are however, two categories of reinforcing elements that have been questioned for Mg-MCs. The earliest and most regularly applied is the ceramic. While, the second is metallic/intermetallic. The Ceramic particles reinforcement are the most frequently studied for Mg-MCs. Several properties of the ceramic materials compose them to be preferable for use as reinforcements. These properties may consist of the lower density and the high of hardness, the high strength and the thermal stability. There are, however, some known setbacks like; the low wettability, the low ductility, and the low compatibility with the Mg matrix.

Found within the numerous ceramic reinforcements, SiC is the commonly know; because of it’s similarly, high wettability and its stability in Mg melt, as opposed to other ceramics. In the Mg-MCs, the popularly, applied reinforcements is accepted as a form of tiny fiber/whisker, or particles, or a grouping of both the two configurations. Tiny fiber/whisker reinforced Mg alloys mostly reveals greater mechanical characteristics than the particles reinforced Mg alloy with an amount of

anisotropic characteristics. The advancement of hybrid Mg nanocomposites provides the likelihood of putting together. The wide and broad development in strength mostly connected with the inclusion of metallic nanoreinforcements with development in the ductility mostly connected with ceramic nanoreinforcements together with the advance Mg nanocomposites with important developments in both strength and ductility [15].

The inclusion of Al_2O_3p to ZX51 alloy refines the microstructure of the matrix by reason of heterogeneous nucleation of Mg grains and restriction on their development stage during solidification. This grain refinement is greatly valuable to mechanical substances of the cast composites. Moreover, the small amounts of porosity are also presented attributable to the fact that; the adding of Al_2O_3p has a deleterious outcome on mechanical characteristics [48].

3.5.2. Matrix

Numerous Mg alloy systems have been used as the matrix for composites. Mg-Al alloys like; AM60 and AZ91 that are currently the most common Mg alloys functional in the automotive industry. They are as well the mainly generally examined and evaluated matrices for Mg-based composites. Other Mg materials, like; pure Mg, Mg-Li alloy, and Mg-Ag-Re (QE22) alloys, have been utilized as a matrix, but less commonly. In the MMCs, the secondary reinforcing phase can relevantly affect the grain size of the matrix.

3.5.3. Interfacial Characteristics

The interface amid the matrix and the reinforcing phase acts profoundly in the carrying-out of composite materials. The base behaviors of the interface are the chemical reactions and the potency of bonding. The interface reactions in the Mg-MCs are predominantly predicted by the composition of the matrix and the reinforcement elements. Porosity moreover creates an impact in the interfacial reactions amongst the matrix and the reinforcing phases.

Q. Yuan et al. [56] have observed and revealed that the presence of MgO nanoparticles amongst the CNTs and the matrix of Mg can relevantly increase the interfacial bonding strength, which grantees the effectiveness of the transmit of load from the matrix to CNTs. The microstructure characterization of WE43 MMC reinforced with SiC particles reveals that homogeneous reinforcement allocation and the occurrence of the little quantity of porosity at the interface [20]. The insertion of nano-size SiC reinforcements to the Mg-5Nb, the microstructure of the composite changed and this leads to refine grains. The empowered presence of nano-sized reinforcements and the hot extrusion procedure helped a lot in the refinement in grains by creating sites for grain nucleation and inhibiting grain developments [21]. The adding of $Mg_2B_2O_5$ whiskers may also lead to the refining of the grain size of AZ31B matrix. With the increment in whiskers volume, the grain size is finer and most orderly uniformed; therefore, the whisker distribution appears a small agglomerated. An MgO interfacial reaction is formed amongst the whisker and matrix in the composites [50].

3.5.4. Porosity and Inclusions

Porosity and inclusions are very important to the mechanical characteristics of Mg-MCs. The happening of porosity in Mg-MCs can be drastically reduced the creep resistance of the composite materials. At a very low porosity levels, the amount of the harm to the mechanical properties, which are caused by the porosity, is the summation of that from each pore, whereas the tensile strength is seen to be a linear function of the porosity density. This happens because the distribution of the stress fields in the locale of each pore does not overlap. When the porosity quantity attains a certain level, the stress fields of the pores overlap with each other, and the strength of the material is no longer linearly affected by the porosity.

CHAPTER 4

LITERATURE REVIEW

4.1. INTRODUCTION

Functionality the MMCs are utilized for an exclusive distinction of purposes as a result of their benefits and the value of their particular substances (from their substances-to- their weight unit) of rigidity and strength as opposed to monolithic metals, which on the other hand presents a hopeful opportunity latent for innovative, creative designs, masterpieces and fabrications [11,12,17,63]. Nevertheless, they are regarded and recognized as; anisotropic, non-homogeneous materials and reinforced with a distinctively rough and abrasive elements which later results to an uneasy (difficult) to machine materials [13,14,64]. This challenges leads to massive damages in the machined areas and in the high-level areas of tool wear.

4.1.1. Magnesium

Mg is recognized and labeled to be; one of the lightest-weight structural metal. Mg alloys are roughly estimated to weight between the size ranges of 33%, 61% and 77% lighter in comparison to aluminum, titanium and the stainless steels categorically respectively [15]. When compared to the other earth crust elements, magnesium is ranked and labeled as the sixth most enriched element, with a roughly estimated 2.1% of earth crust weight [15,16]. However, for the lightweight construction, magnesium provides some extra benefits like; a highly effective – relevant strength, a great damping capacity, recyclability, and a nominal dimensional stability.

Magnesium and its alloys are utilized productively in the numerous fields and scopes of applications either it be in; the aerospace industry, the automobile industry, and as well as, in the chemical and communication industries by reason of of their low-level of density (1.738 g/cm³) [18,19,65]. Remarkably, their low-level of mechanical strength, low-level of elastic modulus, their ever-changing ductility and poor wear resistance, reduces and decreases their capacity and the functionality of their applications [66].

4.1.2. Magnesium Matrix Composites

Technically, MMCs are identified to be made-up by a grouping of light metal that serves as a matrix with other elements that are referred to as reinforcements which otherwise are labeled as particles or fibers (the metal, the non-metal, the ceramic or the organic elements) in the nano or in the micro-size. During the employment of a one matrix reinforced amid more than single element, they are referred to as; the hybrid composites. Basically, the core and fundamental benefits that the MMCs have above that of the monolithic metals are [14,16,67]:

1. Their enormous specific strength.
2. Their high limit of elasticity, stiffness, and fatigue capacity.
3. Their highly superior wear and corrosion prevention resistance.
4. Their improvements on damping.
5. Their high strength-to-weight ratio.
6. Their decrease and reductions of thermal expansion.

Markedly, Mg-MCs has more benefits as oppose to monolithic Mg or its alloys, like its high strength, its high elastic modulus, its super-creep, and its superb wear protective within the ever-changing elevated levels of temperatures [14-16]. Their envisioned substances can be accomplished through a prudent picking and choosing of the size and with a particular type of reinforcement particles.

The commonly and popularly applied reinforced materials are; SiC, Al_2O_3, TiC, B_4C, CNTs and currently, The GNPs [13,15,16,18,19,67]. M. Rashad et al. [16]

fabricated Mg/0.3wt% GNPs in (2015) through a semi powder metallurgy procedure. Through the insertion of 0.3wt%GNPs to Mg matrix which lead to a development in the elastic modulus, the tensile strength, the significant tensile capability and then the Vickers hardness that is up to 10.6%, 5%, 8% and 19.3% remarkably.

Table 4.1. The mechanical characteristics of pure Mg compared to Mg/0.3wt%GNPs MC [16].

Materials	Elastic Modulus (GPa)	0.2%YS (MPa)	UTS (MPa)	Strain Failure (%)	Vickers Hardness (HV)
Pure Mg	13.2±0.3	187±4	219±5	3.45±0.5	57.5±2
Mg/0.3wt %GNPs	14.6±0.2	197±3.1	238±6	3.11±0.4	68.5±2

4.2. MACHINING OF METALS MATRIX COMPOSITES

The MMCs are, however, no homogeneous, anisotropic and are reinforced with some very harsh and rough fundamentals, this guide to formulate tough to machine materials [13,68]. The usual machining procedures, like; the turning process, the drilling process and the milling process, are universally, are utilized for the machining of MMCs. Ever since of that, the reinforcements are brittle and abrasive, the division and the sharing of the chip is realized through the brittle fracture in preference to the plastic deformation while the cutting procedure is ongoing. The machining of MMCs differs from various sides from the machining of usual metals [8,13].

The fundamental challenges in the machining and in the ability assessment of MMCs are classified as the elevated rank of tool wear and under the nominated conditions; these significantly results to the non-inexpensive or unachievable operational. The roughly tough and abrasive reinforcement’s properties bring about a high- level of productive tool wear. This is however, seen and illustrated by investigative the tribological scheme in the cutting of MMCs, as shown in Figure 4.1 [13,14].

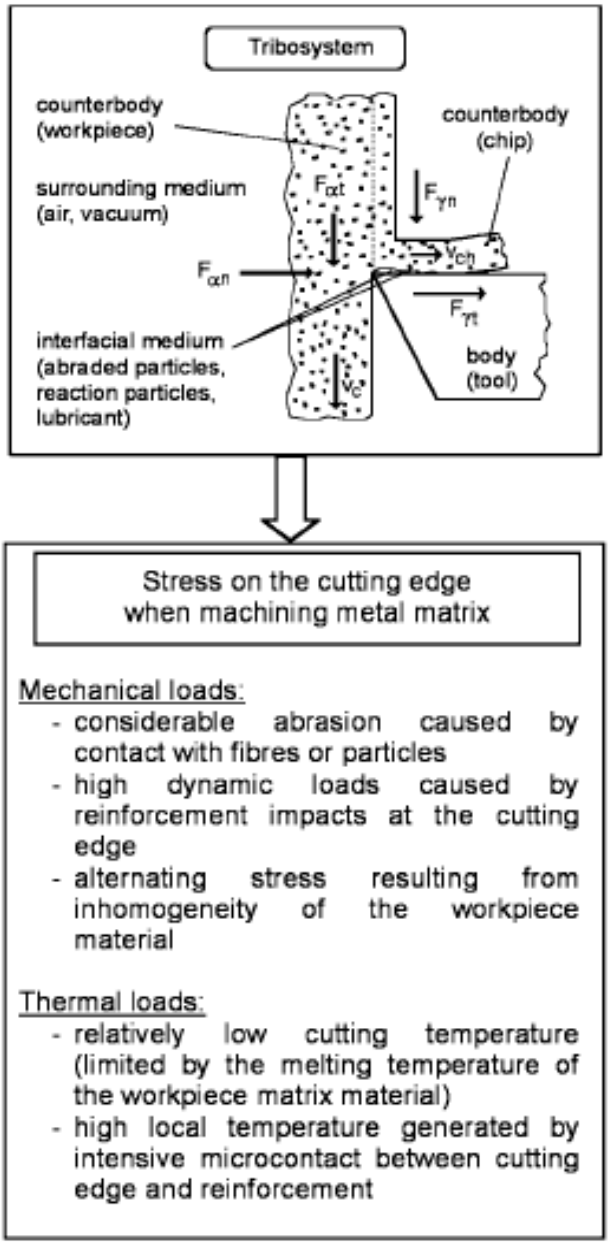

Figure 4.1. The tribological scheme in the machining of MMCs [13,14].

The fundamental shielding tool wear is the contact amongst the elements of reinforcement and the cutting edge; results to the mechanical and thermal loads which creates a negative impacts on the cutting edge [14,67,69]. The wear mechanisms could be occurred during the cutting of MMCs: the micro (cutting), the micro (plowing), the micro (cracking), and the micro (fatigue) [13].

Besides the tool wear, the cut surface (subsurface) integrity of MMCs is also a fundamental and relevant factor to consider. The breakdown of the reinforcement

particles in the friction locale (zone) while the machining is processing, results to and brings about a extremely low down rank in the properties of the machined surfaces of the MMCs. [68-70].

4.3. CHIPS FORMATION

The material in the front of the cutting edge experiences the tough plastic deformation and sequent shearing outcomes in the chip formation. The chip formation approaches of MMCs are quite alike to the behavior of monolithic metals [68,69]. Hence, the occurred transformation in mechanical properties with reinforcement form and directions in the matrix asserts and explains; the mechanism of chip formation such as; (micro shearing, micro plowing, and micro cracking) and the ensuing outcome of the machinability of the MMCs [69]. The chip formation observations and examinations provides an obvious and well understood illustration and presentation of the machining parameters that impacts and control the tool wear and the surface quality of the cut zones.

The observatory and experimental research that was carried out and excellently achieved by W. Pedersen et al. [8], through the utilization of PVD (TiCN/TiN) coated (C2) carbide inserts type (TPG-322) for machining (ZK60A-T5) Mg-MC by the 20vol.% of SiC particles of the 3-4 μm diameter. The chip formed was saw tooth, continuous or semi continuous, as illustrated in Figure 4.2.

Figure 4.2. Serrated and semi-continuous chips formed [8].

According to the research carried out by, M. Saravanakumar et al. [70], they examined the consequences of dry machining on the Mg-MC through the employment of tungsten-coated carbide (K10) type (TNMG 120404). The chip formation was envisioned to be more fragmented and short in length by reason of the brittleness. In addition, with the insertion of 5% graphite it enlarged the fragility of the composite, which results to the situation by which the chips were short in length. The drop off in the ductility of the metal matrix by the insertion of SiC particles assists to create a semi-continuous variety category of chip [7]. The form of produced chip through the drilling process of Al/15%SiC/4%Gr through the employment of coated carbide tools is illustrated in Figure 4.3, the chip is shorten in the length, and the discontinuous and sequence of the chip segments are viewed as linked to one and another [71].

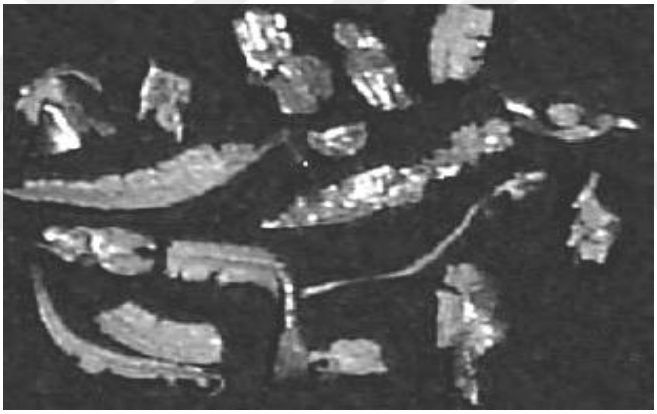

Figure 4.3. The chip formed through the employment of coated carbide in drilling process [71].

4.4. WEAR MECHANISMS AND TOOL LIFE

The cutting tool wear can referred to as, and understood to be the unwanted replacement of tool's material from the cutting edges resulting to an unwanted transformation in the tool geometries [69]. The fundamental reason for tool wear in the machining of MMCs is the straight away contact amid the presence of nature's abrasive reinforcement particles and the tool edges [11,14]. As asserted by; W. Pedersen et al. [8], the basic wear mechanism was abrasion during the employment of the (PVD) (TiCN/TiN) coated carbide inserts for machining of the ZK60A-T5

Mg matrix with the maximum wear on the flank face of the tool edge, as revealed in Figure 4.4 and 4.5.

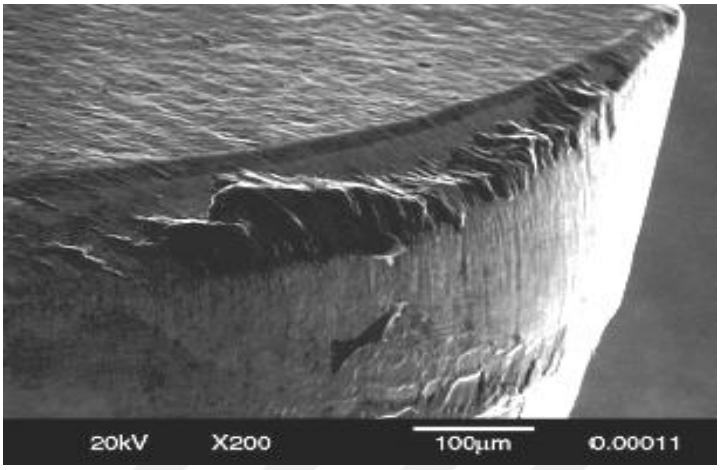

Figure 4.4. The tool edge later than 389m of cutting movement [8].

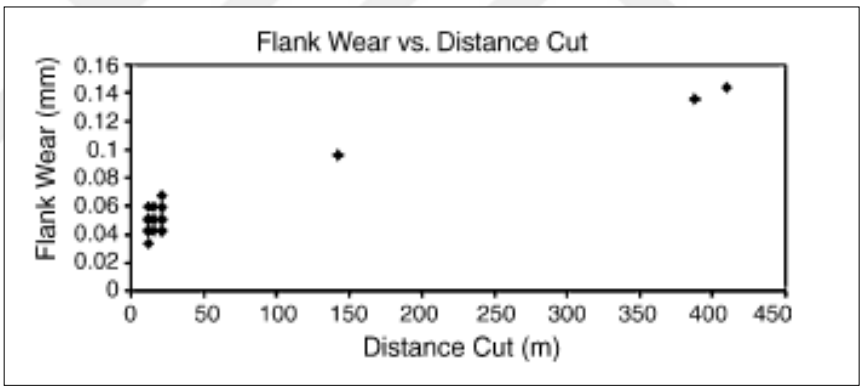

Figure 4.5. Flank wears against cutting length [8].

A. Taskesen et al. [72] carried out a drilling route through the employment of three selection kinds of drills materials (The HSS, uncoated carbide and The TiAlN coated carbide) these were utilized for the drilling of B_4C reinforced Al-alloy. Asserted from the research, the prime tool wear mechanism was the abrasive wear, and next to, it was the flank wear increasing from the cutting edge over the flank surface areas resulting from nature's abrasive outcomes of the B_4C particles, as illustrated in Figure 4.6.

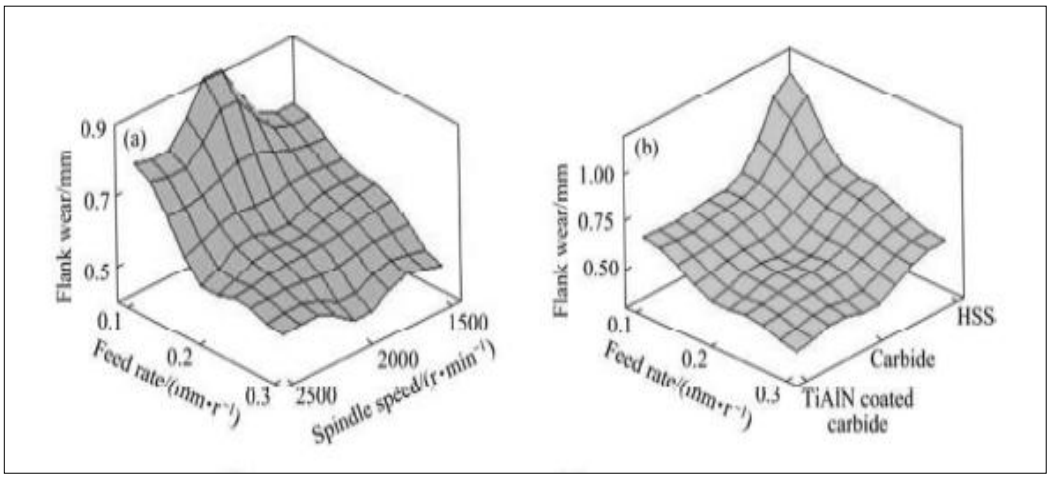

Figure 4.6. The effects of process parameters on flank wear, (a) feed and speed, and (b) feed and cutting tool sort [72].

The observatory and experimental research that had been conducted by X. Wei et al. [40] through the utilization of carbide and PCD tool inserts for the machining procedure of AZ91D Mg alloy reinforced with carbon fibers (C_f). The wear modes of the carbide tool were, however, categorized and grouped into; abrasive, adhesive and micro-breakage wears. The wear modes of the PCD tool were; micro-breakage and abrasive wear. Figure 4.7; presents and clearly illustrates the accomplishments and outcomes of the carbide and PCD tools.

The drilling process of MMCs with SiC reinforced in a prime wear mode is progressed in the flank face, the abrasive is powerfully dominant, and besides that, a magnitude of adhesions are observed [40,73]. The Mg based composite reinforced with the altitude of 1.98vol. % of nano-sized of Ti and TiB_2 were machined by the AlTiN coated tungsten carbide, which was derived from the spot where both the abrasion and the adhesion wear were observed. It was also found; that the chip adhesion impact was to be noticed and clearly seen at the machining with Ti particles as been compared with TiB_2 particles, due to the ductility of matrix metal magnesium and reinforcement particles Ti [74].

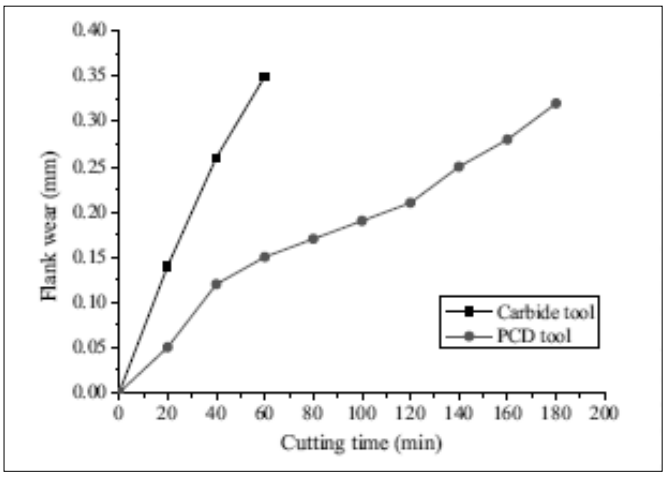

Figure 4.7. Relation curves of VB (max) with cutting time [40].

As inferred by N. Muthukrishnan et al. [75] the wear on the PCD tool take place by reason of the abrasive comportment of the SiC particles. The PCD tools are known to be harder in substances than the SiC particles, and even though the abrasive wear, may be connected to the micro mechanical it breakdown in the place of micro cutting process (Figure 4.8).

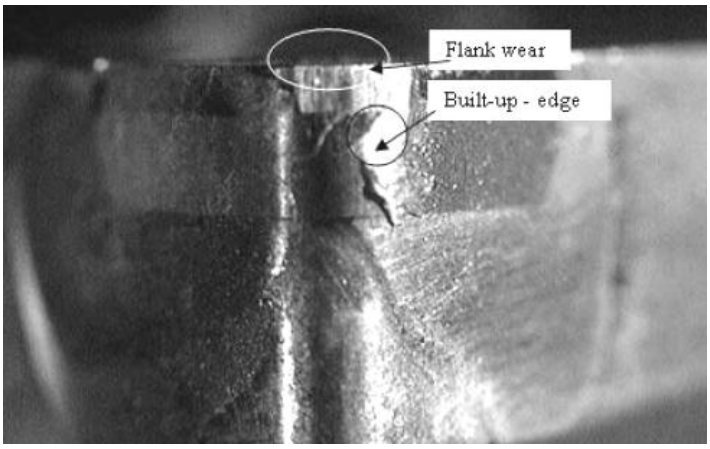

Figure 4.8. Flank wears of PCD tool [75].

According to S. Basavarajappa [76] in a research carried out on the machining investigation for Al2219/15SiC/3Gr and Al2219/15SiC through the utilization of three selection kinds of cutting insert, the uncoated carbide, the coated carbide and the PCD inserts. The flank wears for all tools, which were relatively less during the period of machining of Al2219/15SiC/3Gr. This was, by reason of the slight coating

film, which was, however, formed through and from the presence of graphite (Figure 4.9).

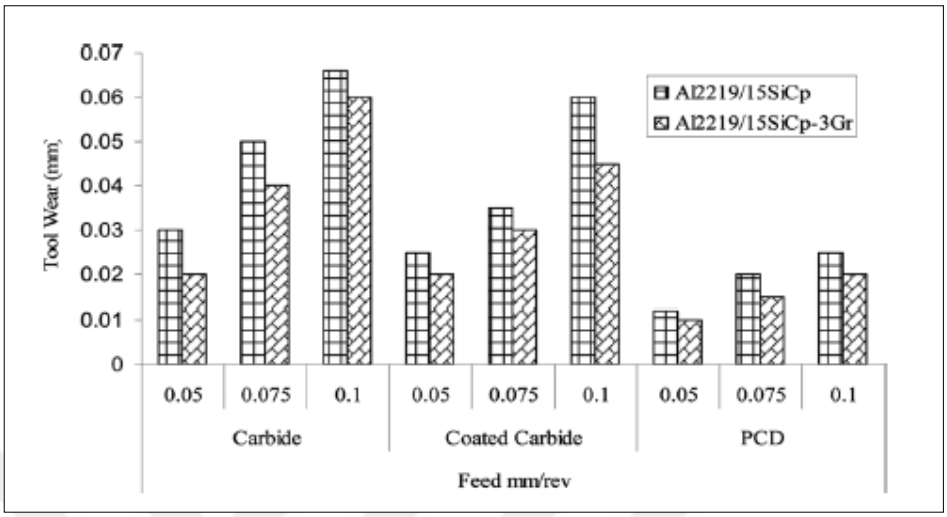

Figure 4.9. The distinctive of tool wear alongside the feed rate for the different types of tools, for a constant distance of 50mm, cutting speed of 80 m/min, and the depth of the cut of 0.3mm [76].

4.5. INFLUENCE OF MACHINING PARAMETERS

The fundamental key to maximizing the efficiency, productivity and sustainability of the MMCs machining routes is the optimization of the process parameters [9]. The optimizing of process parameters initiate sustainable and further efficient process [9,69].

4.5.1. Effect of Feed Rate

Feed rate has a profound and relevant consequence on the surface finishing, the elevated cutting speed and the low down feed rate which initiate preferable and desirable surface finish and conversely. This outcome was observed while examining of the dry machining on the Mg-MC through the utilization of tungsten coated carbide (K10) inserts type (TNMG120404), which was carried out by M. Saravanakumar et al. [70].

Furthermore, when the feed rate is increased, the cutting force becomes more too this is attributable to the detail that there is a rise in the contact locale amid the cutting edge and the composite. It has, however, been discovered that the feed rate causal effects has a relevant and an influential impact on the thrust force and surface roughness rates [71,74,77]. As inferred in [72], flank wear reduces as the feed rates raises, as illustrated in Figure 4.10. The minimal feed rate consequence to the elevated wear of the cutting edge, in addition the surface finishing of the drilled specimen's breaks down by reason of of the increments the feed rate at an unchanging rate of speed [73].

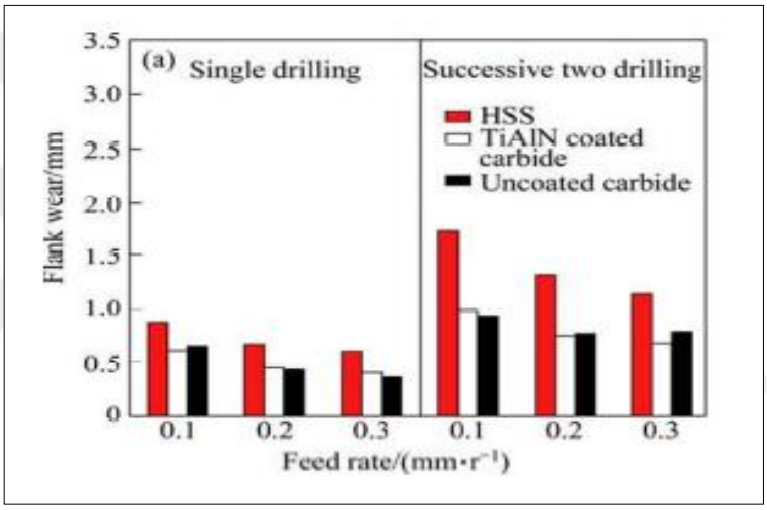

Figure 4.10. The flank wear intended for single and successive two drilling of 15% B_4C composite at 1500 rev/min [72].

The majority essential parameter affects the thrust force in the drilling of the MMCs is the feed rate. The thrust force differs by means of to the feed rate, and also with this; the burr formation, increases once the feed rate raises [10,78]. The feed rate is the fundamental that extremely influences the drilled surface finish in the drilling of MMCs [79].

4.5.2. The Effect of Cutting Speed

A finding, research has been performed to scrutinize the thrust force and the surface finish in the drilling of Al/SiC/Gr hybrid MMC by A. Muniaraj et al. [71]. Which asserted that the thrust force reduces with the rising altitude of spindle speed, and the

drilled surface roughness reduces with the increasing of the spindle speed, as presented in Figure 4.11.

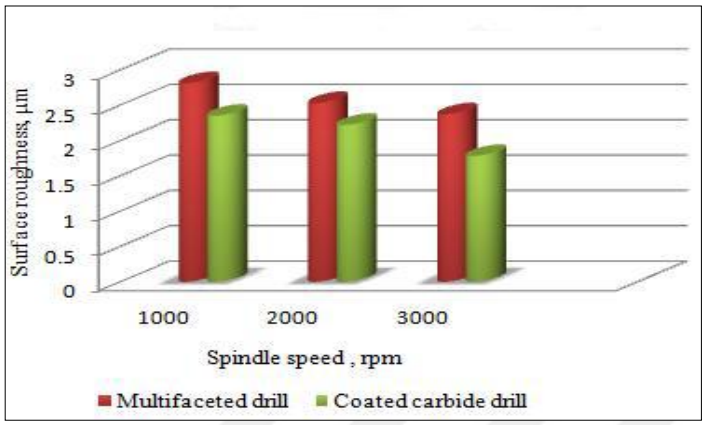

Figure 4.11. The influence of spindle speed on drilled surface roughness while utilization of coated carbide and multifaceted drills [71].

The surface roughness raise by reason of the increments of the both of the feed rate and the rotation speed, and the rotation speed had a highly relevant effect on the surface finishing [74]. As inferred to in [75], the diminution in the surface roughness and to minimization of the tool wear has the chance to be attained throughout the utilization of the elevated cutting speeds while machining of MMCs (Figure 4.12).

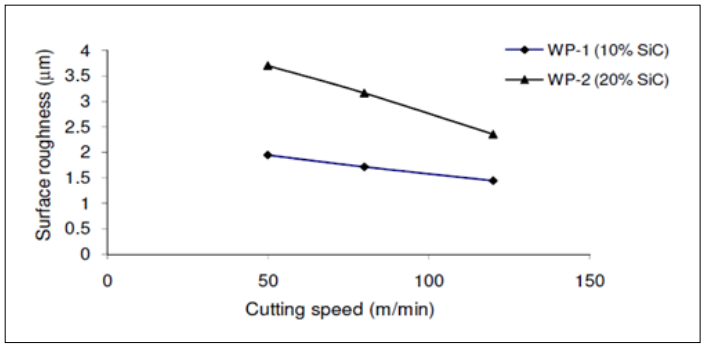

Figure 4.12. The cutting speed along vs. surface roughness at a feed rate level of 0.1 mm/rev and depth of cut 0.5 mm [75].

As inferred to [10,78] when the drilling is ongoing the thrust force reduces as the spindle speed increases, and conversely, the same reactions and occurrence happens in the lower spindle speed which provides a closely more thrust force than the higher spindle speed, as Figure 4.13 shown. In the drilling experiment which was conducted

by J. Paulo Davim et al. [6] the utilization of the PCD drills, reflects and presents clearly that at the constant cutting speed, the surface finish of the drilled surfaces reduces as the feed rate raises, but this does not change drastically during the varying the cutting speed.

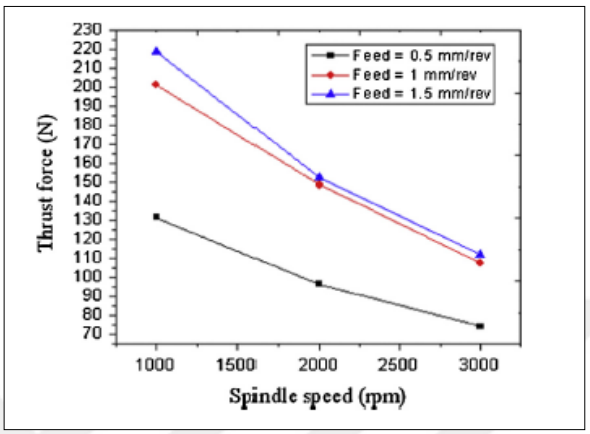

Figure 4.13. The variant of thrust force with speed at diverse feed rates [10].

Figure 4.14 illustrates the variant of the machining force versus to the cutting speed as asserted by M. Fathipour et al. [80] during the orthogonal cutting of Al/SiC composite utilizes the titanium carbide inserts. The tangential force reduces while the cutting speed rises, the causes for this reduction can be understood from the dropping of the depth of the built up edge (BUE) during the raising of the cutting speed.

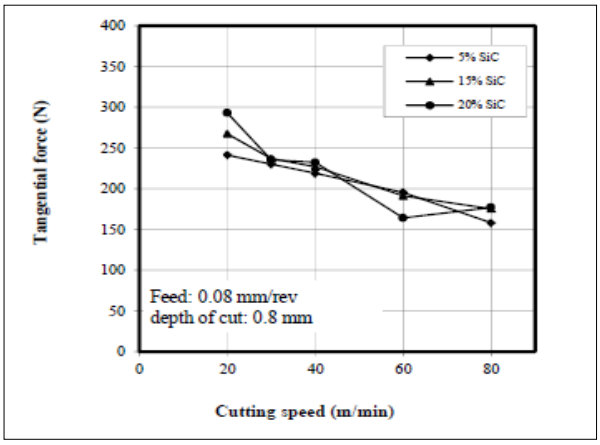

Figure 4.14. The tangential force against the speed whereas the orthogonal cutting of Al/SiC MMC [80].

4.6. INFLUENCE OF TOOL MATERIAL

The machining processes of MMCs with the abrasive reinforcement's increment the cost, the wear and the premature breakdown of the tool [81]. Hence, throughout the machining of MMCs the tool material selected is relevantly important. Figure 4.15 illustrates the placing and ranking of the tool material sorts and variety that was applied in the cutting of the MMCs that was cross-survey through the review observation that was conducted by Carl J. Nicholls et al. [9]. Figure 4.15 presents the detail that majority of the machining processes for the MMCs were carried out through the utilization of carbide or the PCD cutting tools. The CBN and PCD tools are, however, been placed in the first and in the second orders according to their relevance and importance. Which is seen and asserted to be better than the carbide tools in provisions of the wear resistance, while alternatively the carbide tools has the opportunity to be utilized cost effectively, for the roughing machining [13].

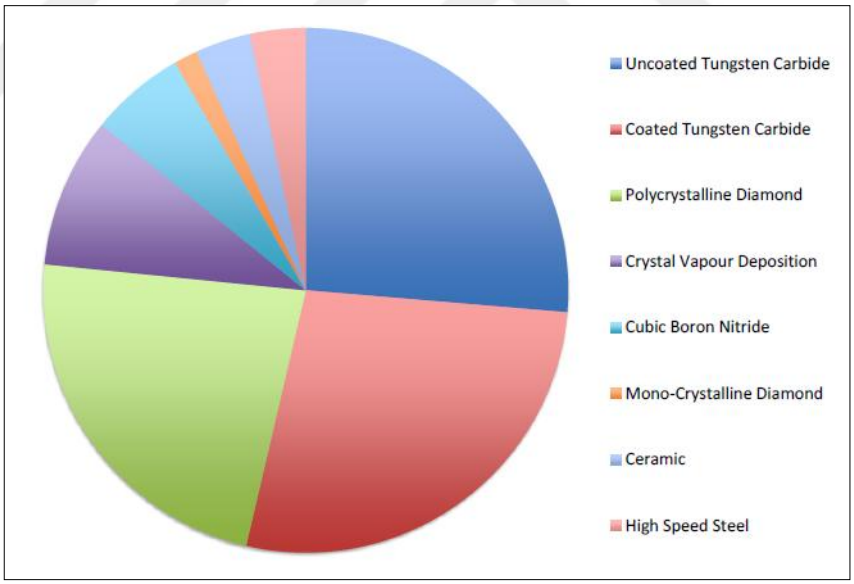

Figure 4.15. Tool materials utilization in the machining of MMCs [9].

According to W. Pedersen et al. [8] which had utilized a PVD (TiCN/TiN) coated carbide inserts to machine ZK60A-T5 Mg-MCs with 20vol. % SiC particles reinforcement, The TiN coating on the inserts was nearly worn instantly upon the start-up of the machining, The coating was totally worn out within the 20 m of the cutting range.

As inferred to in [71], in the encroachment of the surface finish, the coated carbide tool outcome was much more better than the multi-faceted carbide drill during the machining of Al/15%SiC/4%Gr. A further research carried-out by Xinliang Wei et al. [40], through the utilization of uncoated carbide and the PCD inserts for machining of AZ91D Mg alloy reinforced with carbon fiber (C_f), was suggested that the PCD tool had a way more higher wear resistance as disparate to the carbide tools. Although, the carbide tools were more suitable and desirable for cutting (C_f / Mg) composites. X. Teng et al. [74] through the utilization of AlTiN coated tungsten carbide tool for machining Mg-MCs reinforced with nano-sized Ti and TiN particles. It was asserted that the AlTiN coated carbide tool produces a relatively elevated rate and chance to the adhesive to the wok material while the cutting Mg/Ti MMC is ongoing.

As within the employment of carbide tools, the flank wear is recognized as the premier appearance, and the less for the PCD tools [76]. Figure 4.16 reveals the distinctive differentiation in the flank wear and the speed for the entire tools. The PCD tools are ,however, known to be elevated and more superior to the other tools in regards to their tool wear resistance as a result of these acknowledgements they were therefore optional for the mass manufactured and production [76].

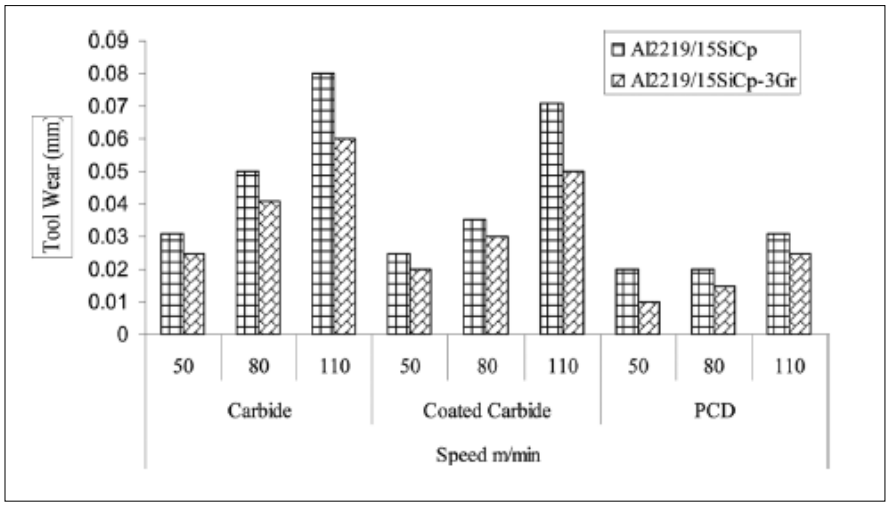

Figure 4.16. The variation of tool wear alongside the speed for the numerous cutting tools and materials for a constant distance of 50mm, the feed rate of 0.075 mm/rev, and depth of cut of 0.3mm [76].

Both the CBN and PCD tools are primary to second in the ranking categorize of level better in the wear resistance than the WC tools. Even though the WC tools could be utilized for the purpose of the roughing machining, the CBN and PCD tools are predominately utilized for the finishing machining, by the reason of that; they can limit and decrease sub-surface breakdown (damages) [82]. A research conducted by M. S. Said et al. [83] had revealed that while under the different cutting parameters, the uncoated carbide bits are exposed to less damages, and are followed by TiN coated carbide which undergoes from a second least damage and breakdown.

4.7. DELAMINATION IN DRILLING OF MMCs

The separation and division of the films of material in a shield is referred to as delamination. There are numerous reasons and a number of effects that leads to the occurrences and presence of delamination. These reasons and possessions of delamination have an effect on the tensile strength originated on the fragment of delamination. Other than the effects and influences of these numerous defects that are created by reason of drilling, delamination is referred to be the majority serious.

In a conducted research by C. C. Tsao et al. [84] illustrated via an observatory and experimental outcomes; which revealed that even if the thrust force is higher with an increment wear, it becomes that delamination will happen by reason of the actual thrust force increment with the wear to high degree. Delamination takes place as a result of many factors such as; the high thrust force and feed rate, other identified factors may incorporate the prompt tool wear [85]. Retrospectively, there have been techniques to avoid delamination, which are to drop off the feed rate, and consecutively lead to diminish the thrust force. The feed rate is recognized to be the parameter that has the prime influence on the delamination factor, the precinct of delamination raises according to the increment in the feed rate and the diminution in the spindle velocity [86].

The delamination mechanisms are categorized into sets of; push-down and peel-up classes, founded on the laminating side it happens to occur; either through the drilling exit point or the entrance point, interchangeably. The peel-up category

occurs by reason of the cutting force that pushes the abraded which later cuts the materials to the flute surface. To begin with, the cutting edge of the drill abrades the lamination. While the drill moves further, it pulls the abraded material along the flute surface area, and the material spirals up right before it is effectively cut. This process leads to a peeling force that is upwards and has the possibility to detach the upper laminas of the plate, as illustrated in Figure 4.17 (a).

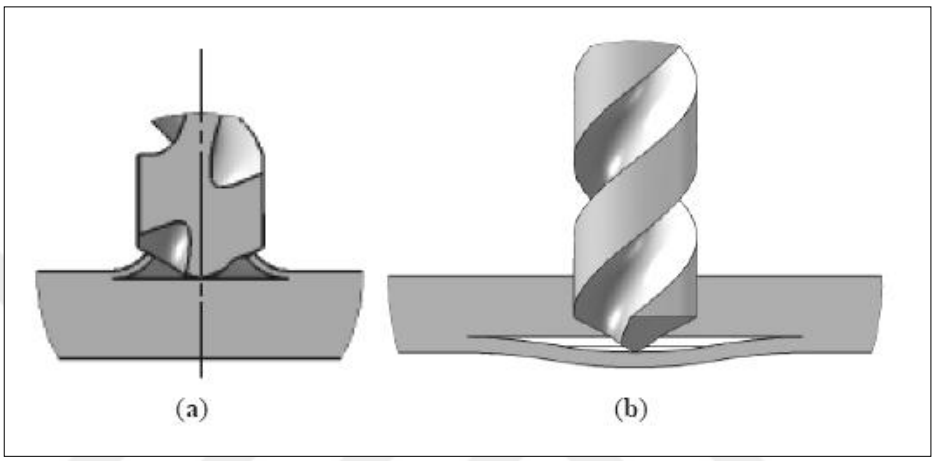

Figure 4.17. (a) Peel-up delamination sort at the entrance of the drill, (b) Push-down delamination sort at the exit of the drill [87].

While the push-down category is the outcome, end-result and aftermath of the compressive thrust force which reveals why the chisel edge of the drill clearly exerts on the workpiece. The laminate throughout the drilling creates the opportunity to be moved afar from the upper plies, thereby breaking the inter-laminar bond in the region surrounding the hole. While the drill is in motion towards the last part of the laminate, it reduces the volume of the uncut depth and the resistance to the deformation reduces. It is noticed that; the loading process exceeds the inter-laminar bond strength and therefore, delamination occurs (Figure 4.17 (b)).

4.8. LITERATURE REVIEW SUMMARY

Currently, there is an increasingly interesting concern and focus on MMCs. This growing interest is prompt appropriate an intellectual phenomenon in the broad field of science. Which is now reinforcing and reexamining nano particles like; nano SiC, CNT and GNPs. There is as well a rising attention in the findings and investigations on the hybrid composites, the composing of varied matrix and (or) the reinforcement of materials. In the broad field of the machining of Mg as derived from the MMCs, the available literature reports are found to be limited. Nevertheless, the difficulties of machining magnesium-based composites are, however, close on that of aluminum-based composites while been compared.

The machining of the MMCs is noticeably distinct on various levels and scales of rating like; from the machining of monolithic metals. It is reported that while the machining of MMCs, is undergoing a process their behavior is not homogeneous and anisotropic, and thus it relies on the various reinforcement and matrix properties, and the content of reinforcement and the metal matrices. Therefore, the mechanical characteristics transforms according to and in the uniformity of the reinforcement format and the allocation in the metal matrix which indicates the chip formation mode which are; (the shearing mode, the plowing mode and the cracking mode) and thereafter it influences and impacts the machinability of MMCs. The abrasion is the prime wear mechanism; and adhesions to be slightly observed. It is, however, essential to reminder that; delamination occurs based on a numeral of reasons and as a response to a number of effects. It could either be affected by the tensile strength outcome as influenced by the locale of delamination. The feed rate is the parameter that has the prime assertive influence on the delamination factor.

CHAPTER 5

EXPERIMENTAL WORK

5.1. INTRODUCTION

The functionality of the machining characteristics of the graphene-reinforced Mg based hybrid nanocomposite that has not completely recognized and acknowledged yet. Researchers have eventually conducted observations, studies and examinations on the microstructure and mechanical characteristics of these novel materials.

This research aims to machining of these materials through an investigation study of; their microstructure, the influence and impact of process parameters, the cutting forces, the machined surface integrity, the delamination, the cutting tool failure and the wear mechanisms, in order to realize a clear comprehension of the processing mechanism and to eliminate of the effects.

Derived from the open literature reported, only limited researches dealt with the drilling of Mg-MCs. The two categories of the Mg-MCs were produced: the Mg/0.25w.t%GNPs MMC and The hybrid Mg/10wt.%SiC/0.25wt.%GNPs MMC throughout the appliance of the powder metallurgy procedure. The specimens dimensions were within: the diameter of (ϕ=25 mm) and the thickness of (h=10mm). The observatory research findings of the drilling characteristics of the two categories of the Mg-MCs are enlisted below:

1. The microstructure of the fabricated composite materials.
2. The cutting thrust force and the torque.
3. The surface roughness of the drilled sub-surface.
4. The delamination formation mechanism and its measurements.

5. The tools wear mechanism.
6. The morphology of the drilled surfaces.
7. The chip formation and morphology.

5.2. HYBRID MAGNESIUM MATRIX COMPOSIRES SYNTHESIS

5.2.1. Magnesium (Mg)

Mg is a favorably, desired lightweight structural metal. Mg alloys are classified as; 33%, 61% and 77% measured as lighter than the aluminum, the titanium and the stainless steels accordingly [15]. This explains why they are have attained a desirable attention and prospective attraction as an alternative or a substitute material for the other metals. Besides the earth crust elements, Mg is acknowledged to be the sixth abundant element, with having around 2.1% of earth crust weight [15,16].

Mg and its alloys are utilized and applied technically, in the various sectors of the applications in the aerospace industry, the automobile industry, the chemical and communication industries by reason of their low down density of 1.738 g/cm³ [18,19,65]. In addition to, their low mechanical strength, low elastic modulus, low ductility and poor wear resistance that technically slows down the limit of their applications. Hence, in order to attain and achieve the required and demanded properties, the composites of the various other kinds of the reinforcements are needed and required [66].

Mg-MCs provide several benefits that are much than the monolithic Mg or its alloys that could be found in; their elevated strength, their lofty elastic modulus, their excellent creep characteristics, and their outstanding wear resistance that is at the elevated altitude of temperatures [14-16]. The most wanted properties acquired from the thoughtful process of choosing their size and their sort of the reinforcement particles used.

5.2.2. Graphene Nano-platelets (GNPs)

Since from the time it was found in 2004 [88], the graphene has increasingly created an attention both academically and concerning the technical application of its industrial purposes by reason of its unique properties. Graphene, is an individual atomic layer made-up of (sp2-hybridized carbon), which has gained a remarkably successful attention and attraction because of its awesome and excellent electrical, thermal and mechanical characteristics. The modulus of elasticity and intrinsic fracture strength of monolayer graphene are 1TPa and 125GPa respectively [16]. GNPs are acknowledged to be the stack of the multi-layer graphene sheets that form the platelet morphology. With the addition of GNPs as reinforcement to the metal matrix, it results to the increment of thermal conductivity, raise in the electrical conductivity, advances the barrier properties, decreases the component mass while the advancement of the properties, the increment in its stiffness and the increment in its toughness (impact strength) [89].

5.2.3. Silicon Carbide (SiC)

The SiC is noted to have been unintentionally discovered in the year 1890 by Edward G. Acheson [90]. Silicon carbide is a favorably desired material for demanding mechanical and high temperature applications, in addition to its utilization in abrasive and corrosive media [91]. The application and utilization of SiC as the reinforcement in the MMCs is continuously been on a high increase through the last years as a result of their profoundly and outstanding properties like; their light weight, their high strength, their high specific modulus, their high fatigue strength, their high hardness and their low density. Among these numerous ceramic reinforcements, SiC is the prime regularly known by reason of its relatively high wettability and its identified stability in the Mg melts process [92].

5.2.4. Powder Metallurgy Technique

Powder metallurgy can be understood and referred to as; the forming and fabricating method that is made-up through three main processing stages. The primary stage

which is; the primary materials are physically powdered, by mean of separated into fine particles. Then, in the next stage the powders mixture is injected into a mold or pushed through a die to fabricate and achieve a weakly cohesive structure (through the cold welding) closely to the dimensions of the product specifically to be produced. Conclusively, the final stage is formed through the appliance of pressure, high temperature, long setting times right when the self-welding happens.

5.2.4.1. Characteristics of Metal Powders

The outcome of the functions of the metal powders while the process of the powder metallurgy rely upon the characteristics of the metal powders that are utilized.

The following enlisted details and specifications are the vital characteristics of the metal powders.

1. The profile of the particle: The particle shape deeply relies on the method and technique of powder manufacture. The shape is recognized to be; nodular, irregular, angular, and dendrite. The shape of the particle influences and creates an impact on the flow characteristics of the powders. Specially shaped particles have perfect sintering properties. Moreover, the irregularly shaped particles are perfect at green strength because they have to capability to interlock on computing.
2. The size of the particle: The size of the particle influences and creates an impact on the control of the porosities and the compressibility. The size of the particle is ascertained through the passing of the powder through the standard sieves or by applying the microscopic measurements.
3. The size of the particle distribution: This is detailed in the specification and in term of a sieve analysis, the amount and volume of powder passing through specific ranges from mess sieves. The size of the particle distribution affects the stuffing of powder and its performance and behavior throughout the moulding and sintering operations.
4. The flowing rate: It is in the aptitude of the powder to flow instantly and frequently as it confirms to the mould cavity. It predicts the rate of production.

5. The compressibility function: This refers to the volume of the prime powder to the volume of the compacted piece. The compressibility relies on the particle size, its distribution and its shape.
6. The apparent degree of density: This particularly relies on the particle size and it is referred to as the percentage of the volume to the weight of the loosely filled mixture.
7. The purity degree: The powders must to be without charge of impurities that work to diminish in the life of dies and it affects the sintering procedure. The oxides and the gaseous infection could be cleared from the piece while sintering through the application of the controllably reduced atmosphere.

5.2.4.2. Advantages of Powder Metallurgy Procedure

1. Besides the fact that the price of making powder is high there is technically no loss of material. The components created are cleaned and all set for employ.
2. the most significant benefits of this process are the control and management of the composition of the product.
3. Products could be fabricated through the execellent surface finishing and the close up a tolerance.
4. The production rates are high.
5. The complexity profiles could be fabricated.
6. A broad variety of the properties like density, porosity and particle size can be achieved through some particular functions.
7. There are usually no requirements for the subsequent machining or finishing processes.
8. This process helps to guide the mixing of both metallic and non-metallic powders in order to provide the products with particular characteristics.
9. The porous parts can be fabricated that, however, could not be achieved through other means or techniques.
10. The impossibilities of the parts (cutting tool bits) can be fabricated.
11. The sophisticatedly- qualified or skilled-labor are neither required nor necessary.

5.2.4.3. Limitation of Powder Metallurgy Procedure

1. The metal powders and the equipment applied and utilized are highly priced.
2. The storage of the powders leads to high challenges and uneasiness by reason of the hazard of the fire and the explosion.
3. The parts fabricated through this technique have poor ductility.
4. The sintering of the low down melting point powders such as; the lead, the zinc, the tin etc., these can, however, create some very profound challenges and uneasiness.

5.3. SYNTHESIS PROCESS OF Mg-MMCs THROUGH POWDER METALLURGY METHOD

The Mg/0.25wt.%GNPs and the hybrid Mg/10wt.%SiC/0.25wt.%GNPs were formulated throughout the employment of the powder metallurgy route. According to the literature, the fraction volume of the SiC particles utilizing into Mg-MMCs as reinforcement is restricted around 10 Vol.%. The major reason is that it is very hard to mix more SiC particles into the matrix metal homogeneously.

The matrix material was utilized for the fabrication of the composites that is the Mg powder with 99.7% of purity with an average particles size of 100 μm. GNPs and SiC particles were applied and utilized as the reinforcements. With the GNPs obtaining, achieving and consisting of an average thickness of 5–8 nm and the surface area was about 750 m^2/g. The SiC particles of 99.7% purity with particles average size of 40 μm. The Mg powder and the two reinforcement (GNPs and SiC) were therefore supplied by the Nanografi Co. Ltd.

Two categories of Mg-MCs are produced through the employment of the powder metallurgy technique (Figure 5.1): the Mg/0.25wt%GNPs and the hybrid Mg/10wt%SiC/0.25wt%GNPs MMCs. The specimen's dimensions were 25 mm in diameter with a thickness of 10 mm.

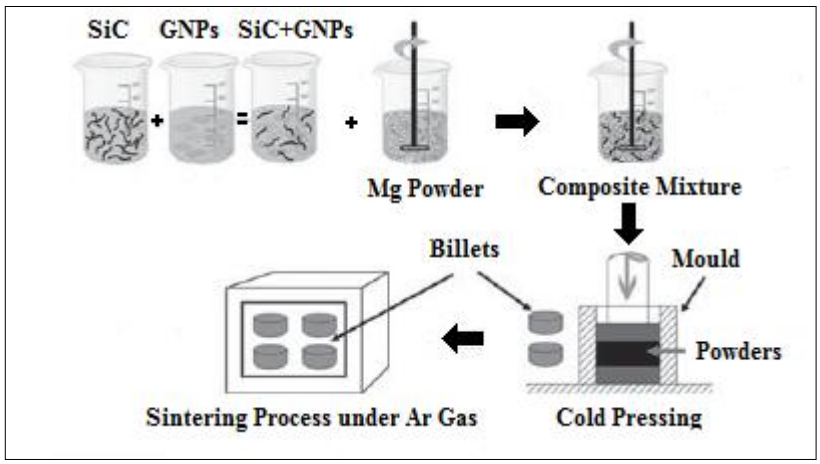

Figure 5.1. The sketch diagram of powder metallurgy process {adapted from [22]}.

The composites were fabricated through the utilization of the powder metallurgy technique through the three main stages, the blending process, the compacting process and the sintering process:

1. The blending of powders stage: In this stage, the weights of Mg and the reinforcement powders were calculatedly measured in accordance with their molecular weight, then the mechanical alloying for the powders were utilized for two hours with mechanical alloying mixer speed of 250 rpm. The mechanical alloying device was used is presents in Figure 5.2. After the mixing and the blending of the powders, an excellent homogeneous combined-mixture ought to have been accomplished.

Figure 5.2. A mechanical alloying device used.

2. The cold compacting stage: The cylindrical stainless steel mold of 25 mm internal diameter was utilized for this process. The powders compressed at a room temperature through the application of a hydraulic press machine with applied pressure of 500 MPa, as publicized in Figure 5.3. In this stage, the green compact specimens were produced.

Figure 5.3. The hydraulic press machine used during the fabrication of the Mg-MC.

3. The sintering process stage: The green compact specimens were then sintered through the usage of a Protherm atmosphere controlled sintering furnace (Figure 5.4). The sintering route was applied in two cycles. In the key cycle, the green compact specimens were heated for 1.5 hours at a temperature level of 550 Cº under a controlled atmosphere of high purity Argon gas to avoid and prevent the oxidation by reason of the low oxidation resistance of the Mg.

Figure 5.4. The Protherm atmosphere controlled sintering furnace.

Whereas in the second cycle, the specimens were permitted to cool-down inside the sintering furnace in order to attain an accurate room temperature level. At the end of the production procedure, the specimens were ready for the next classification and observation for the characterization and examination.

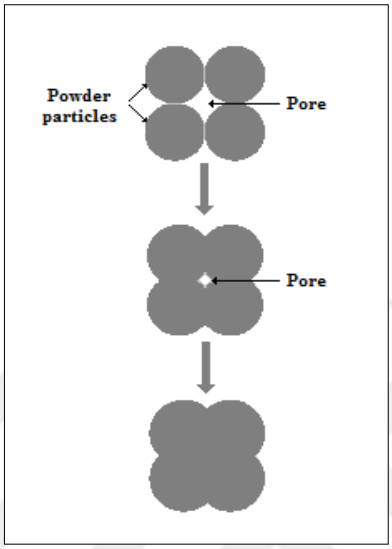

Figure 5.5. The composite particles under sintering process.

5.4. EXPERIMENTAL DESIGN AND DRILLING CONDITIONS

In accordance with the focus and aim of this research, a systematic drilling experimental work was carried out to further investigate the drilling of the Mg-MCs characteristics. The material system examined in this research was the Mg-MCs that were reinforced with the nano-sized of GNPs and the micro-sized of SiC particles. The microstructure, the thrust forces, the torque, the drilled surface morphology, the surface roughness and ultimately delamination were all categorized with an aim to understand a better comprehension of the machinability in the drilling of the two categories of the Mg-MMCs: the Mg/0.25wt.%GNPs and the hybrid Mg/10wt.%SiC/0.25wt.%GNPs, that were fabricated through the powder metallurgy route.

The Taguchi's method is identified to be a very powerful tool in the parameter design, which was applied for the conducting of the experiments. The L27 (3^3) orthogonal array with 27 rows (which matched the number of experiments) accordingly was utilized for the experiments for each composite material. It provided

a simple, effective and systematic approach to the optimization of the design for the better functionality, quality and cost. Three levels of cutting speed, the feed rate and the carbide drill bits types were utilized in the observatory experiments, are illustrated in Table 5.1.

Table 5.1. Taguchi orthogonal array design.

Exp.#	Drill bit type	Cutting speed (m/min)	Feed rate (mm/rev)
1	D_1	V_1	f_1
2	D_1	V_1	f_2
3	D_1	V_1	f_3
4	D_1	V_2	f_1
5	D_1	V_2	f_2
6	D_1	V_2	f_3
7	D_1	V_3	f_1
8	D_1	V_3	f_2
9	D_1	V_3	f_3
10	D_2	V_1	f_1
11	D_2	V_1	f_2
12	D_2	V_1	f_3
13	D_2	V_2	f_1
14	D_2	V_2	f_2
15	D_2	V_2	f_3
16	D_2	V_3	f_1
17	D_2	V_3	f_2
18	D_2	V_3	f_3
19	D_3	V_1	f_1
20	D_3	V_1	f_2
21	D_3	V_1	f_3
22	D_3	V_2	f_1
23	D_3	V_2	f_2
24	D_3	V_2	f_3
25	D_3	V_3	f_1
26	D_3	V_3	f_2
27	D_3	V_3	f_3

5.4.1. Cutting Conditions (Parameters)

Based on the literature papers cross-examined, the range and variety of cutting speed and the feed rate that were all utilized by most of the researchers were (30 to 50 m/min) and (0.05 to 0.30 mm/rev) accordingly as presented in Table 5.2. Table 5.3 lists the cutting parameters were employed in this observatory experimental study.

Table 5.2. Cutting parameters and levels were utilized in the experimental work.

Level	Cutting Speed levels	Feed rate levels	Drill material levels
1	v_1=30 m/min	f_1=0.10 mm/rev	Uncoated carbide
2	v_2=40 m/min	f_2=0.15 mm/rev	PVD (TiN) coated carbide
3	v_3=50 m/min	f_3=0.20 mm/rev	CVD (AlTiN) coated carbide

5.5. SPECIMEN AND HOLE NUMBERING SYSTEM

The two types of workpieces were fabricated and utilized: the Mg/GNPs and the hybrid Mg/SiC/GNPs. The choosing of the workpieces sizes were based on the internal diameter of the available functional stainless steel mold that was utilized in the cold compacting route for the fabrication of the composites workpieces. The thickness choices were inspired and directed by the demands to achieve the full engagement of the cutting lips in the drilling process. Hence, all the workpieces were produced to the following dimensions: with the diameter of 25 mm and the thickness of 10 mm, as revealed in Figures 5.6 and 5.7.

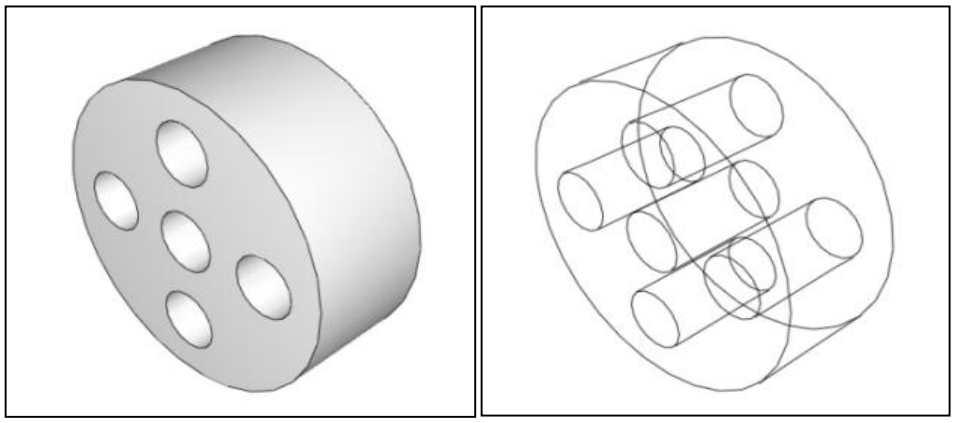

Figure 5.6. Work-piece material specimen.

Table 5.3. Based on the literature papers cross-examined.

REF.#	DATE	AUTHORS	MATERIAL	CUTTING PARAMETERS	TOOL MATERIAL	INVESTIGATION
5	2016	Avinash A. Thakre et al.	Al6061/SiCp	Vc=40,60,80 m/min f=0.10,0.25,0.20 mm/rev D=10 mm	Solid carbide	Chip formation Surface morphology Burr formation
6	2001	J. Paulo Davim et al.	A356/20SiCp	Vc=30,40,50 m/min f=0.05,0.10,0.15,0.20 mm/rev D=15 mm	PCD	Tool wear Surface finish
8	2006	W. Pedersen et al.	ZK60A-T5/SiCp	Vc=420, 532,700 rpm f= 0.112,0.157,0.203 mm/rev	PVD coated carbide (TiCN/TiN)	Tool wear Cutting forces Surface roughness
10	2014	K. Palanikumar et.al.	Al6061/15SiCp/4Gr	Vc=1000,2000,3000 rpm f=0.05,010,0.15 mm/rev D=4,8,12 mm	Uncoated carbide TiN coated carbide	Cutting forces Surface roughness Burr formation
12	2012	T. Rajmohan et al.	Al356/SiCp/mica	Vc=1000,2000,3000 rpm f=50,100,150 mm/min D=6 mm	Uncoated carbide TiN coated carbide PCD	Cutting forces Surface morphology
26	2013	Ahmet Taskeen et al.	Al-5Zn-3.5Cu-2.5Mg/B_4Cp	Vc= 1500,2000,2500 rpm f=0.10,0.20,0.30 mm/rev D=8 mm	HSS Uncoated carbide TiAlN coated carbide	Thrust force Chip formation
35	2017	Ergun Ekici et al.	Al/10B_4Cp/5Gr	Vc=1,25,35 m/min f=0.08,0.112,0.16 mm/rev D=5 mm	Uncoated carbide K10	Thrust force Burr formation Surface roughness
36	2017	G. S. Samy et al.	Al/10B_4Cp	Vc=2200,2500,2800rpm f=0.10,0.20,0.30 mm/rev D=8mm	TiN coated carbide	Cutting forces Surface morphology Temperature

To be continued

REF.#	DATE	AUTHORS	MATERIAL	CUTTING PARAMETERS	TOOL MATERIAL	INVESTIGATION
39	2012	Yahya Altunpak et al.	Al[LM2]/20SiCp/10Gr	Vc=3500,4000,4500rpm f=0.10,0.13,0.16 mm/rev D=5 mm	Coated DLC drill	Thrust force Surface roughness
41	2010	A.Riaz et.al.	Al/5SiCp/5B_4Cp	Vc=180,315,630 rpm f=0.125,0.20,0.315 mm/rev D=5 mm	HSS	Tool wear Surface morphology
71	2013	A.Muniaaraj et.al	Al6061/SiCp/Gr	Vc=1000,2000,3000 rpm f=0.05,0.10,0.15 mm/rev D=4 mm	TiN coated carbide	Cutting forces Chip formation Surface roughness
72	2013	A.Taskesen et al.	Al/B_4Cp	Vc= 1500,2000,2500 rpm f=0.10,0.20,0.30 mm/rev D=8 mm	HSS Uncoated carbide TiAlN coated carbide	Tool wear Dimensional accuracy
73	2001	J. P. Davim	A356/20SiCp	Vc=30,40,50 m/min f=0.05,0.10,0.15,0.20 mm/rev D=5 mm	PCD	Thrust force Tool wear Surface roughness
77	2015	M. Ay et al.	Al/SiCp/Gr	Vc=3500,4000,4500rpm f=0.10,0.13,0.16 mm/rev D=5 mm	Coated DLC drill	Cutting parameters optimization
78	2014	Vikas K. Doomar et al.	Al1100/SiCp	Vc=900,1800,2700rpm f=0.12,0.18,0.30 mm/rev D=8 mm	HSS	Cutting forces
83	2016	M. S. Said et.al.	AlSi/10AlN	Vc=1000,1500,2000rpm f=50,100,150 mm/min D=6 mm	Uncoated carbide TiN coated carbide TiCN coated carbide	Optimal cutting parameters Tool wear

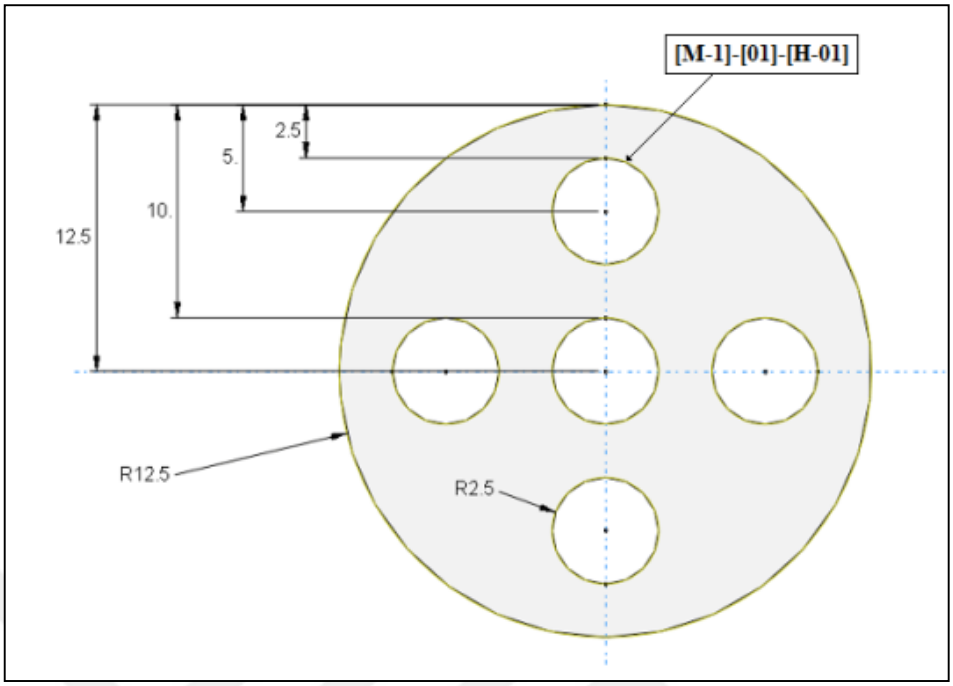

Figure 5.7. The hole configuration on the specimen and hole numbering system (all dimensions in mm).

The specimen and the hole numbering system as presented in figure 5.8.

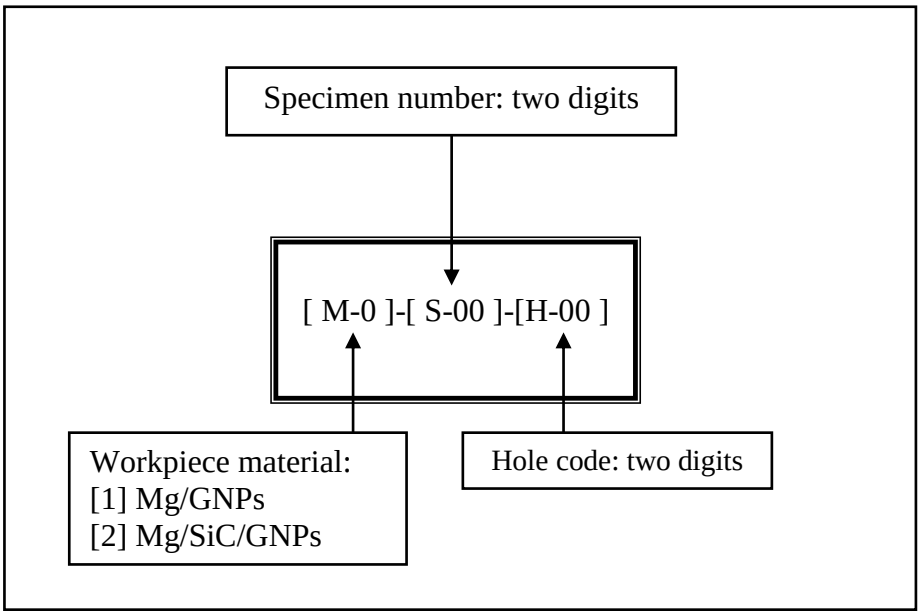

Figure 5.8. The specimen and the hole numbering system.

5.6. CUTTING TOOLS (DRILL BITS)

There were, however, no proceedings found of the drilling bits designed particularly for the drilling purpose of the hybrid Mg-MC, in an attempt of searching for what was hoped to have been performed on the hybrid Mg-MC. It therefore found a Chinese company (The Blue-rock Precision Tools CO., LTD) that providing high quality coated drill bits for metallic alloys. There was a two-facet twist drill, which tended to be the right technical fit and quite suitable for the drilling of the light metals and the MMCs materials. The standard twist drills were then employed in the experimental studies on the drilling of the MMCs materials published in the literature (i.e. [5, 6, 10, 12, 26, 27, 28, 35-38, 41, 49, 71, 73, 78, 84, 87] etc). The carbide drill bits details and specifications that were produced by the (Changzhou Blue-rock Precision Tools CO., LTD) enlisted below:

5.6.1. The Uncoated Carbide Drill Bits

Table 5.4 lists the mainly important features and specifications of the uncoated drill bits, and Figure 5.9 shows the image of the drill tool used in the tests.

Table 5.4. The features and the specifications of the uncoated drill bits.

Code	Flute diameter D (mm)	Flute length (mm)	Shank diameter SD (mm)	Overall length L (mm)
DNGCUS-C06M0500	5.0	22	6.0	60

Drill bit material	Coating material	Coating thickness (µm)	Hardness (HRC)	Point angle (º)	Helix angle (º)
Tungsten carbide	-	-	92	135	28

Figure 5.9. The uncoated drill bit used in the tests.

5.6.2. PVD-Coated Carbide Drill Bits

Table 5.5 lists the mainly important features and specifications of the PVD-coated drill bits, and Figure 5.10 shows the image of the drill tool used in the experiments.

Table 5.5. The features and the specifications of the PVD-coated drill bits.

Code	Flute diameter D (mm)	Flute length (mm)	Shank diameter SD (mm)	Overall length L (mm)
DNGCUS-C06M0500/PVD	5.0	22	6.0	60

Drill bit material	Coating material	Coating thickness (µm)	Hardness (HRC)	Point angle (º)	Helix angle (º)
Tungsten carbide	TiN	3.0	92.5	135	28

Figure 5.10. The PVD-coated drill bit used in the tests.

5.6.3. CVD-Coated Carbide Drill Bits

Table 5.6 lists the mainly important features and specifications of the CVD-coated drill bits, and Figure 5.11 shows the image of the drill tool used in the tests.

Table 5.6. The features and the specifications of the CVD-coated drill bits.

Code	Flute diameter D (mm)	Flute length (mm)	Shank diameter SD (mm)	Overall length L (mm)
DNGCUS-C06M0500/CVD	5.0	22	6.0	60

Drill bit material	Coating material	Coating thickness (µm)	Hardness (HRC)	Point angle (º)	Helix angle (º)
Tungsten carbide	AlTiN	5.0	92.5	135	28

Figure 5.11. The CVD-coated drill bit used in the tests.

5.7. THRUST FORCE AND TORQUE MEASUREMENT

The drilling experiments were carried-out and function through the computer numerical control (CNC) vertical machining center type (JOHNFORD VMC-550) specifically with the absence of the utilization of coolant (under dry conditions). Table 5.7 has a listed detail of the technical specifications of the machining center utilized for the investigation work.

Table 5.7. The CNC vertical machining center technical specifications.

Y axis	500	mm
X axis	550	mm
Z axis	450	Mm
Power	7.5	kW
Max rotation speed	6000	rev/min
Precision	0.001	mm
Control system	Fanuc	

The thrust force and torque were, however, captured through the utilization of the computer controlled data acquisition system.

The dynamometer employed was the piezo-electric type KISTLER 9272-A. the dynamometer was coupled to the multi-channel charge amplifier type KISTLER 5070-A 4. First, signals were captured and sent from the dynamometer to the data

reading card (type KISTLER PCIM DAS 1602/16) and thereafter to the KISTLER 5070-A multi-channel amplifier, via the (1677-A5), (1500-B15), and (RS232) data cables, and at the end, the captured signals preserved and processed with KISTLER Dynoware 2825D-02 software.

The Figure 5.12 illustrates the images of both dynamometer and multi-channel amplifier, which were utilized throughout the entire drilling process of the experiments, and the Figure in 5.13 reveals and illustrates the experiment and the applied set-up for the measuring of the thrust and the torque.

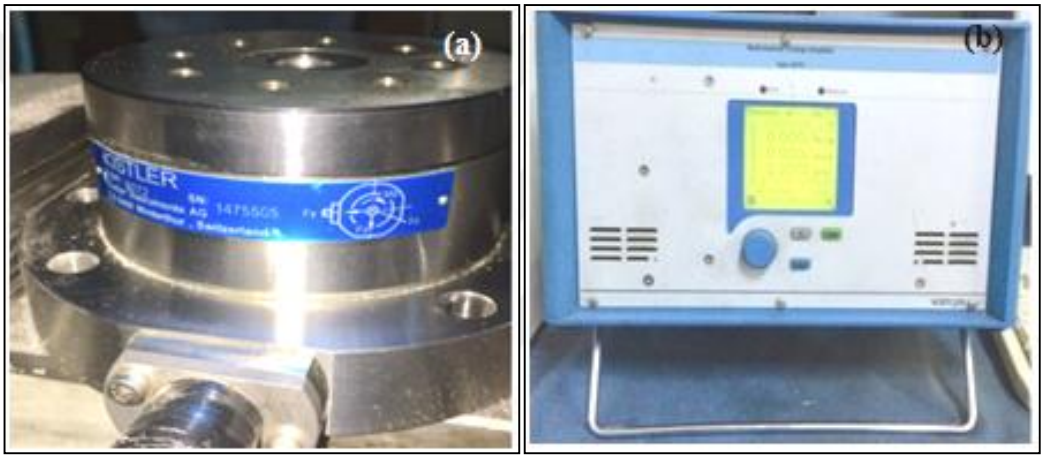

Figure 5.12. (a) The KISTLER 9272-A dynamometer, and (b) The KISTLER 5070-A multi-channel amplifier.

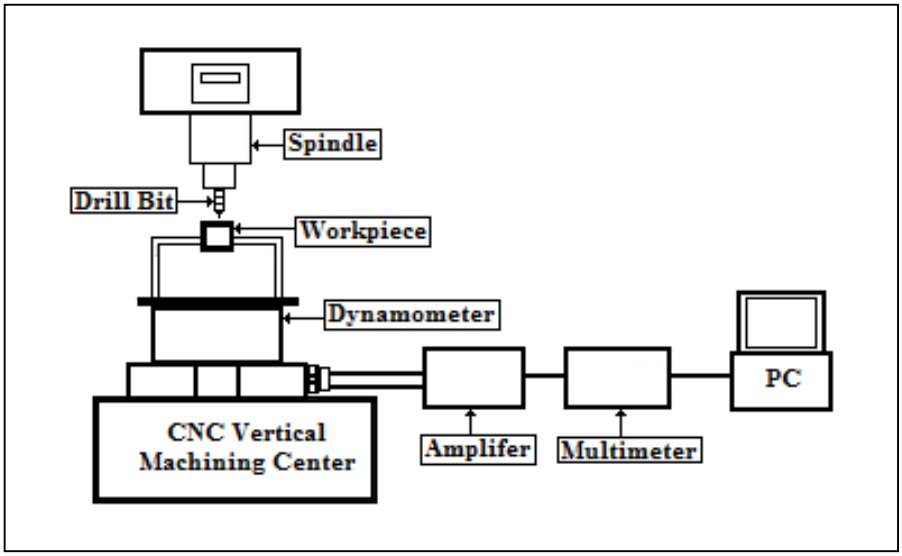

Figure 5.13. Schematic of experiment set-up for measuring thrust and torque.

The usual thrust force and torque practical in the drilling of the MMCs were revealed in the Figure 5.14, where the hole making process dealt with six different stages. The first stage revealed the initial drill entry into the MMC material, where the thrust force and torque examined was the minimal values.

In the second stage, the cutting edge entered the workpiece and the drilling procedure starts, which showed the increased thrust force and torque. In the third stage, the drill passed through into the workpiece material and the drilling procedure was carried out. The fourth stage illustrated the drilling phase; the tool cutting edge had a full contact with the workpiece the thrust force and torque with the utmost maximum values. The fifth stage presented the exit of the tool, which revealed the sharp drop in thrust force and torque. Right at the end of the stages was the observation of the thrust force as it dropped to the zero. The mean thrust force values were, however, calculatedly measured at the full engagement phase of the drill bit and the MMC material interface, as illustrated in Figure 5.14.

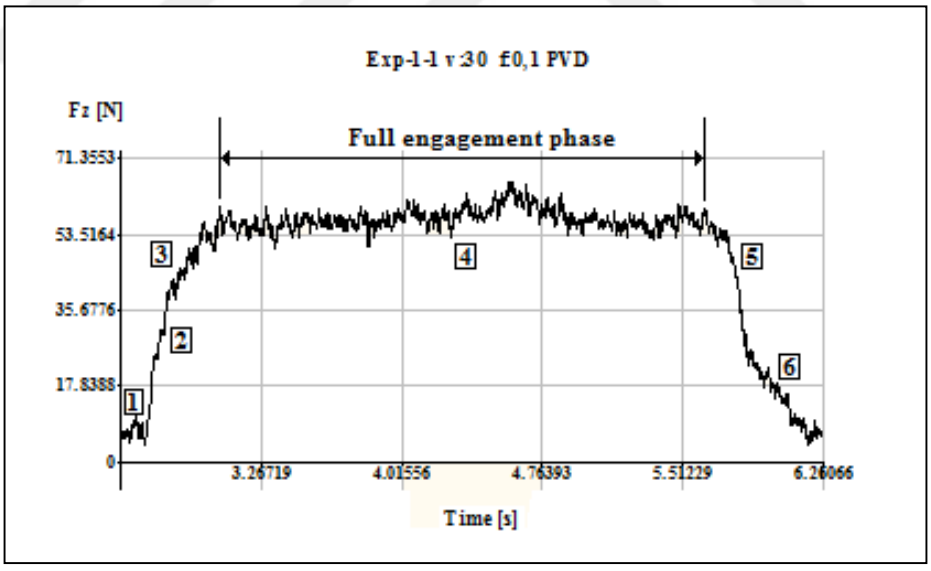

Figure 5.14. Machining thrust force vs. cutting time for an experimental run.

5.8. HARDNESS AND SURFACE ROUGHNESS MEASUREMENT

The Qness hardness instrument (type Q10A+) was utilized to measure the Vickers hardness (HV), as obtained in Figure 5.15. Vickers hardness (HV) was measured

under a test load of 500 gf within the time interval of 15 seconds alongside the surface of the test specimen. For each test specimen, three measurements were made with an interval of about 3 mm with an intention to avoid and prevent the effects by the neighboring indentations, and then the average of the hardness measurements is taken into the contemplation.

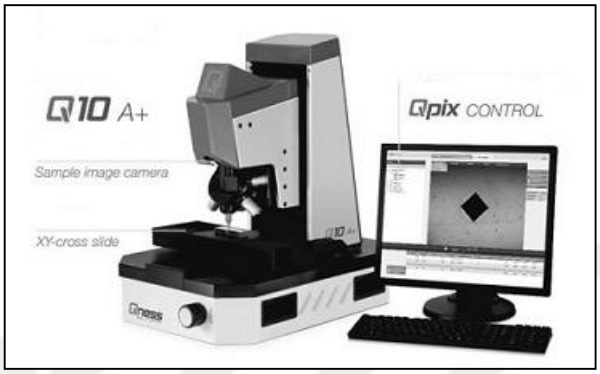

Figure 5.15. The Qness hardness instrument (type Q10A+) was employed to measure the Vickers hardness (HV).

The surface roughness (R_a) was therefore, calculatedly measured with a Mitutoyo SJ-410 surface instrument with a cut-off distance of 4.8 mm and speed of 0.5 mm/s. Surface roughness which was utilized to categorize and classify the surface quality. The R_a was thereafter measured in parallel to each hole axis from three different positions, and the average value of the R_a measurements were then examined, assessed and then accepted and considered in the analysis. The schematic arrangement of the observatory experimental setup is presented precisely in Figure 5.16.

Figure 5.16. The schematic arrangement of R_a measurements.

5.9. DELAMINATION MEASUREMENT

The delamination is acknowledged to be one of the prime forms of failure in the drilled materials by reason of the composite's lack of strength in the direction of drilling. This sort of failure has lead to diminish in the compressive load with a carried capability of the structure.

While, several of the vital causes for the happening of the delamination in the first place were the high thrust force and feed rate, while reasons specifically included the rapid tool wear. With some previous methods that avoided the delamination formation were able to diminish the feed rate and, which sequentially lead to reduce in the thrust force.

Once later than the drilling process, the delaminated sector around each drilled hole is examined through the utilization of the Nikon zoom stereomicroscope (type SMZ 745T) with the Clemex vision lite software (version 7.0.369 (11281)) as presented and revealed in the figures in 5.17. With every captured image it computationally processed the identify and the classification of the zones of the interest: hole zone, delaminated and then the non-delaminated regions, as revealed in Figure 5.18.

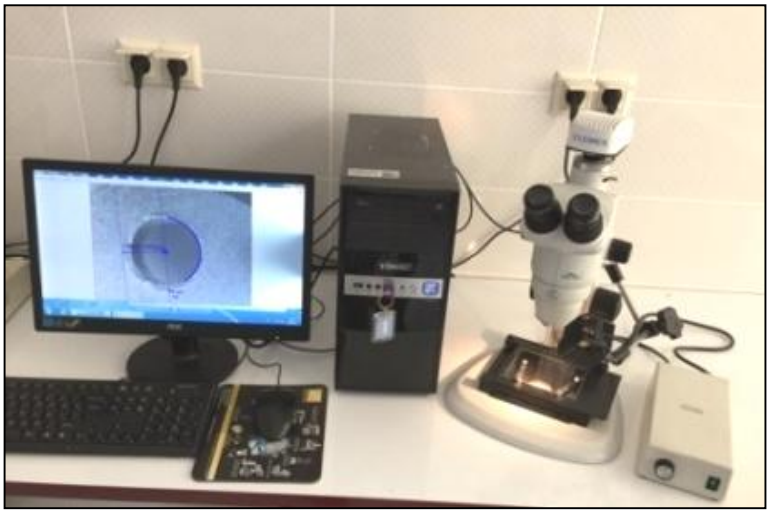

Figure 5.17. The Schematic arrangement for delamination measurements.

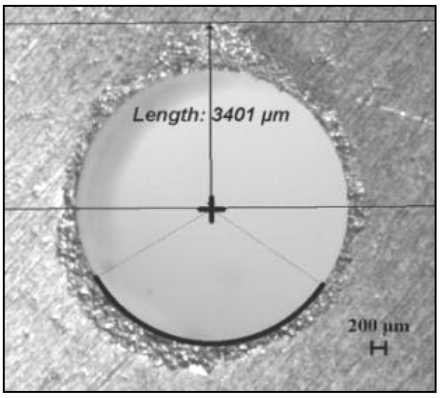

Figure 5.18. The captured image for the delaminated zone around the drilled hole.

Although, it is possible to perform the quantification of the damaged zone to measure the factor that numerically expressed the damaged zone extension. Wen Chou Chen [93] revealed a comparing factor that empowered the examination and the analysis of the delimitation's capacity in the laminated composites. That ratio was referred to as the delamination factor (F_d), and it was, therefore precisely labeled and referred to as the quotient amid the maximum delaminated diameter, D_{max}; and the hole nominal diameter, D_o as equation 5.1 revealed, and the Figure 5.19 illustrates the measurement of the maximum delaminated and nominal hole diameters:

$$f_d = \frac{D_{max}}{D_o} \tag{5.1}$$

The Wen Chou Chen methodology revealed in [93] was applied to calculate the delamination factor in this thesis study.

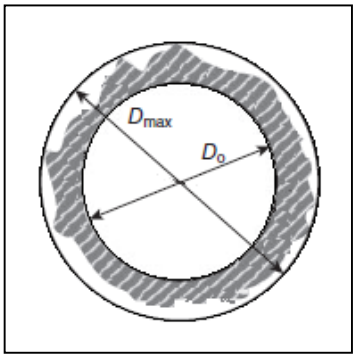

Figure 5.19. The measurement of the maximum delaminated and nominal hole diameters.

After taking the measurements of the holes delamination, selected holes based on the optimization procedure were cut, with the purpose of conduct the SEM examination for the delaminated areas.

CVD (Chemical Vapor Deposition) and PVD (Physical Vapor Deposition) are procedures that utilization to form an extremely thin layer of coating over the tool surfaces. The major difference between CVD and PVD is the procedure that employed. During PVD coating, pure sources substances are gasified through evaporation and then condense on the tool surfaces to form the wanted coating layer. However, during CVD coating, the source substance is not pure; it is a mixture with an unstable ancestor. The mixture then will be injected in a chamber that holds the tool. While the mixture is adhered to the tool surfaces, the ancestor finally decomposes and forms the wanted coating layer. The surfaces development of PVD and CVD coatings comprise surprising and higher hardness, low friction, high corrosion protection, high heat transfer, and high thermal resistance.

CHAPTER 6

RESULTS AND DISCUSSION

6.1. INTRODUCTION

Technically the thrust force while the drilling could be recognized as "the force acting alongside the center line of the drill throughout the machining process". In the drilling the thrust cutting forces assist to screen the tool wear, hence the forces usually raise with the tool wear progressing. The thrust force is also utilized to professionally monitor the wearable tools and, in turn, it is utilized as the means to monitor of the tools life.

Besides this, the thrust force is highly regarded, and recognized to be the core and fundamental contributor of the delamination that is extremely noticeable during the drilling procedure. Through the assertions of most greatly considerable researches that have been conducted to prove, and provide facts that there is a "critical thrust force" that results to the delamination, and thrust force below, which comes the constrains or the elimination of the delamination through drilling process.

M. Fernandes and C. Cook [94] furthermore divided of the drilling procedure into five major stages:

stage (1) the entrance process,
stage (2) the drilling process,
stage (3) the drilling and reaming process,
stage (4) the reaming, and
stage (5) the backing out process.

The force and torque graph for their experiments is revealed in Figure 6.1.

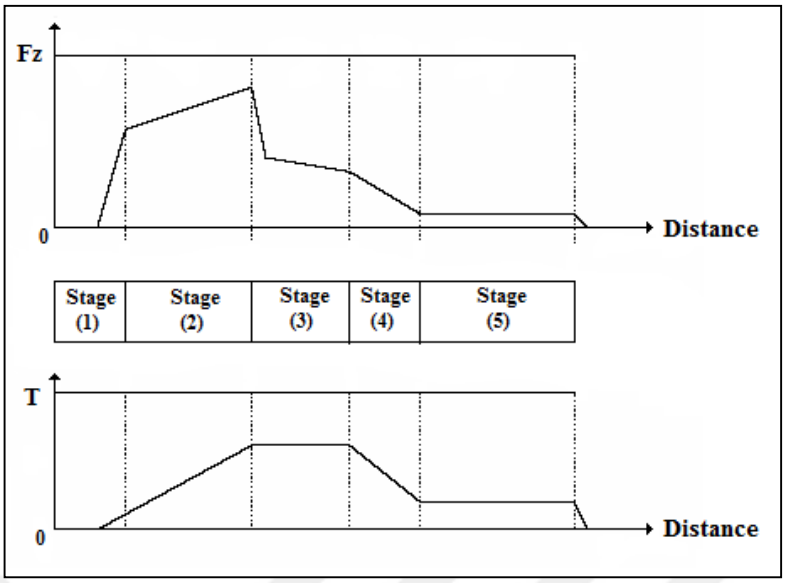

Figure 6.1. Thrust force and torque plots for the five stages {adapted from [94]}.

During stage (1), this is where; the drill bit meets and encounters the specimen and a quick raise in the thrust force can be observed, whereas a slow increase and rise is clearly observed for the torque generated. A usual problem during this Stage (1) that the drill bit could be sliding. Other problem that can, somehow, occur is the wandering problem or the deflection of the drill bit. These problems might have an effect on the hole size and positioning.

During stage (2), this is where; the removal of material takes place. The graph shows a steady enhance in the thrust force, while a hasty raise in the torque can be clearly observed. The delamination and tool wear are general problems related with this stage. The delamination is supposed to occur by reason of the existence of elevated thrust force in this stage.

During stage (3), as generated from and presented on figure; the drill bit outlets the work-piece after takes away the material. The graph illustrates that the thrust force reduces until the tool exits the material. A minor raise in torque is observed. This is due to that the tool is in touch with the maximum surface region during this moment. A set of more peculiar problems related with this stage had surfaced which finish at the exit and at the occurrence of delamination at the exit. The hazard of delamination

happening is greatly more smaller when compared to the earlier stages because the thrust force is much smaller when compared to the drilling stage.

During the stage (4), this is when the drill bit reams the hole to its finishing dimension. The problem related with this stage is the final size and the finishing of the hole. A stable turn down in the thrust force and torque values was observed.

During stage (5), this is where the drill bit backs out from the work-piece. Reaming goes on as extended as the contact among the work-piece and the drill tool. This, however, influences the dimension and the finishing of the hole. The values of torque and thrust force stay as the same of which in the previous stage.

The only dissimilarity among this stage and the previous stage is the track of the movement of the drill bit. The problems connected with this stage are the same as the ones connected with the previous stage.

As illustrated and shown in Figure 6.2, it reveals a typical thrust force and torque signals for the drilling experiment of hybrid Mg/SiC/GNPs composite while using PVD-coated drills at V_C=30 m/min and f=0.10 mm/rev.

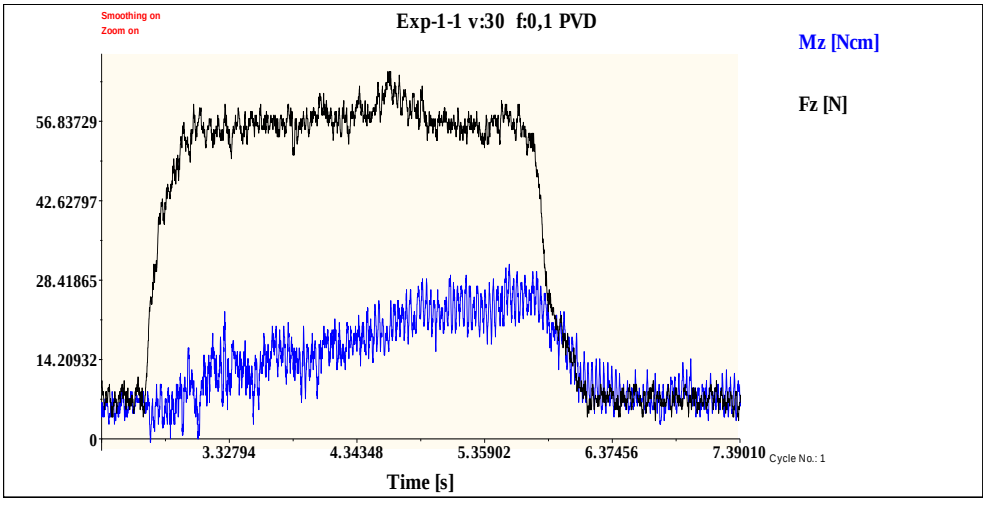

Figure 6.2. Typical thrust force and torque signals observation at V_C=30 m/min and f=0.10 mm/rev while drilling of hybrid Mg/SiC/GNPs MC.

As accountable at the drilling-process of MMCs the height (peaks) and troughs in the thrust force are come out which are linked with the contacts between the tool edge and the reinforcements particles [43].

Figure 6.3 illustrates the conditions of interface amid the tool edge and the reinforcement particles: (a) the diminution in the cutting force that is there by reason of the particle fracture and the debonding, (b) the ever-changing rise in the cutting force, which is also there by reason of the particle depress without the crack beginning, (c) the fracture in the particle results a hasty drop in the cutting force, and (d) The drop in the cutting force which is by reason of the particle fracture and the crack expansion in the matrix material.

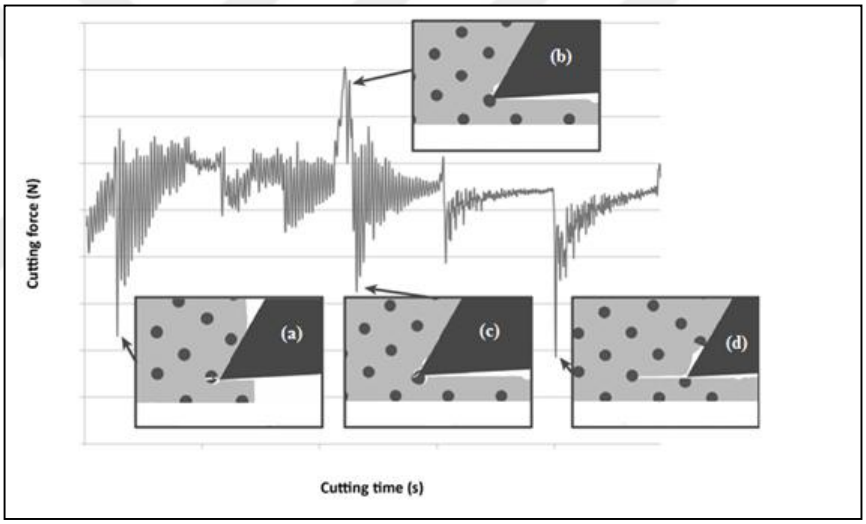

Figure 6.3. Cutting forces variation during machining of MMCs materials [43].

6.2. HARDNESS RESULTS

The aftermaths, results from the hardness test show that hybrid Mg/SiC/GNPs composite has a much higher hardness as contrasted to the Mg/GNPs composite and pure Mg. This is allied to the fact that the atomic bonding between SiC particles and the Mg matrix which is strong. Figure 6.4 illustrates the resulted Vickers hardness (HV) values.

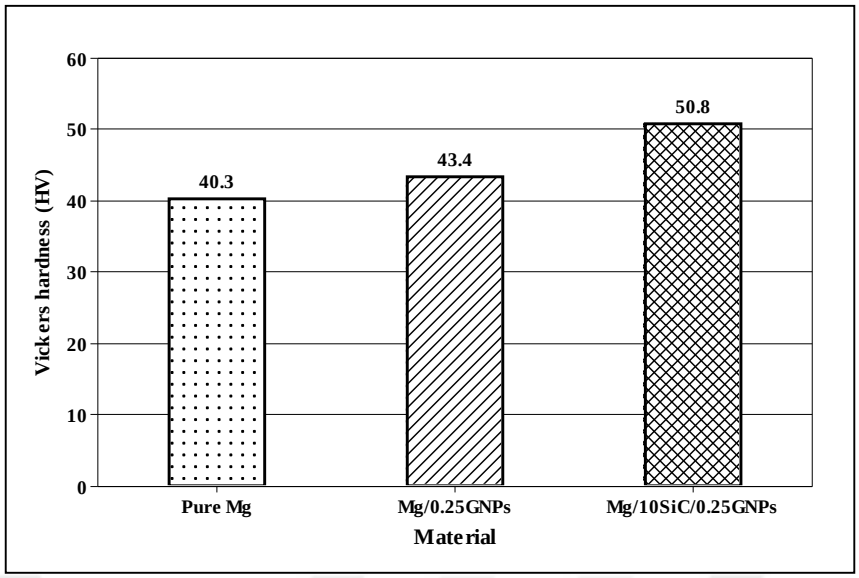

Figure 6.4. Vickers hardness (HV) measured values of the composites and pure Mg.

6.3. MICROSTRUCTURAL CHARACTERIZATION

The SEM was utilized for the investigation procedure of the surface morphology of the two categories of the composites that were fabricated: Mg/GNPs and hybrid Mg/10wt%SiC/0.25wt%GNPs Mg-MMCs. As revealed in Figure 6.5 its explanations illustrate the SEM images of the Mg/GNPs MC, which it is clear sufficient to assert that the GNPs distributed homogenously around the Mg particles boundaries. There also, exists a major significant bonding amid the GNPs and the Mg particles.

Figure 6.5 (a) reveals an amount of micro-pores and very clear grain boundaries on its surface. Although the incidence of GNPs nanoparticles into the Mg matrix are hardly to categorize by reason of the extremely few volume of GNPs nanoparticles (0.25wt%). However, the technical presence of the GNPs nanoparticles into the Mg matrix that was certain with X-ray mapping as pointed up in Figure 6.5 (c), which proves that the GNPs are homogeneously embedded into the Mg matrix.

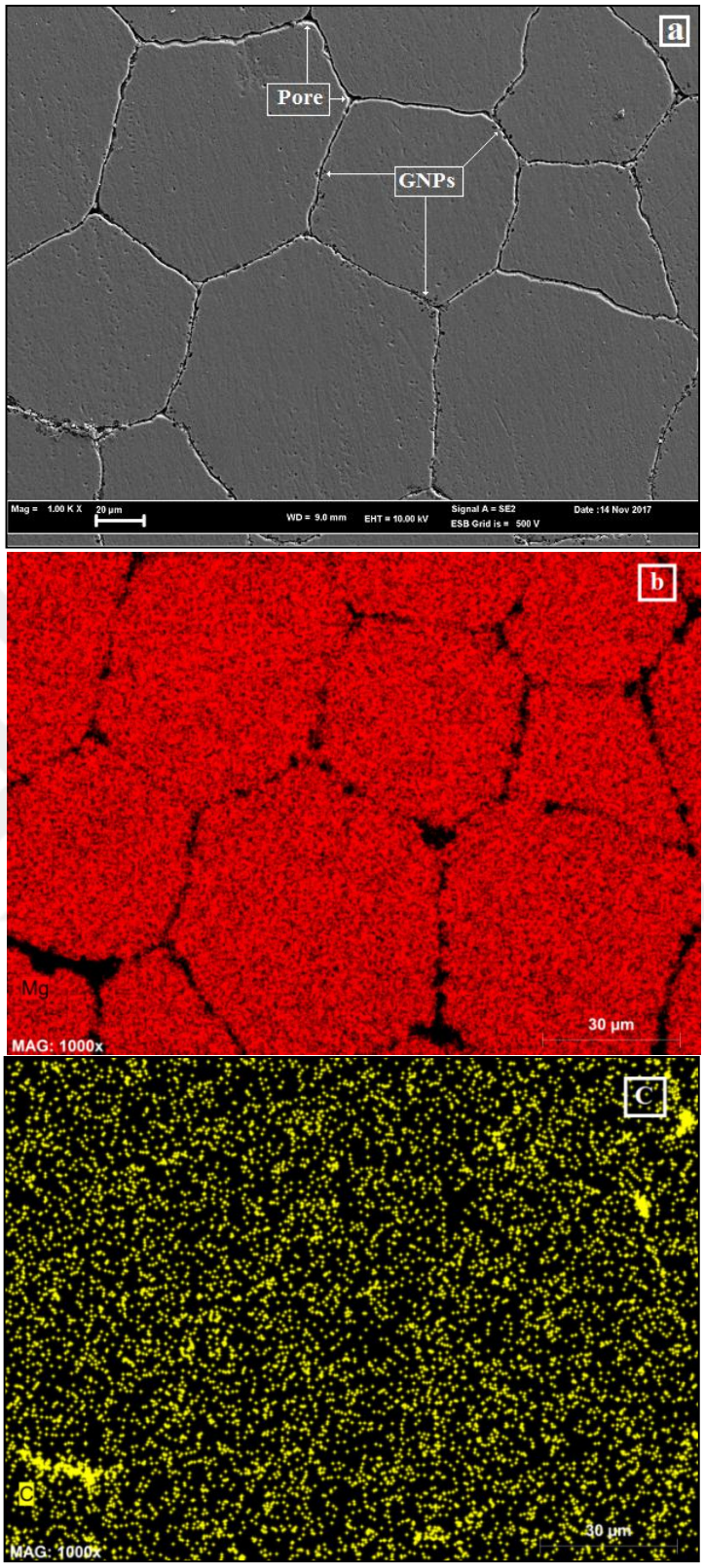

Figure 6.5. (a) The SEM image for Mg/0.25wt%GNPs MC, (b) X-ray mapping of the Mg matrix, and (c) X-ray mapping of the allocation of carbon (GNPs).

The SEM was employed furthermore in order to explore the surface morphology of the hybrid Mg/SiC/GNPs MMC. Figure 6.6 (a-d) shows the SEM images of the hybrid MMC. The allocation of the reinforcement (GNPs and SiC) into the Mg matrix is also provided in the figure. The homogeneous allocation of the SiC particles technically misses the end-results and outcomes from the excellent wettability of SiC into the molten Mg [20,51,52,57]. The reinforcement particles are positioned mostly all along the matrix grain boundaries.

The Figures reveal that the microstructure is entirely free of macro-structural defects, like the macro-porosities and the cracks. However, there were partial oxidations in the matrix material since the low corrosion resistance of the Mg based composites. The images show that existence significant bond between the (GNPs, SiC) and the Mg matrix particles.

A precise assessment of the SEM image is been publicized in Figure 6.6 (b), which shows that a medium and fine SiC particles be situated. In addition, the SEM image in Figure 6.6 (d) illustrates the uniform allocation of carbon (GNPs) in the matrix with miniature clusters. Furthermore, as derived from Figure 6.6 (d), it can be clearly observed that the SiC particles are likely to situate around the GNPs clusters.

The explanation in Figure 6.7 (a) reveals the SEM surface image of Mg/SiC/GNPs hybrid MMC with chosen locale for EDS (Energy Dispersive Spectroscopy) peaks as shown in Figures 6.7 (b–d). The Carbon peak in the EDS confident the existence of a carbonaceous composition in the Mg/SiC/GNPs hybrid MMC, while the little peak of oxygen revealed the small altitude of oxidation all the way through the sintering procedure. The locale 1 has extra carbon content than other locales since of the existence of both the SiC and the GNPs.

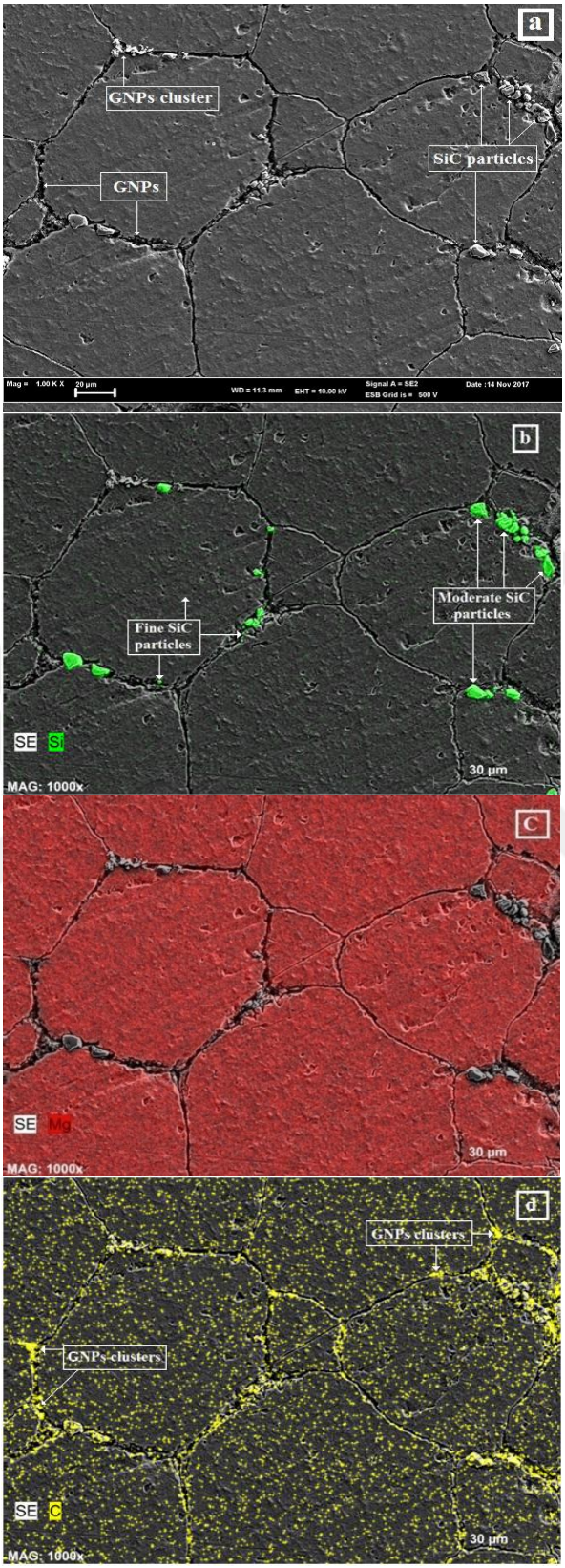

Figure 6.6. (a) The SEM image of hybrid Mg/SiC/GNPs MC, (b) X-ray mapping of SiC particles, (c) X-ray mapping of Mg matrix, and (d) X-ray mapping of the distribution of carbon (GNPs).

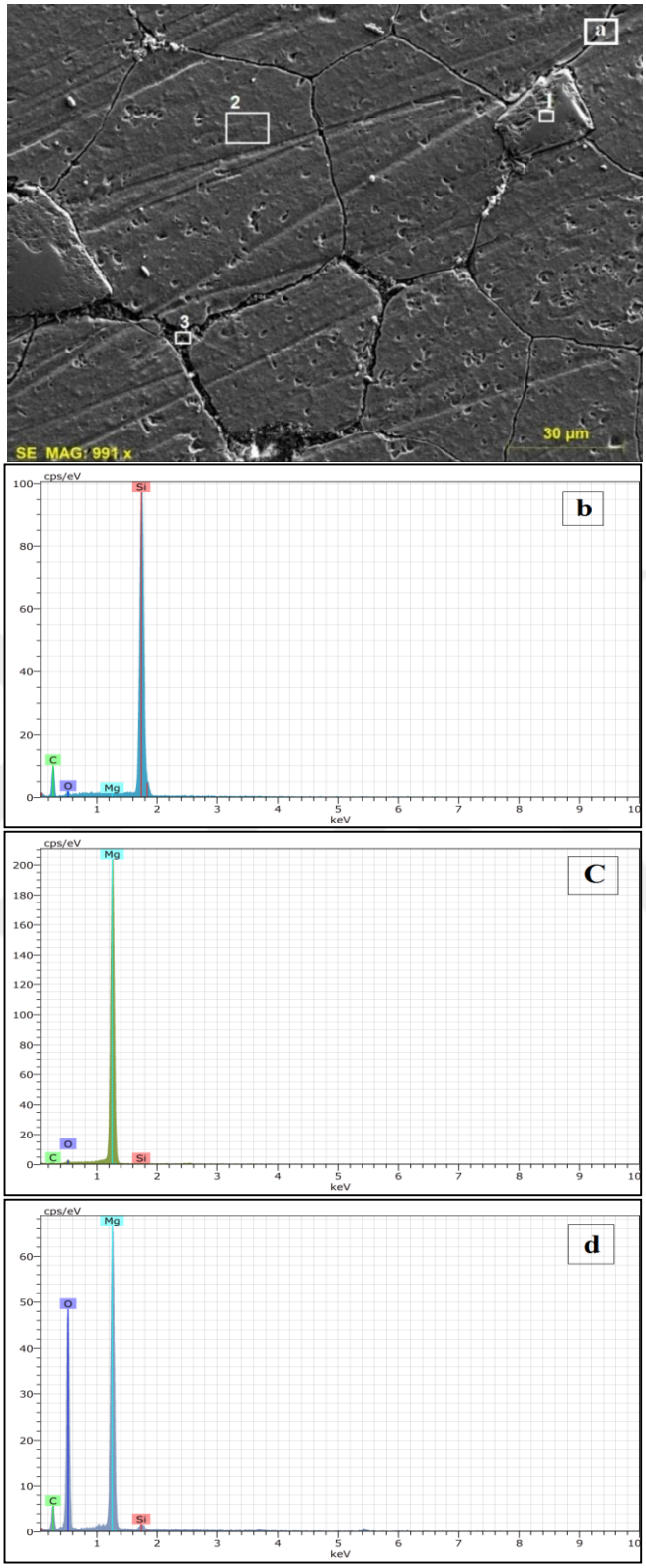

Figure 6.7. (a) Surface SEM image of hybrid Mg/10wt%SiC/0.25wt%GNPs MC, (b) EDS peaks for the selected locale number 1, (c) EDS peaks for the selected locale number 2, and (d) EDS peaks for the selected locale number 3.

6.4. THRUST FORCE AND TORQUE RESULTS

Thrust force mean values in (*N*) and the mean torque values in (*N.cm*) which were captured during the drilling with the one shot drill for each individual hole which were been considered for the complete engagement stage of drill bit cutting edge and the MMC material interfacial through the utilization of KISTLER Dynoware (2825D-02) software.

6.4.1. Thrust Force and Torque While Drilling of Mg/GNPs MC

6.4.1.1. Thrust Force and Torque Measured Values While Drilling of Mg/GNPs MC

Through the cutting force which are principally dependant and reliant on the matrix and reinforcement's elements structure, interface and properties. As Figures 6.8 (a-c) illustrate the variant of the thrust force along with the feed rates at the different cutting speeds levels for the Mg/GNPs MMC while utilizing the uncoated, PVD- and CVD-coated drill bits. The figures are illustrated that the thrust force is extremely reliant on the feed rate, the cutting speed, and the category of drill bit. Purposely, the figures are been revealed in a way that the thrust force are vastly reliant on the feed rate and cutting speed levels [10,26,27,39]. The experimental outcome in the figures illustrated that the thrust force was increased through the increment of the feed rate, which by the way, while the thrust force decreases with the increment of the cutting speed for the sorts of the drill bit types that are used.

These outcomes was highly linked to the reality that elevate of the heat on the cutting locale softened the Mg matrix and ultimately lead to an easier plastic deformation; it is recognized to have weakened the bond among the GNPs and the matrix [41]. Nearly all the tests illustrated that the thrust forces were low down while drilling of Mg/GNPs MC. This conclusion can be linked to the fact that; the GNPs lessened the friction on the interface of tool cutting edge-composite and as well among the tool cutting edge and chips which were shaped as a outcome to its natural solid lubricant assets [10,39].

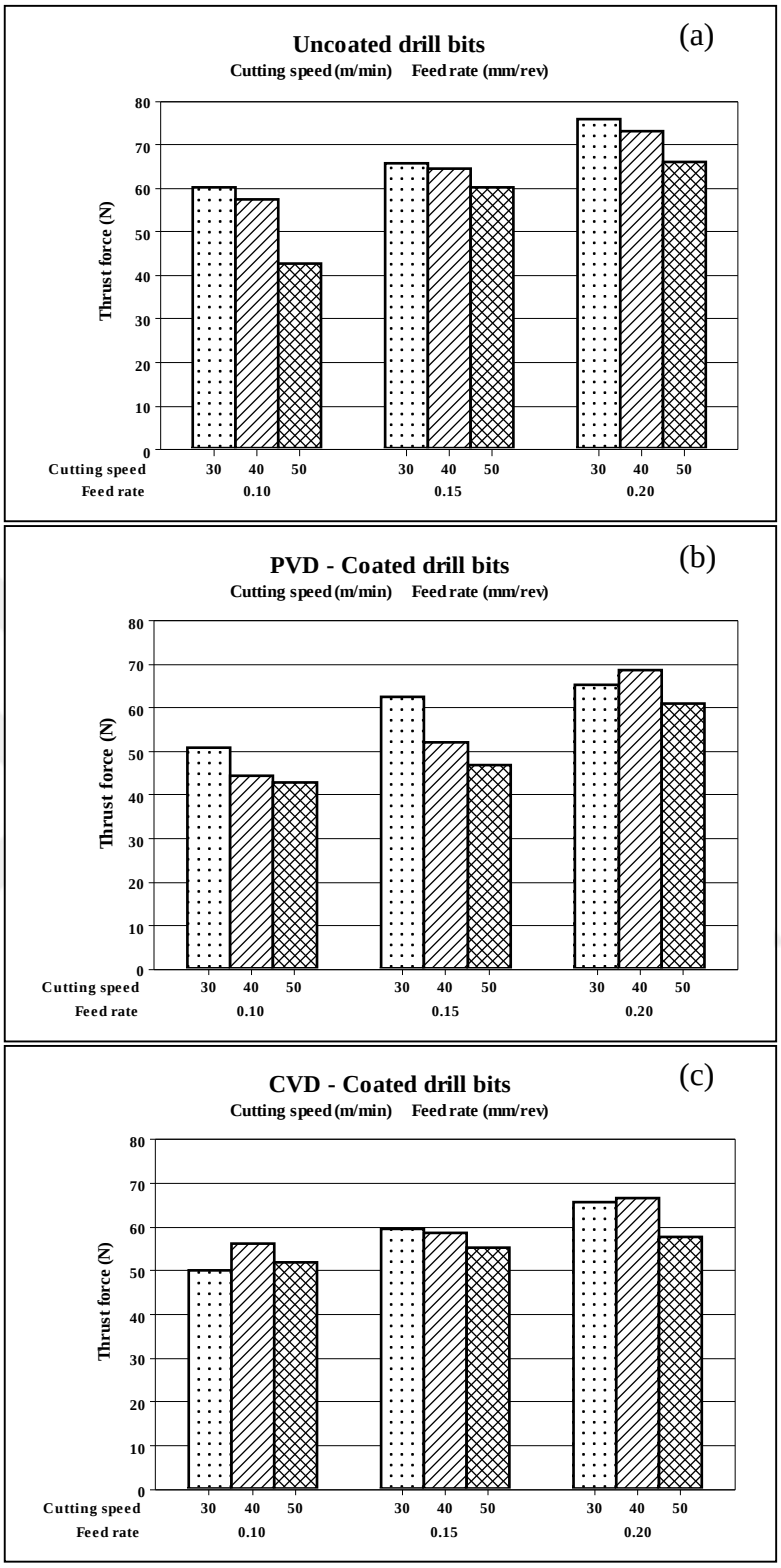

Figure 6.8. Thrust force vs. feed rate at different cutting speeds while using: (a) uncoated, (b) PVD-coated and (c) CVD-coated drill bits, while the drilling of Mg/GNPs MC.

Noticeably, the feed rate has constantly been the predominant factor, with which the feed rate enlarged from 0.10 to 0.20 mm/rev, the thrust force values enlarged all the way through 54.58%, 42.25% and 10.87% at cutting speed of 50 m/min for the uncoated, PVD- and CVD-coated drill bits correspondingly. This was for the reason that; the rise of the feed rate enlarges the cutting pressure on the tool edge that sequentially increases the thrust force. In the most of the tests, the figures exposed that as feed rate increases the thrust force raise as well.

According to Y. Altunpak et al. [39], the authors asserted that the insertion of graphite (Gr) in Al/SiC_P MMC led to reduce of the cutting force and the feed rate that was the key factor, which notably had an influencial impact on the cutting force.

The highest thrust force value that was reached when the cutting speed was of 40 m/min with an elevated feed rate in cases where the PVD- and CVD-coated drill bits were employed. Although, while utilized the uncoated drill bits the highest thrust force achieved at cutting speed of 30 m/min and feed rate of 0.20 mm/rev.

In general, from a much-more broader sense of view, the generated thrust force are high though the utilizing of the uncoated drill bits weighed against to the coated drill bits at the used levels of cutting speed and feed rate. This could be allied to the hard coating layers over the drills surfaces, which diminish the built-up-edge (BUE) formation throughout the drilling action; this experimental study was done under the dry cutting environment, which produced important increment in the drilling temperature, which meant that the environment was probable to be appropriate for the formation of a BUE.

Additionally, to this result that has been indicated prove that the high cutting velocities and lower feed rate were supreme in the drilling of Mg/GNPs MC.

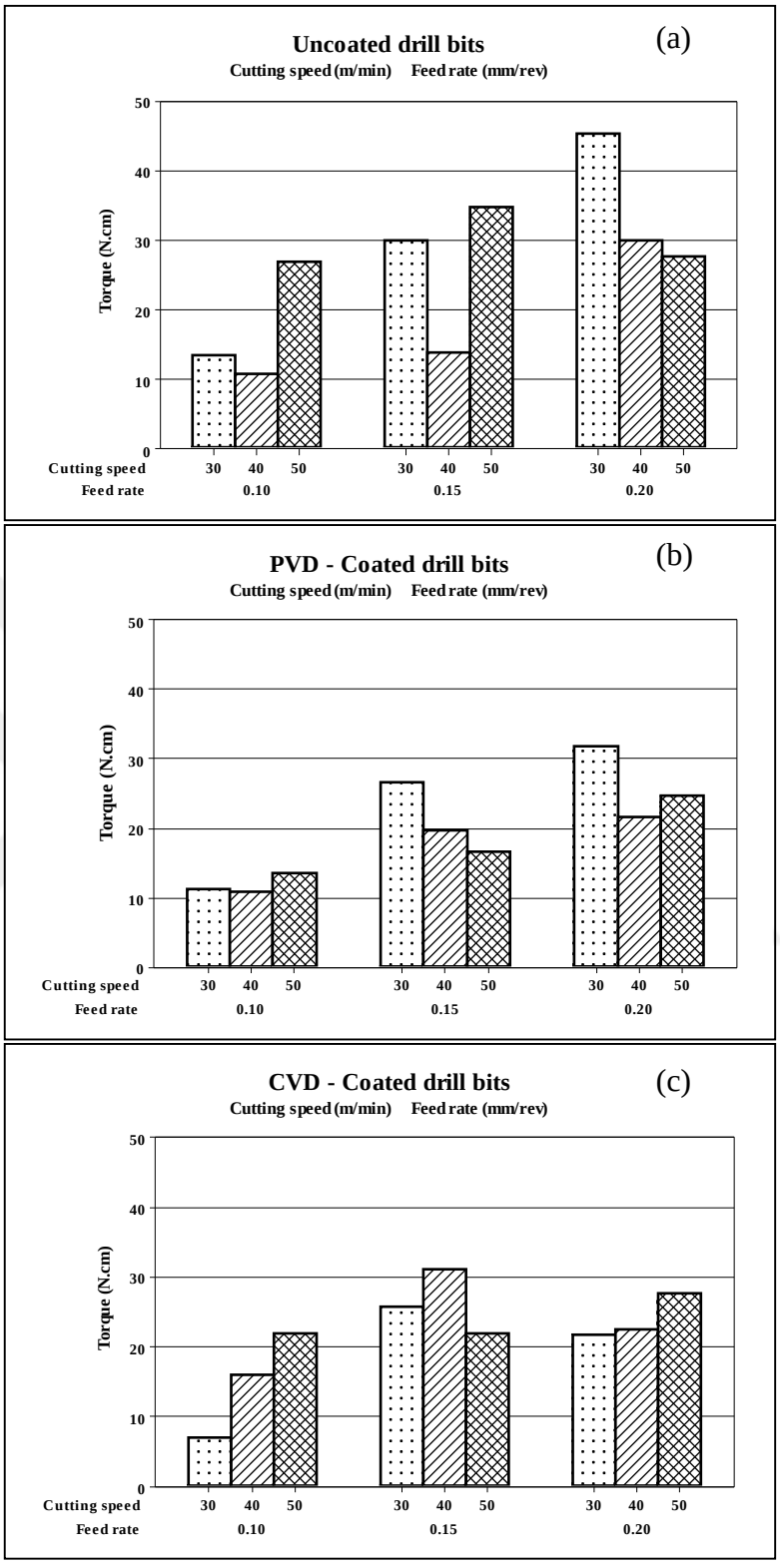

Figure 6.9. Torque with respect to feed rates at different cutting speeds when utilized: (a) uncoated, (b) PVD-coated and (c) CVD-coated drill bits, while drilling of Mg/GNPs MC.

The results from the measured torque values while the drilling procedures of Mg/GNPs MC are been exist in Figure 6.9 (a-c). The results indication reveals that; for the nearly all parts of the tests the torque raises with the increment in the feed rate for the all categories of the drill bits. The results also reveal an indication that the torque shows a discrepancy with the cutting speed levels for each feed rate level. This could be because that the rise of the rotating speed which increases the torque in the drilling of the MMCs that was consequently of the abrasive reinforcement, which works to rising the friction amid the drill bit surface and the composite. From this result, this research-study could draw a conclusion that torque is controlled by the abrasive reinforcement, not the matrix material.

It is notice to pinpoint that the highest value of torque has been reached at V_C=30 m/min and f=0.20 mm/rev while utilizing the uncoated carbide drills. Whereas the lowly value was at V_C=30 m/min and f=0.10 mm/rev.

6.4.1.2. Taguchi's Method Optimization for Thrust Force and Torque While Drilling of Mg/GNPs MC

The process of the Taguchi's procedure applies the signal/to/noise ratio (S/N ratio) to computation of the attribute value that is deviate from the desired value. The S/N ratio is utilized with the purpose of state the control factor that minimizes the outcome of the noise on the response. Smaller rate reveals a better property category of the (S/N) ratio, which was utilized in this analysis. The formula for the smaller is the better (S/N) ratio is:

$$S/_N = -10 \log_{10}\left(\frac{1}{n}\sum_{i=1}^{n} Y_i^2\right) \tag{6.1}$$

Where; Y is the specified responses for the factor level grouping and n that is the response number in the factor level grouping.

The experimental outcome were turned into the S/N ratios, the factor with the higher differentiation among the mean of S/N ratios was the majority important control

factor. The response table can then identify which factor has the majority level of influence on the response (thrust force and torque) and whose factor level is linked to the upper or the lower response characteristic rates. Taguchi's procedure employs the following procedure to form the response table: (1) by computing, the chosen response characteristic for each factor level is show through a combination. (2) for each parameter, calculates the prime of the response characteristic at each factor level. (3) for each factor, computes the delta value that is the peak prime response characteristic value minus the lowly prime response characteristic value for the factor levels. (4) by calculating the order which is the (rank) of the factors, in the order of the delta values from high to low. The drill bits (uncoated, PVD- and CVD-coated), cutting speed, and feed rate were chosen as control factors as scheduled and revealed in Table 6.1.

Table 6.1. The cutting parameters levels were utilized in the experimental work.

Level	**Cutting Speed levels (V_C)**	**Feed rate levels (f)**	**Cutting tool levels (C_T)**
1	V_{C1}=30 m/min	f_1=0.10 mm/rev	Uncoated carbide
2	V_{C2}=40 m/min	f_2=0.15 mm/rev	PVD-coated carbide
3	V_{C3}=50 m/min	f_3=0.20 mm/rev	CVD-coated carbide

Table 6.2 reveals that the ranks of the parameters resulted by S/N ratio intended for the parameter levels for the thrust force, whilst the drilling of Mg/GNPs MMC. As the Table 6.2 presented, the major parameter that has an effect on thrust force was to be the feed rate, which tag along by the cutting speed and then the type of drill.

Table 6.2. The S/N ratio response table (smaller is better) of thrust force for Mg/GNPs MC.

	Control factors		
Level	**Cutting speed (m/min)**	**Feed rate (mm/rev)**	**Drill type**
1	-35.75	**-34.05**	-35.23
2	-35.51	-35.28	-34.68
3	-34.52	-36.45	-35.86
Delta	1.23	2.41	1.17
Rank	2	**1**	3

The interaction and their effects are noticeably and relevantly important in the reaching point of a more general inference in parametric studies. To recognize the interaction among parameters, the graph of the average responses at each action combination this is illustrated in Figure 6.10.

As exemplifies in Figure 6.10 (a), it reveals the versus order plot, the plot which illustrates that there are technically no systematic effect in the records, consequently of the time or experimental arrange. The figure 6.10 (b) is shown the normal probability chart of the residuals for the thrust force, the data tracks almost the straight line, which implies and reveals that the model proposed is sufficient and accurate. The plot of S/N ratio main effects of thrust force for Mg/GNPs MMC is shown in Figure 6.10 (c), which shows that the optimal parameters combination to reach the minimum value of thrust force that are the PVD-coated drill bit, 50 m/min cutting speed and 0.10 mm/rev feed rate.

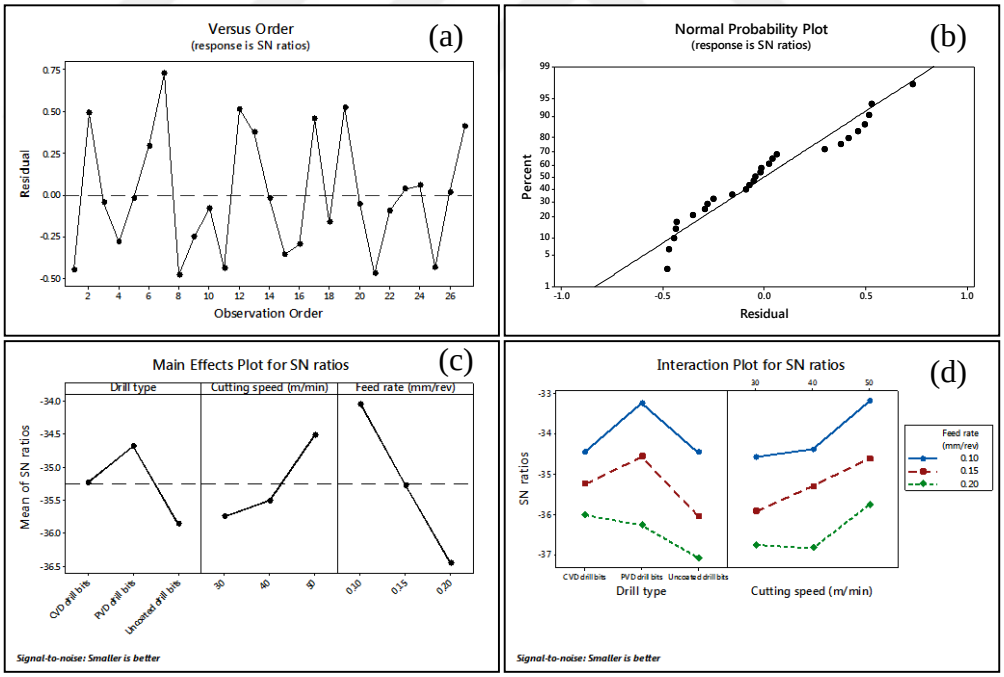

Figure 6.10. (a) Versus order plot for S/N ratio, (b) normal probability plot for S/N ratio, (c) main effects plot for S/N ratio and (d) interaction plot for S/N ration; for thrust force while the drilling of the Mg/GNPs MC.

As seen in Table 6.3 the ranks of the parameters were generated by the S/N ratio analysis for the parameter levels for the torque, while the drilling of Mg/GNPs MC.

The most importantly relevant parameter affecting the torque was the feed rate followed by the cutting speed parameter.

Table 6.3. The S/N ratio response table (smaller is better) for torque whilst drilling of Mg/GNPs MC.

	Control factors		
Level	**Cutting speed (m/min)**	**Feed rate (mm/rev)**	**Drill type**
1	-26.30	**-22.65**	-26.16
2	-25.24	-27.43	-25.33
3	-27.29	-28.75	-27.34
Delta	2.05	6.09	2.01
Rank	2	**1**	3

Importantly, the plot of S/N ratio main and its effects of torque for the Mg/GNPs MMC which is revealed in Figure 6.11 (c), this reveals that the optimal parameters combination to reach the minimum value of torque are the PVD-coated drill bit, 40 m/min of cutting speed and 0.10 mm/rev of feed rate.

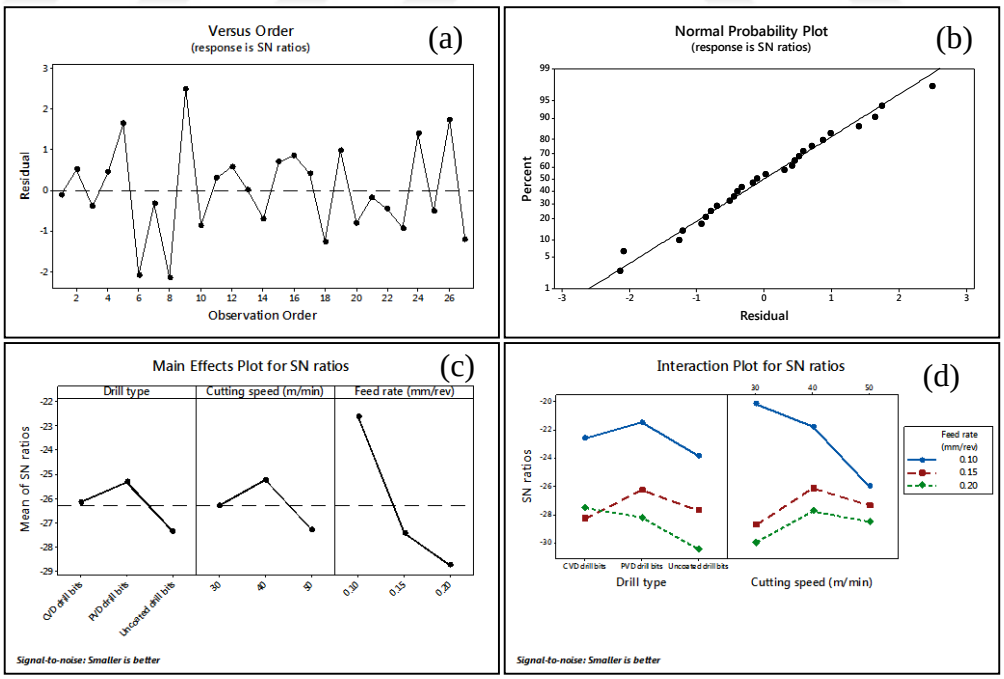

Figure 6.11. (a) Versus order plot for S/N ratio, (b) normal probability plot for S/N ratio, (c) main effects plot for S/N ratio and (d) interaction plot for S/N ration; for torque while drilling of Mg/GNPs MC.

6.4.1.3. ANOVA and Regression Analysis for Thrust Force and Torque Whilst Drilling of Mg/GNPs MC

ANOVA is a statistical methodological approach that can be utilized in order to determine the individual interactions of the power factors in the tests. In this research study, the ANOVA was utilized and applied to evaluate the effects of the feed rate (f), the cutting speed (V_c) and the type of drill bit (C_T) on the thrust force and torque. The ANOVA analysis outcomes for the thrust force and torque are shown in the Tables 6.4 and 6.5 respectively. The analysis was then carried out at a (5%) of significance level and the confidence level of (95%). The last column of the table reveals the contribution rate percent that shows a signal of the rate of the influence of the process parameters.

Given the Table 6.4, the most significant factor on the thrust force was found to be the f with the contribution rate of 56.51%, which is followed by the V_C factor (14.17%), and then by the C_T factor (13.93%), the same result that was found throughout the utilization of the Taguchi's approach.

Table 6.4. The ANOVA analysis results for the thrust force (Mg/GNPs MC).

Variance source	DF	SS	MS	F-value	P-value	Contribution (%)
V_c	1	285.68	285.68	26.92	0.000	14.17%
f	**1**	**1139.39**	**1139.39**	**107.36**	**0.000**	**56.51%**
C_T	2	280.91	140.46	13.23	0.000	13.93%
V_c *V_c	1	35.97	35.97	3.39	0.086	1.78%
f* f	1	0.76	0.76	0.07	0.793	0.04%
V_c *f	1	0.12	0.12	0.01	0.918	0.01%
V_c *C_T	2	47.95	23.97	2.26	0.139	2.38%
f *C_T	2	66.22	33.11	3.12	0.074	3.28%
Error	15	159.20	10.61			7.90%
Total	26	2016.19				100%

DF: Degree of freedom, SS: Sum of squares, MS: Mean square.
V_C: Cutting speed factor, f: Feed rate factor, C_T: Drill type factor. **(R-sq=92.10%)**

Table 6.5. The ANOVA analysis results for the torque (Mg/GNPs MC).

Variance source	DF	SS	MS	F-value	P-value	Contribution (%)
V_c	1	0.44	285.68	26.92	0.000	0.02%
f	**1**	**819.45**	**1139.39**	**107.36**	**0.000**	**40.65%**
C_T	2	172.66	140.46	13.23	0.000	8.56%
V_c *V_c	1	107.50	35.97	3.39	0.086	5.33%
f* f	1	58.68	0.76	0.07	0.793	2.91%
V_c *f	1	202.79	0.12	0.01	0.918	10.06%
V_c * C_T	2	85.15	23.97	2.26	0.139	4.22%
f * C_T	2	53.08	33.11	3.12	0.074	2.63%
Error	15	516.24	10.61			25.61%
Total	26	2015.97				100%

DF: Degree of freedom, (SS): Sum of squares, MS: Mean square.
V_C: Cutting speed factor, (*f*): Feed rate factor, C_T: Drill type factor. **(R-sq=74.39%)**

As derived from Table 6.5, it is now been seen that; the most prominent factor affecting on the torque is found to be the *f* with the contribution rate of 40.65% which was followed by the C_T factor (8.56%).

The regression analysis was applied for the modeling development and the analyzing of a numeral of variables where there are found relationship between a dependent variable and individual or extra of independent variables. In our case, the dependent variables are the thrust force and torque, whereas the independent variables are the *f*, V_C and the C_T. In attaining the predictive formula for the thrust force and torque based on the outcome whilst the drilling of the Mg/GNPs composite, the regression analysis was utilized. The analytical equations were formed for the full quadratic regression models for the thrust force and the torque, which are specified below.

-Regression equations for the thrust force and torque whilst the employment of the uncoated drills:

$$F_{th}\ (N) = 24.3 + 1.37V_c + 131f - 0.0245V_c^2 + 142f^2 + 0.2V_cf \qquad (6.2)$$

$$T\ (N.cm) = -11.1 - 2.14V_c + 877f + 0.0423V_c^2 - 1251f^2 - 8.22V_cf \qquad (6.3)$$

-Regression equations for the thrust force and the torque whilst the employment of the PVD-coated drills:

$$F_{th}\ (N) = 11.7 + 1.46V_c + 140f - 0.0245V_c^2 + 142f^2 + 0.2V_cf \quad (6.4)$$

$$T\ (N.cm) = -2.2 - 2.4V_c + 846f + 0.0423V_c^2 - 1251f^2 - 8.22V_cf \quad (6.5)$$

-Regression equations for the thrust force and the torque whilst the employment of the CVD-coated drills:

$$F_{th}(N) = 15.8 + 1.76V_c + 55f - 0.0245V_c^2 + 142f^2 + 0.2V_cf \quad (6.6)$$

$$T(N.cm) = -13.6 - 1.87V_c + 794f + 0.0423V_c^2 - 1251f^2 - 8.22V_cf \quad (6.7)$$

Where F_{th} is the thrust force, T is the torque, V_C is the cutting speed and then f is the feed rate. The comparison of this prediction and estimation (based on the full quadratic regression models which is given in equations 6.2, 6.4 and 6.6) and the experimental outcome which are presented in Figure 6.12 for the thrust force (R^2=0.921) according to the experiment order numbers. Moreover, Figure 6.13 presented the comparison for the torque (R^2=0.7439) which is based on the full quadratic regression models given in equations 6.3, 6.5 and 6.7.

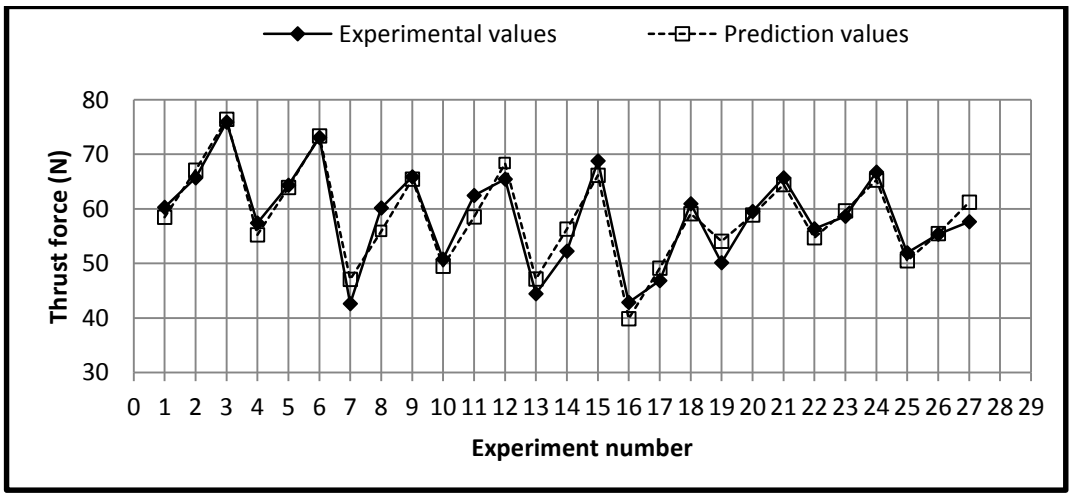

Figure 6.12. The comparion plot of the experimental and predicted outcome for the thrust force (R^2=0.921) while drilling of Mg/GNPs MC.

These results revealed that the regression models could be applied effectively in the predictions of the thrust force and torque whilst the drilling of Mg/GNPs MC.

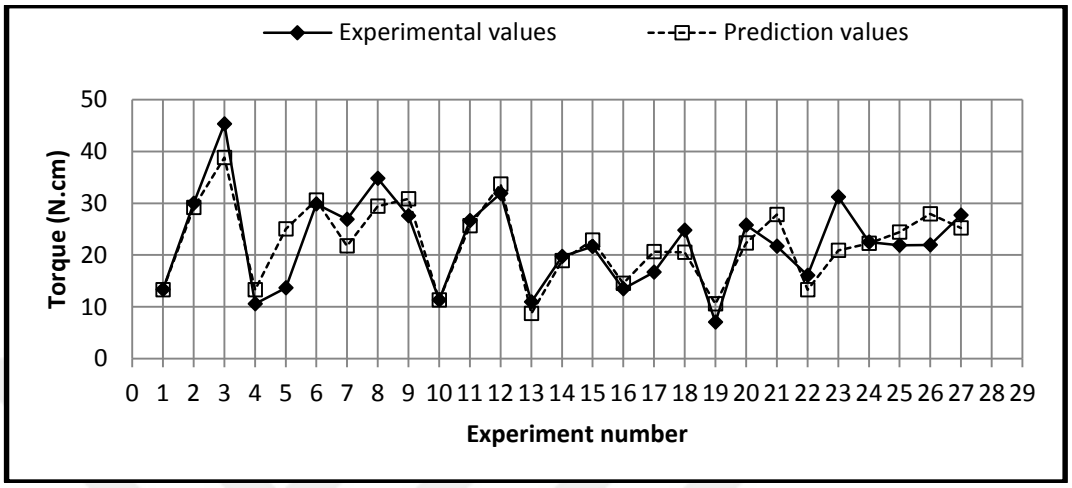

Figure 6.13. The comparion plot of the experimental and predicted outcome for the torque (R^2=0.7439) while drilling of Mg/GNPs MC.

6.4.2. Thrust Force and Torque While Drilling of Hybrid Mg/SiC/GNPs MC

6.4.2.1. Thrust Force and Torque Measured Values While Drilling of Hybrid Mg/SiC/GNPs MC

As showed in Figure 6.14 (a-c) it technically reveals the variant of the thrust force with the feed rates at cutting speeds levels for hybrid Mg/SiC/GNPs MMC during the utilization of the uncoated, PVD- and CVD-coated drills correspondingly. The thrust force in the drilling of MMCs generally relies on the matrix and the reinforcement elements composition, the interface, and their assets.

The relevant differences amid the thrust force are lower at the points of 30 and 40 m/min of cutting speeds throughout the utilization of the PVD-coated drills whilst compared to the upper cutting speed (50m/min). For almost all of the tests, the experimental outcome show a signal that; the thrust force enlarged by the rise of the feed rate, while the thrust force diminish with the rising of the cutting speed. This has coupled to the growth of the temperature produced at the cutting environment, which softens the matrix (Mg) that could attend to the easy plastic deforming.

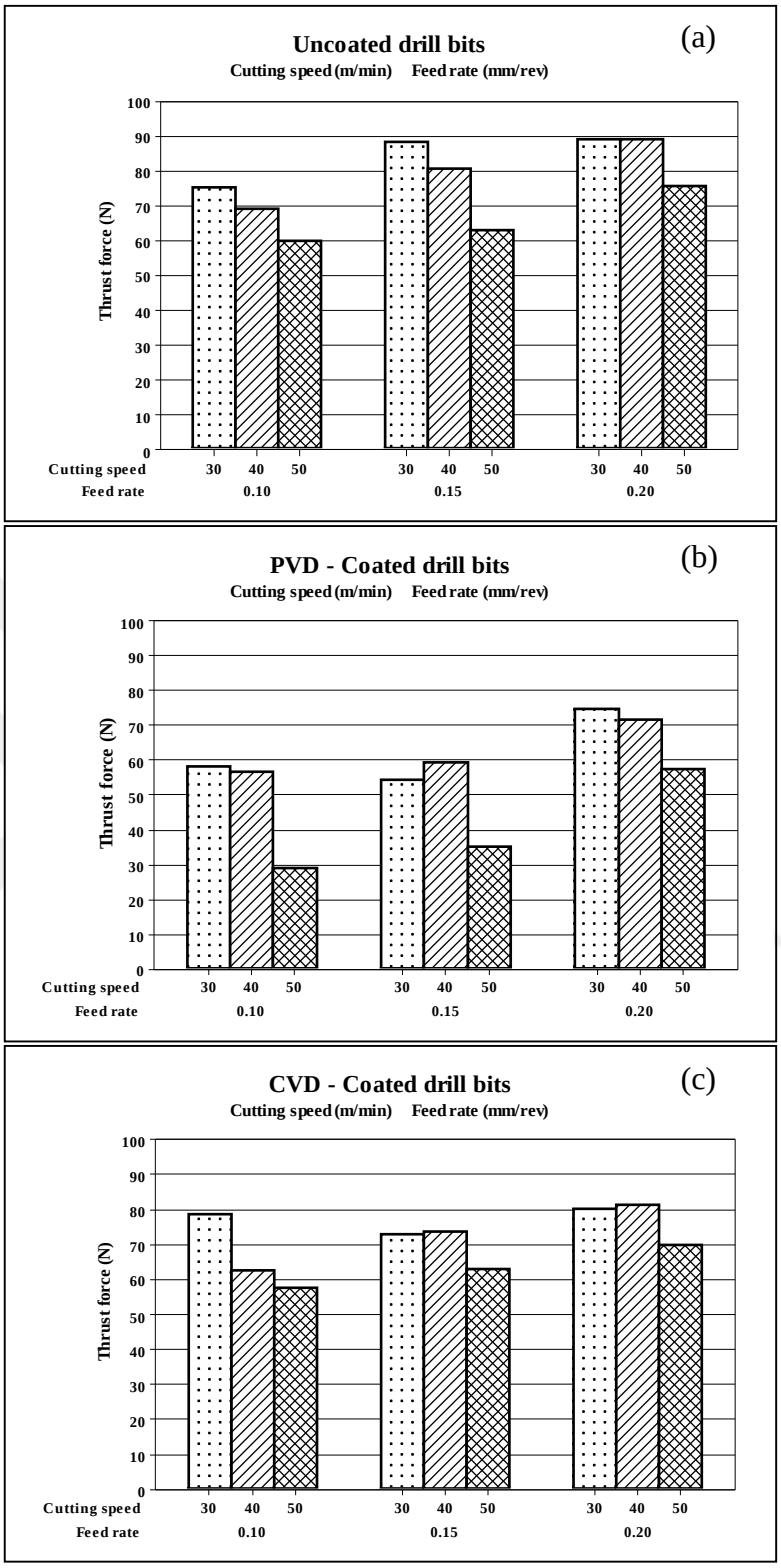

Figure 6.14. Thrust force vs. feed rates at diverse cutting speeds while utilizing: (a) uncoated, (b) PVD-coated and (c) CVD-coated drill bits, whilst the drilling of hybrid Mg/SiC/GNPs MC.

This works to declining of the bonds amid the GNPs, SiC and the Mg matrix. Moreover, in nearly all of the experiments, the thrust force was low down whereas the employment of the coated drills. The GNPs reduces the friction on the cutting edge-material interface, and with a tough covering layer play a role for the diminution of the BUE creation, this direct to proficient lubrication surroundings [70,81].

Further, the lowly thrust force was throughout the employment of the PVD-coated drills at the all levels of the feed rate, as publicized in Figure 6.14 (b). The figure as well shows that with the rising of the feed rate, the thrust force raise as well. Figure 6.14 (c) which clarifies that the thrust forces are almost equal at 30m/min and 40 m/min of cutting speeds, with the levels 0.15 and 0.20 mm/rev of feed rates, however in attendance is a considerable difference among them at the level 0.10 mm/rev of feed rate.

The outcome of torque with respect to feed rates at employed levels of cutting speeds while the utilization of the uncoated, the PVD- and the CVD-coated drills, whilst drilling of hybrid Mg/SiC/GNPs MC are furthermore been existing in Figure 6.15 (a-c). It becomes clear that as the feed rate increases, the torque values also increase in nearly all cases during the employment of the uncoated and coated drill bits. The highest torque value is reached at a high cutting speed with the upper feed rate during the usage of the uncoated drill. This result could be related to the rough SiC particles, which at high speed peel out from the composite and work for raising the friction amid the tool edge and the composite, and then leads to increment of the torque.

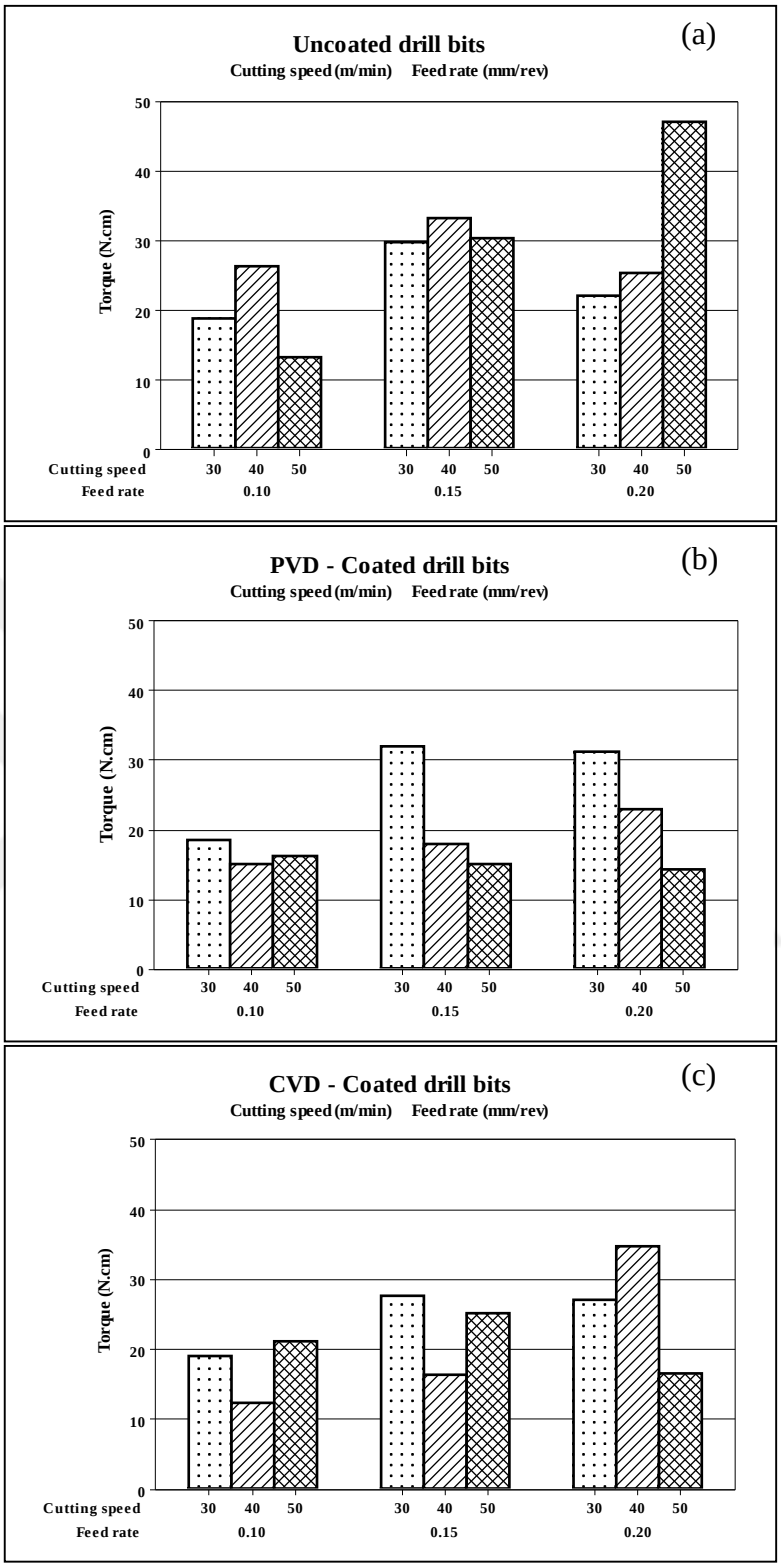

Figure 6.15. Torque vs. the feed rate at diverse speeds whilst utilizing: (a) uncoated, (b) PVD-coated and (c) CVD-coated drill bits, while drilling of hybrid Mg/SiC/GNPs MC.

6.4.2.2. Taguchi's Method Optimization for Thrust Force and Torque While Drilling of Hybrid Mg/SiC/GNPs MC

The ranks of the parameters that were generated by S/N ratio analysis for the diverse parameter levels for the thrust force, through the cutting of the hybrid Mg/SiC/GNPs composite are revealed in Table 6.6. The mainly significant parameter has an effect on the thrust force was the coating category of drill; go after by the cutting speed and after that the feed rate parameter.

Table 6.6. The S/N ratio response table (smaller is better) of thrust force for hybrid Mg/SiC/GNPs MC.

	Control factors		
Level	**Cutting speed (m/min)**	**Feed rate (mm/rev)**	**Drill type**
1	-37.36	-35.41	-36.98
2	-37.01	-36.08	**-34.51**
3	-34.74	-37.61	-37.60
Delta	2.62	2.21	3.09
Rank	2	3	**1**

the plot of S/N ratio main effects of the thrust force for the hybrid Mg/SiC/GNPs MMC has been revealed in Figure 6.16 (c), which reveals that the optimal parameters grouping to reach the lowly value of the thrust force are the PVD-coated drill bit, cutting velocity of 50 m/min and feed rate of 0.10 mm/rev.

As well, Table 6.7 reveals the ranks of the parameters created by the S/N ratio analysis for the diverse parameter levels for the torque, whilst the machining of the hybrid Mg/SiC/GNPs MC. According to the Table 6.7, the majority significant parameter has an effect on the torque in an order happens to be the feed rate, the category of drill and the cutting speed.

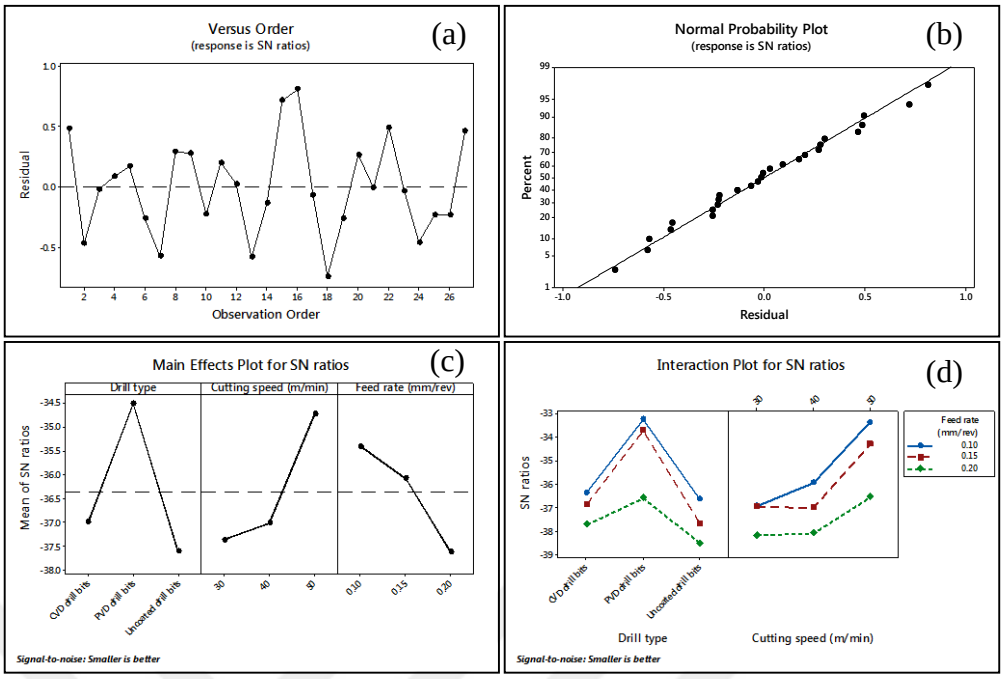

Figure 6.16. (a) The versus order plot for S/N ratio, (b) normal probability plot for S/N ratio, (c) main effects plot for S/N ratio and (d) interaction plot for S/N ration; for thrust force while drilling of Mg/SiC/GNPs MC.

Table 6.7. The S/N ratio response table (smaller is better) of the torque for the hybrid Mg/SiC/GNPs MC.

	Control factors		
Level	**Cutting speed (m/min)**	**Feed rate (mm/rev)**	**Drill type**
1	-27.81	**-24.82**	-26.55
2	-26.64	-27.72	-25.81
3	-26.15	-28.06	-28.24
Delta	1.66	3.23	2.43
Rank	3	**1**	2

The plot of S/N ratio main effects of the torque for the hybrid Mg/SiC/GNPs MMC are revealed in Figure 6.17 (c). This is where the optimal parameters grouping reaches the minimum value of the torque which are the PVD-coated drill bit, the 50 m/min of cutting velocity and the feed rate of 0.10 mm/rev.

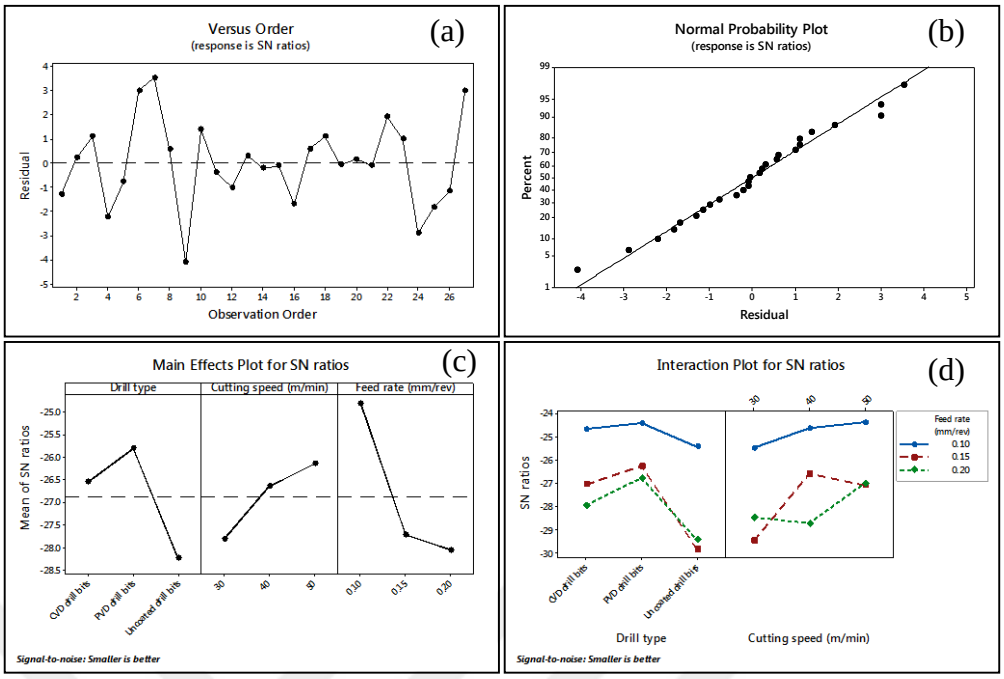

Figure 6.17. (a) versus order plot for the S/N ratio, (b) normal probability plot for the S/N ratio, (c) main effects plot for the S/N ratio and (d) interaction plot for the S/N ration; for torque while the drilling of Mg/SiC/GNPs MC.

6.4.2.3. ANOVA and Regression Analysis for Thrust Force and Torque While Drilling of Hybrid Mg/SiC/GNPs MC

Analytically, the ANOVA analysis outcome for the thrust force and the torque whilst the drilling procedure of the hybrid Mg/SiC/GNPs MMC are publicized in the Tables 6.8 and 6.9 respectively. The analysis were accomplished at a 5% of the significance level and the confidence level of 95%. The most principal factor has an effect on the thrust force was found to be the coating category of the drill bit (C_T) with the contribution rate of (40.01%), go after by the cutting velocity factor (V_C) (26.00%) and subsequently the feed rate factor (f) (20.10%).

As resulting from the Table 6.9, throughout the ANOVA analysis the majority significant and relevant factor has an effect on the torque was found to be the feed rate (f) with the contribution rate of (20.65%) which was tracked by the drill bit coating type (C_T) (13.07%).

Table 6.8. ANOVA analysis outcome for the thrust force (hybrid Mg/SiC/GNPs MC).

Variance source	DF	SS	MS	F-value	P-value	Contribution (%)
V_c	1	1438.45	1438.45	62.17	0.000	26.00%
f	1	1111.72	1111.72	48.05	0.000	20.10%
C_T	**2**	**2213.31**	**1106.65**	**47.83**	**0.000**	**40.01%**
V_c *V_c	1	206.70	206.70	8.93	0.009	3.74%
f* f	1	57.12	57.12	2.47	0.137	1.03%
V_c *f	1	47.80	47.80	2.07	0.171	0.86%
V_c *C_T	2	48.02	24.01	1.04	0.378	0.87%
f *C_T	2	62.08	31.04	1.34	0.291	1.12%
Error	15	347.06	23.14			6.27%
Total	26	5532.26				100%

DF: Degree of freedom, (SS): Sum of squares, MS: Mean square.
V_C: Cutting speed factor, (f): Feed rate factor, C_T: Drill type factor. **(R-sq=93.73%)**

Table 6.9. The ANOVA analysis results for the torque (hybrid Mg/SiC/GNPs MC).

Variance source	DF	SS	MS	F-value	P-value	Contribution (%)
V_c	1	40.65	40.65	0.79	0.388	2.32%
f	**1**	**361.98**	**361.984**	**7.04**	**0.018**	**20.65%**
C_T	2	229.08	114.542	2.23	0.142	13.07%
V_c *V_c	1	4.96	4.963	0.10	0.760	0.28%
f* f	1	52.29	52.294	1.02	0.329	2.98%
V_c *f	1	0.97	0.975	0.02	0.892	0.06%
V_c *C_T	2	266.31	133.155	2.59	0.108	15.20%
f *C_T	2	25.20	12.602	0.25	0.786	1.44%
Error	15	771.09	51.406			44.00%
Total	26	1752.55				100%

DF: Degree of freedom, (SS): Sum of squares, MS: Mean square.

V_C: Cutting speed factor, (f): Feed rate factor, C_T: Drill type factor. **(R-sq=56.00%)**

Furthermore from the analysis outcome the predictive formulas were created for the full quadratic regression for the thrust force (F_{th}) and the torque (T) while the cutting of the hybrid Mg/SiC/GNPs MC which is been given below.

-Regression equations for the thrust force and the torque whilst the employment of the uncoated drills:

$$F_{th}\ (N) = 47.7 + 3.2V_c - 366f - 0.0587V_c^2 + 1234f^2 + 3.99V_cf \quad (6.8)$$

$$T\ (N.cm) = -11.4 - 0.48V_c + 452f + 0.0091V_c^2 - 1181f^2 + 0.57V_cf \quad (6.9)$$

- Regression equations for the thrust force and the torque whilst the employment of the PVD-coated drills:

$$F_{th}\ (N) = 28.7 + 3.01V_c - 331f - 0.0587V_c^2 + 1234f^2 + 3.99V_cf \quad (6.10)$$

$$T\ (N.cm) = 28 - 1.42V_c + 394f + 0.0091V_c^2 - 1181f^2 + 0.57V_cf \quad (6.11)$$

- Regression equations for the thrust force and the torque whilst the employment of the CVD-coated drills:

$$F_{th}(N) = 42.1 + 3.41V_c - 421f - 0.0587V_c^2 + 1234f^2 + 3.99V_cf \quad (6.12)$$

$$T(N.cm) = 9.2 - 0.99V_c + 418f + 0.0091V_c^2 - 1181f^2 + 0.57V_cf \quad (6.13)$$

Where the F_{th} is the thrust force, the T is the torque, V_C is the cutting velocity and f which is the feed rate. The similarity of the predicted (based on the full quadratic regression models given in the equations 6.8, 6.10 and 6.12) and experimental outcome are then been revealed in the Figure 6.18 for the thrust force (R^2=0.9373) with respect to the experiment order.

The Figure 6.19 presents the comparison for the torque results (R^2=0.56) which is based on the full quadratic regression given in the equations 6.9, 6.11 and 6.13. These results are been revealed which shows that the regression models could be applied effectively through the predictions of the thrust force and torque through the drilling procedure of hybrid Mg/SiC/GNPs MC.

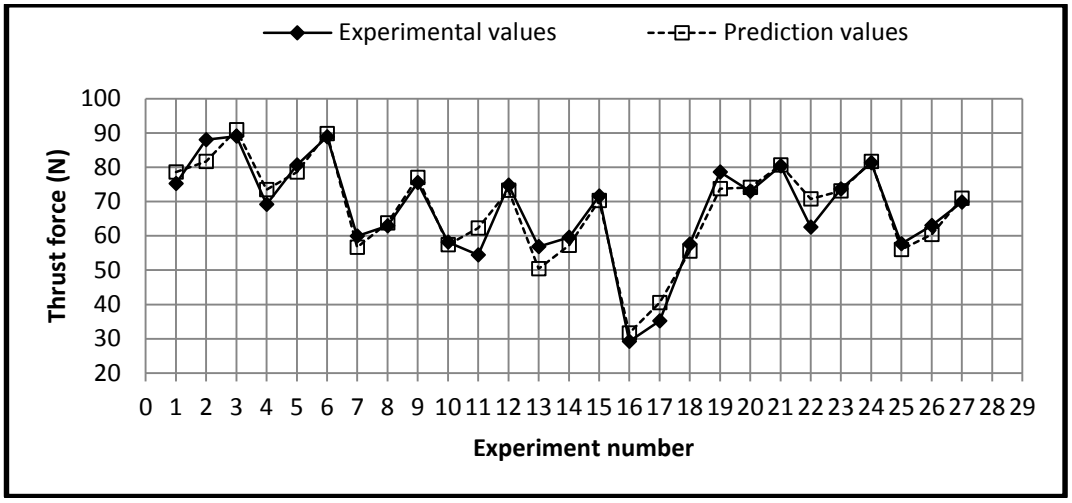

Figure 6.18. The similarity plot of experimental and predicted results for the thrust force (R^2=0.9373) whilst the machining of hybrid Mg/SiC/GNPs MC.

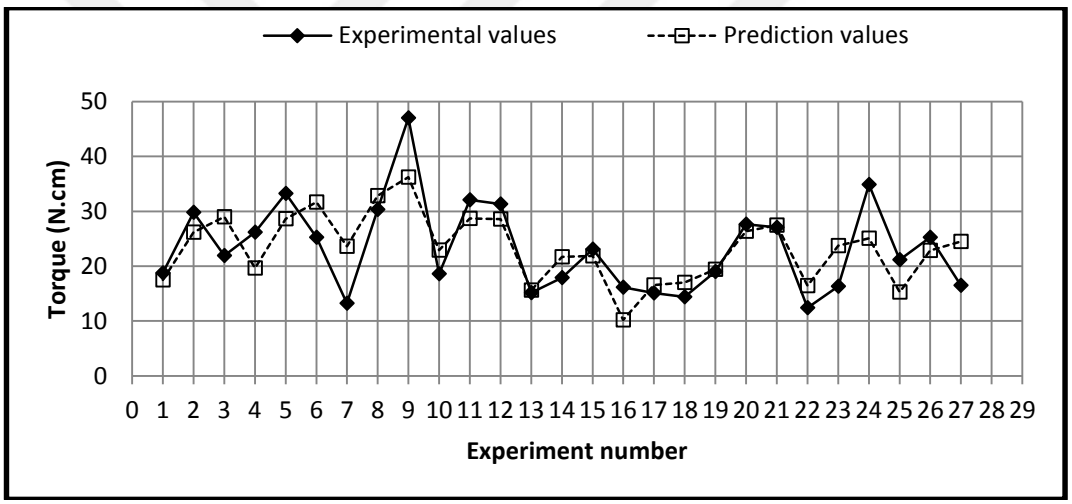

Figure 6.19. The similarity Plot of experimental and predicted results for the torque (R^2=0.56) whilst the drilling of the hybrid Mg/SiC/GNPs MC.

6.5. SURFACE ROUGHNESS RESULTS

The manufacturing parts are necessitated through a high-quality surface texture with the dimensional precision. The surface finish of the produced parts extremely affects the performance of the machined products. The visual manifestation, the load hauling ability, the resistance alongside the corrosion and the wear, and the capability to hold the stress in the produced parts, they are reliance on the surface texture.

For a better and clearer understanding, it is not achievable to fabricate an ideal surface. The surfaces that are created from the machining processes constantly have some kind of wrongdoing and some categories of defects and this explains why they never attain excellence. These degrees of irregularities are mostly found in the machined surface that is defined by the height, the spacing, the direction, and other unsystematic characteristics that are not of a geometric character; this is expressed to be the surface roughness, the surface finish, the face texture or the surface quality. The mean value of the deviations around the centerline within the assessment distance is defined as the arithmetical roughness (R_a). This is as well referred to as the arithmetic average altitude. It is the majority frequent utilized issue for formative the roughness of the machined exterior and for the excellence control of the surface finish.

6.5.1. Surface Roughness while the Drilling of Mg/GNPs MC

6.5.1.1. Surface Roughness Measured Values while the Drilling of Mg/GNPs MC

The Figure 6.20 (a-c) reveals the variant in the surface roughness (R_a) results of the drilled surfaces for the Mg/GNPs MMC under the cutting parameters for the uncoated, PVC- and CVD-coated drill bits correspondingly. As the figures illustrate, as evaluated to the uncoated drills, the coated drills realize a considerable effect to diminish the surface roughness at the upper of the feed rate whilst the drilling of the Mg/GNPs MC, the alike outcomes are been reported by [26].

Precisely, the R_a outcome values of the drilled surfaces are lesser through the drilling of the Mg/GNPs MC while the utilization of the coated drills bits; T. Rajmohan et al. [28] their research findings had obtained the same result.

Nevertheless, the higher values of R_a were reached during the employment of the uncoated drills at a higher feed rate; this could be attached to the BUE formation on the drill edge surfaces and as well on the drilled surfaces. Through the quickness of the BUE formation because of the nature of the Mg matrix and the heat produced through the drilling resulted in the changing the tool geometry that directly affects

the conditions in the deformation locale, this consecutively has an effect on the surface finish.

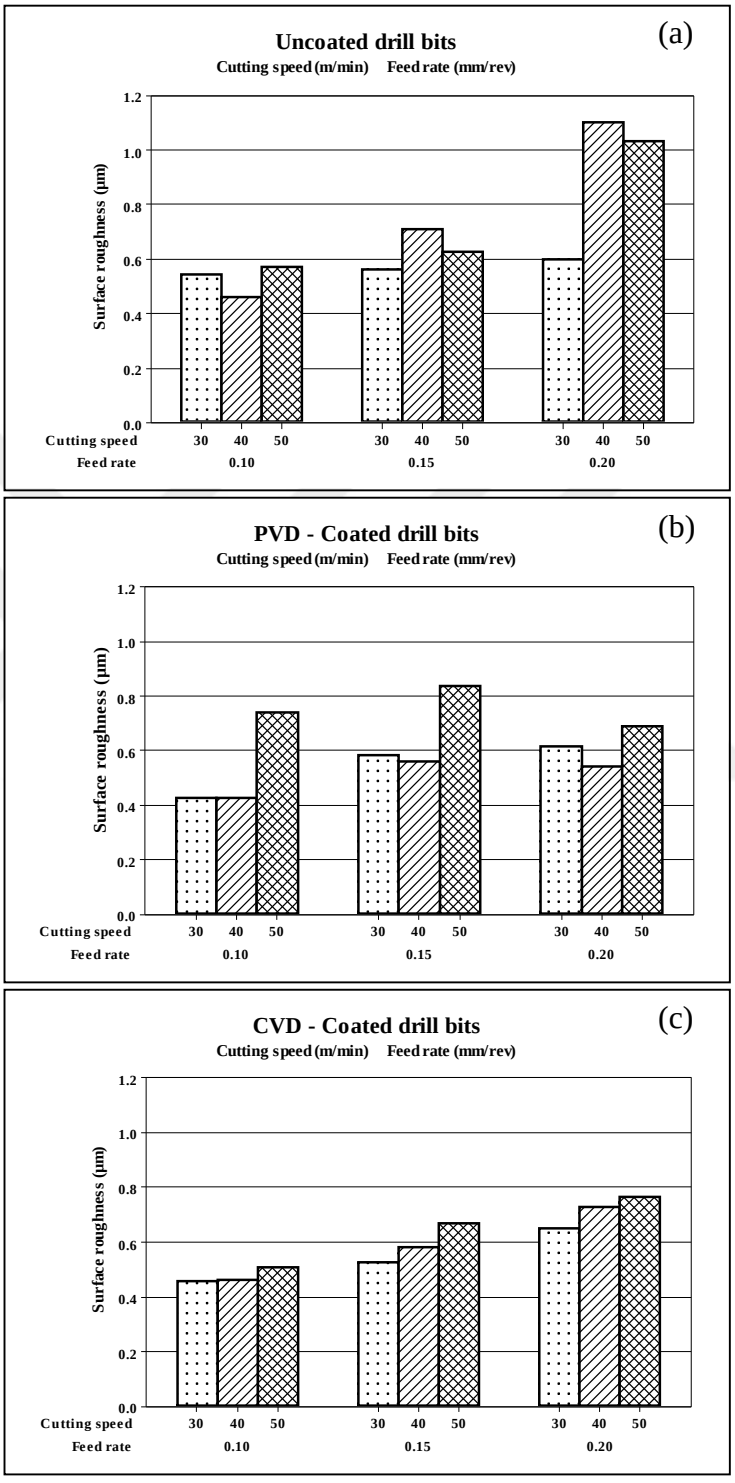

Figure 6.20. Surface roughness (R_a) vs. the feed rate at the diverse cutting speeds while the utilization of: (a) uncoated, (b) PVD-coated and (c) CVD-coated drill bits, whilst the machining of Mg/GNPs MC.

Based on G. Samy and S. Kumaran pieces of conducted researches [36] it was revealed that the rise in the thrust force directed to diminution in the surface quality. The Figures 6.20 (c) points out that the rise of the cutting velocity and the feed rate raises the R_a throughout the employment of the CVD-coated drills. While, with the employment of the PVD-coated drills, the higher values of the R_a are reached at a high cutting speed as reveled in the Figure 6.20 (b). From Figure 6.20 (b), it could be inferred that there is a prime deviation in the R_a when the increasing of feed rate for the high cutting velocity (50 m/min), the alike variation which was found by Y. Altunpak [39].

Based on the outcomes were achieved in the above figures, the lower R_a values were observed at a lower feed rate at the cutting velocities and the drill bits categories employed for the drilling of the Mg/GNPs MC. This was linked to the detail that the chip formed at higher feed rate, which increases the rubbing take action among the composite and the tool edge interface and then the R_a is increased [36].

In accordance, the increase in the cutting velocity, which raises the heat that was produced whilst the drilling that softens the Mg matrix and operates in a ductile behavior and the BUE formation in that case happens, this functions to increase the R_a. As resulting from [12] the lowly feed rate was favored in the drilling of the MMCs and guides to the good quality surface finishing.

6.5.1.2. Taguchi's Method Optimization for Surface Roughness While Drilling of Mg/GNPs MC

As could be seen in Table 6.10, it lists the ranks of the parameters attained from the employment of the S/N ratio analysis for the various parameters levels of the R_a for the Mg/GNPs MC. The table reveals the majority significant parameters that have an effect on R_a which are the feed rate that is followed by the cutting velocity and then the coating type of drill. The feed rate is the parameter, which is extremely influenced the R_a in the drilling of the MMCs [6,12,27].

Table 6.10. The S/N ratio response table (smaller is better) of surface roughness for Mg/GNPs MC.

	Control factors		
Level	**Cutting speed (m/min)**	**Feed rate (mm/rev)**	**Drill type**
1	5.244	**5.969**	4.665
2	4.542	4.131	4.609
3	3.091	2.777	3.603
Delta	2.153	3.193	1.063
Rank	2	**1**	3

The plot of the S/N ratio of the R_a for the drilled surfaces of the Mg/GNPs MC is obtained the same result as revealed in the Figure 6.21 (c). The feed rate is the majority and relevant organize factor. The figures, however, illustrate that the optimal grouping of the parameters to attain the minimum values of R_a are the CVD-coated drills, along with the cutting velocity of 30 m/min and the feed rate of 0.10 mm/rev. The Figure 6.21 (c) as well reveals that in order to attain a low R_a it is desirable to apply a low down feed rate and the cutting velocity.

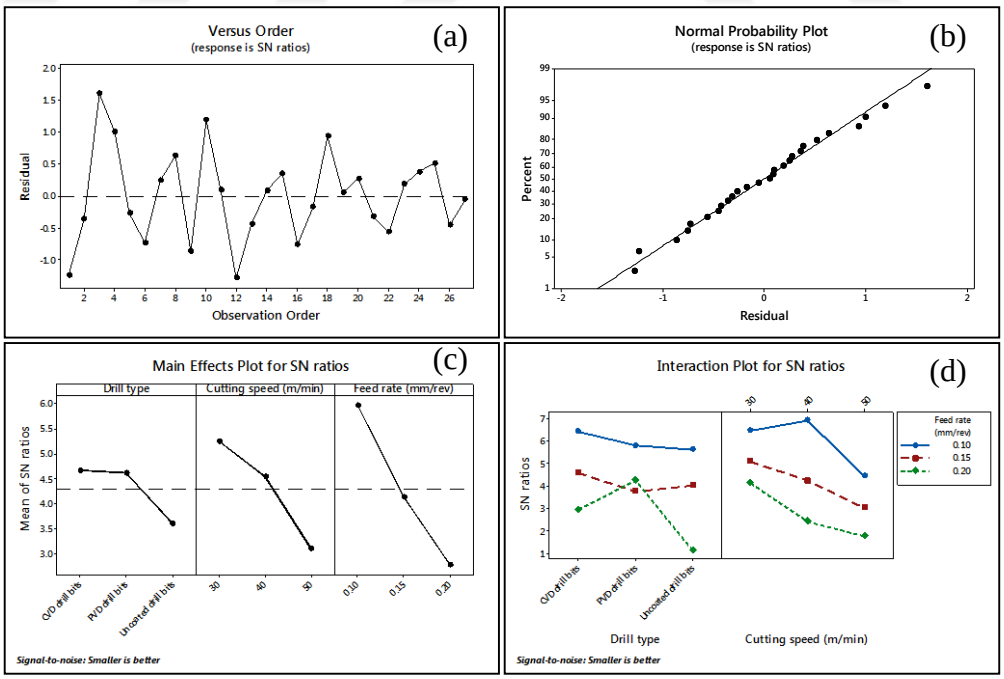

Figure 6.21. (a) versus order plot for S/N ratio, (b) normal probability plot for S/N ratio, (c) main effects plot for S/N ratio and (d) interaction of the plot for the S/N ration; for R_a whilst the drilling of Mg/GNPs MC.

6.5.1.3. ANOVA and Regression Analysis for Surface Roughness While Drilling of Mg/GNPs MC

The ANOVA analysis results for R_a while the drilling of Mg/GNPs MMC are revealed in the Table 6.11. The analysis was carried out at a 5% of the significance level and the confidence level of 95%. The majority principal factor has an effect on the R_a was found to be *f* factor with the contribution rate of 35.53% followed by the cutting speed factor (V_C) (17.06%) and then the drill coating type of (C_T) (6.99%).

Table 6. 11. The ANOVA analysis outcome for the R_a (Mg/GNPs MC).

Variance source	DF	SS	MS	F-value	P-value	Contribution (%)
V_c	1	0.120213	0.120213	8.94	0.009	17.06%
f	**1**	**0.250396**	**0.250396**	**18.62**	**0.001**	**35.53%**
C_T	2	0.049249	0.024624	1.83	0.194	6.99%
V_c *V_c	1	0.001262	0.001261	0.09	0.764	0.18%
f* f	1	0.000004	0.000004	0.00	0.986	0.00%
V_c *f	1	0.004408	0.004408	0.33	0.575	0.63%
V_c * C_T	2	0.009670	0.004835	0.36	0.704	1.37%
f * C_T	2	0.067807	0.033904	2.52	0.114	9.62%
Error	15	0.201689	0.013446			28.62%
Total	26	0.704699				100%

DF: Degree of freedom, (SS): Sum of squares, MS: Mean square.
V_C: Cutting speed factor, (*f*): Feed rate factor, C_T: Drill type factor. **(R-sq=71.38%)**

The predictive formulas were created for the full quadratic regression models for the R_a although the utilization of the three coating categories of drill bits that are given below.

- The outcome of the regression formula for the R_a although the employment of the uncoated drills:

$$R_a\ (\mu m) = 0.217 - 0.0085V_c + 2.22f + 0.000145V_c^2 + 0.3f^2 + 0.0383V_cf \quad (6.14)$$

- The outcome of the regression formula for the R_a although the employment of the PVD-coated drills:

$$R_a\ (\mu m) = 0.509 - 0.0067V_c - 0.79f + 0.000145V_c^2 + 0.3f^2 + 0.0383V_cf \quad (6.15)$$

- The outcome of the regression formula for R_a although the employment of CVD-coated drills:

$$R_a\ (\mu m) = 0.494 - 0.0123V_c + 0.74f + 0.000145V_c^2 + 0.3f^2 + 0.0383V_cf \quad (6.16)$$

Where R_a is the surface roughness, V_C becomes the cutting velocity and f then becomes the feed rate. The assessment of the predicted (based on the full quadratic regression models as given in equations 6.14, 6.15 and 6.16) and the experimental result are been existed in the Figure 6.22 for (R^2=0.7138) according to experiment order.

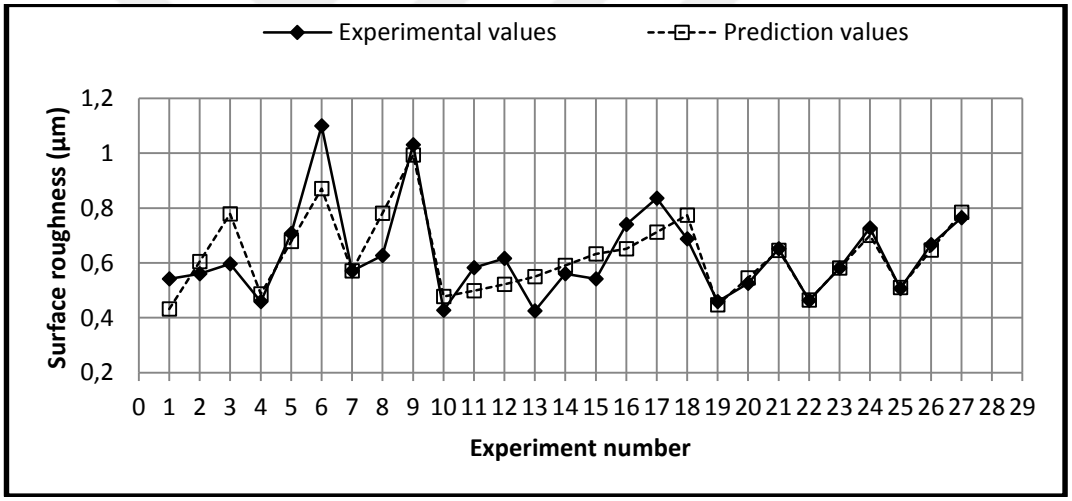

Figure 6.22. The comparison plot of the experimental and predicted results for the R_a (R^2=0.7138) through the drilling of Mg/GNPs MC.

6.5.2. Surface Roughness Whilst Drilling of Hybrid Mg/SiC/GNPs MC

6.5.2.1. Surface Roughness Measured Values Whilst Drilling of Hybrid Mg/SiC/GNPs MC

The variant in R_a the outcome for the drilled surfaces of the hybrid Mg/SiC/GNPs MMC, which are under the utilization of the uncoated, PVC- and CVD-coated drills were obtained in the Figure 6.23 (a-c). The increase in the cutting velocity decreased the R_a in the drilling of the hybrid Mg/SiC/GNPs MMC while the utilization of the CVD-coated drills. At the high cutting velocity the cutting edge pressure had increased and then cut the hybrid MMC smoothly thereby generating less R_a, and the vice versa at the lower cutting speed.

As seen and inferred from the above figures, R_a values are seen to be lower with the employment of the PVD-coated drills within the cutting velocity of 30 m/min at a 0.15 mm/rev level of feed rate, and also with the usage of the CVD-coated drills at *Vc*=50m/min and *f*=0.15mm/rev. This shows up by reason of the hard coating layers over the bits surfaces, which had reduced the BUE throughout the drilling progression. Figure 6.23(b) infers that the lowest rate of the R_a was found during the employment of the PVD-coated bits with a cutting velocity rate of 30 m/min and feed rates of 0.10 and 0.15 mm/rev respectively.

The figures have also exposed that the R_a values are nearly equal at the cutting velocities of 40 and 50 m/min with the feed rates of 0.15 and 0.20 mm/rev. As derived from nearly all tests, the outcomes specify that the lower feed rate (0.10 mm/rev) and the lower cutting velocity (30 m/min) are ideal for drilling of the hybrid Mg/SiC/GNPs MMC, the increase in the feed rate raises the forces and this then has an effect on the surface finishing.

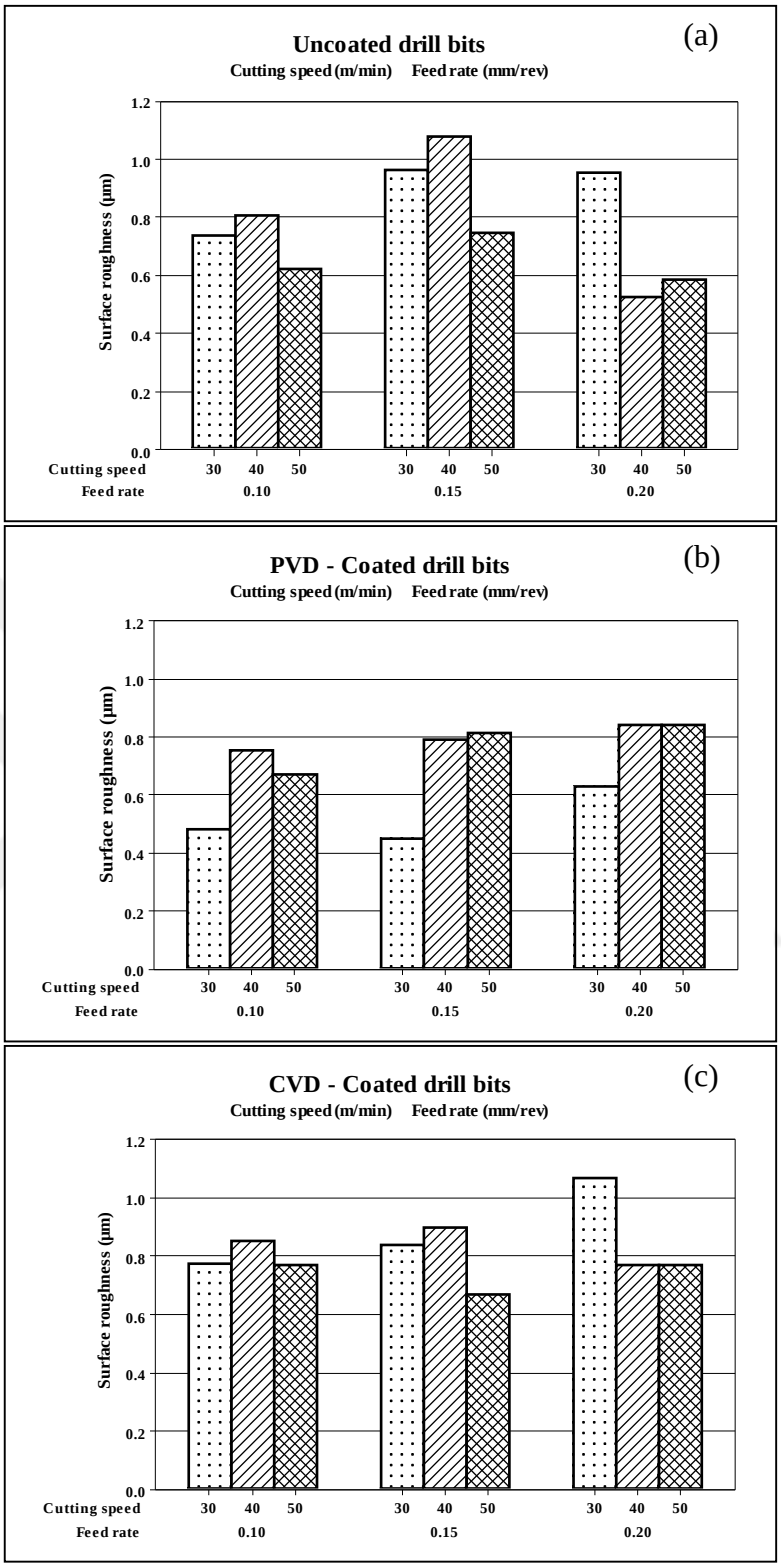

Figure 6.23. The variation of R_a vs. the feed rates at diverse cutting velocities while utilization: (a) uncoated, (b) PVD-coated and (c) CVD-coated drill bits, whilst the drilling of the hybrid Mg/SiC/GNPs MC.

R_a is tends to increase, during the employment of the higher feed rates (0.20mm/rev) while the usage of the coated drills at the lower (30 m/min) and higher cutting velocities (50 m/min). This is by reason of the growth in the friction among the cutting edge and the composite surfaces, which furthermore increases the temperature in the cutting locale. When the uncoated bits are utilized, the maximum value of the R_a is then obtained during the usage of the cutting velocity of 40 m/min at a feed rate of 0.15 mm/rev, afterward an important diminish in the value of the R_a takes place at a feed rate of 0.20 mm/rev.

6.5.2.2. Taguchi's Method Optimization for Surface Roughness While Drilling of Hybrid Mg/SiC/GNPs MC

The ranks of the parameters result recoded through the S/N ratio for the diverse parameters levels of R_a for Mg/SiC/GNPs hybrid MMC are been revealed in Table 6.12. The table illustrates that the considerable parameters that have an effect on the R_a are the coating type of drills that is followed by the cutting velocity and then by the feed rate.

Table 6.12. The S/N ratio response table (smaller is better) of R_a for the hybrid Mg/SiC/GNPs MC.

	Control factors		
Level	**Cutting speed (m/min)**	**Feed rate (mm/rev)**	**Drill type**
1	2.651	2.978	1.758
2	1.929	2.105	**3.327**
3	2.909	2.406	2.404
Delta	0.980	0.874	1.569
Rank	2	3	**1**

The plot of the S/N ratio's main effects of R_a for the hybrid Mg/SiC/GNPs MC is shown in the Figure 6.24(c). The figure illustrates that the optimal parameters grouping that reaches the minimum value of the R_a are the PVD-coated drills, cutting velocity of the 50 m/min and the feed rate of 0.10 mm/rev.

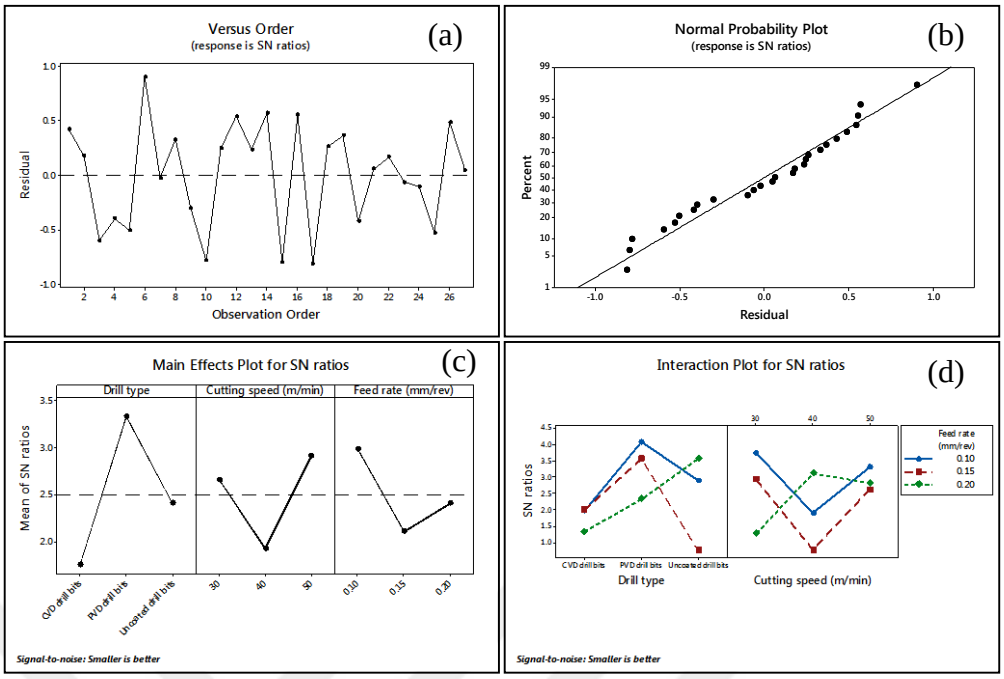

Figure 6.24. (a) Versus order plot for S/N ratio, (b) normal probability plot for S/N ratio, (c) main effects plot for S/N ratio and (d) interaction plot for S/N ration; for R_a while the drilling of Mg/SiC/GNPs MC.

6.5.2.3. ANOVA and Regression analysis for Surface Roughness While Drilling of Hybrid Mg/SiC/GNPs MC

The ANOVA analysis outcomes for the R_a are illustrated in the Table 6.13. The analysis was conducted at a 5% rate of the significance level and the confidence level of 95%. According to the Table 6.13, the majority prominent factor influence on the R_a while the drilling of the hybrid Mg/SiC/GNPs composite was found to be the drill coating type (C_T) with the contribution rate of 11.33% which was tracked by the feed rate (f) with the contribution rate of (2.34%) and the cutting velocity factor (V_c) (1.48%).

As illustrated, the predictive formulas were created for the full quadratic regression for R_a through the drilling of the hybrid Mg/SiC/GNPs composite with the employment of the diverse types of the drills, which are given below.

- The outcome of the regression formula for R_a whiles the employment of the uncoated drill bits:

$$R_a\ (\mu m) = -0.78 + 0.0575V_c + 10.09f - 0.000701V_c^2 - 23.1f^2 - 0.0875V_cf \quad (6.17)$$

- The outcome of the regression formula for R_a whiles the employment of the PVD-coated drill bits:

$$R_a\ (\mu m) = -2.1 + 0.0819V_c + 11.78f - 0.000701V_c^2 - 23.1f^2 - 0.0875V_cf \quad (6.18)$$

- The outcome of the regression formula for R_a whiles the employment of the CVD-coated drill bits:

$$R_a\ (\mu m) = -1.05 + 0.0612V_c + 11.14f - 0.000701V_c^2 - 23.1f^2 - 0.0875V_cf \quad (6.19)$$

Table 6.13. The ANOVA analysis outcome for the R_a (hybrid Mg/SiC/GNPs MC).

Variance source	DF	SS	MS	F-value	P-value	Contribution (%)
V_c	1	0.009476	0.009476	0.59	0.455	1.48%
f	1	0.014964	0.014965	0.93	0.350	2.34%
C_T	**2**	**0.072608**	**0.036304**	**2.26**	**0.139**	**11.33%**
V_c *V_c	1	0.029447	0.029447	1.83	0.196	4.60%
f* f	1	0.019991	0.019991	1.24	0.282	3.12%
V_c *f	1	0.022969	0.022969	1.43	0.250	3.58%
V_c *C_T	2	0.208447	0.104224	6.48	0.009	32.53%
f *C_T	2	0.021777	0.010889	0.68	0.523	3.40%
Error	15	0.241088	0.016073			37.62%
Total	26	0.640768				100%

DF: Degree of freedom, (SS): Sum of squares, MS: Mean square.
V_C: Cutting speed factor, (f): Feed rate factor, C_T: Drill type factor. **(R-sq=62.38%)**

Where the R_a is the surface roughness, and then the V_C is the cutting velocity and f is the feed rate. The similarity of the predicted (based on the full quadratic regression which is given in the equations of 6.17, 6.18 and 6.19) and the experimental outcome are existed in Figure 6.25 for R_a (R^2=0.6238) according to the order of the experiment numbers.

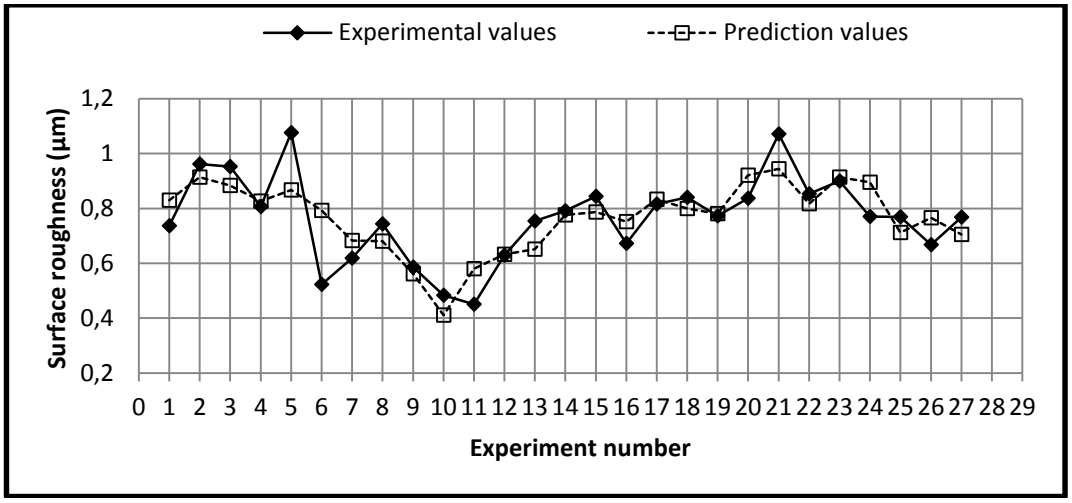

Figure 6.25. The similarity plot of the experimental and predicted results for R_a (R^2=0.6238) while the drilling of the hybrid Mg/SiC/GNPs MC.

6.6. DELAMINATION RESULTS

According to the explanation of the delamination in the composite materials that could be defined as the partition of the layers of the material in a laminate. The delamination could influence the tensile strength utility depending on the locale of the delamination. Amongst the defects that caused by the drilling procedure, the delamination could be documented to be the majority serious. The delamination could be the result of the diminution of the ductility of the MMCs and could cause a drop in the strength of the MMCs and the structural reliability, which results into several of the performance problems.

The most important and core reasons for the happening of the delamination are the high forces and the high feed rate, other causes might comprises the hasty tool wear. The earlier techniques and approaches that have been found to avert the delamination that reduced the feed rate. According to the experimental outcome, the delamination formation was the push-down category at the existence face of the drilled hole, and no essential peel-up category of the delamination formation was observed at the entrance side of drilled holes as shown in Figure 6.26.

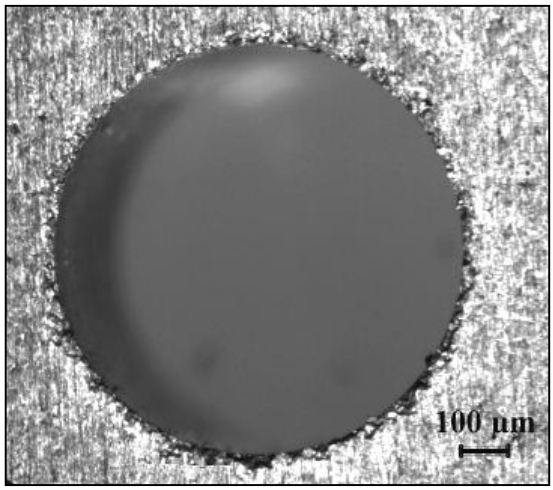

Figure 6.26. The low magnification optical image for the entrance of drilled hole while the employment of the uncoated drills at V_C=30 m/min and f=0.20 mm/rev whilst the drilling of Mg/GNPs MC.

The delamination factor has been assertively referred to as the ratio of the maximum diameter of the delaminated sector on the surface of the composite to the nominal hole diameter which is described in chapter 5-section 5.9.

6.6.1. Delamination While Drilling of Mg/GNPs MC

6.6.1.1. Delamination Factor Measured Values While Drilling of Mg/GNPs MC

When the drilling procedure is completed, the delaminated zone around each drilled hole is examined and observed through the employment of the Nikon zoom stereomicroscope (type SMZ 745T) with the Clemex vision lite software (version 7.0.369 (11281)), as presented in chapter (5)-section 5.9. The Figures 6.27, 6.28 and 6.29 illustrate the low magnification optical images for the delamination measurements and its distribution around the holes during the usage of the uncoated, PVD- and the CVD-coated drill bits respectively. It is noticeable from the images that the delamination is distributed around the whole margins of the drilled holes, but within the dissimilar outline and disparity.

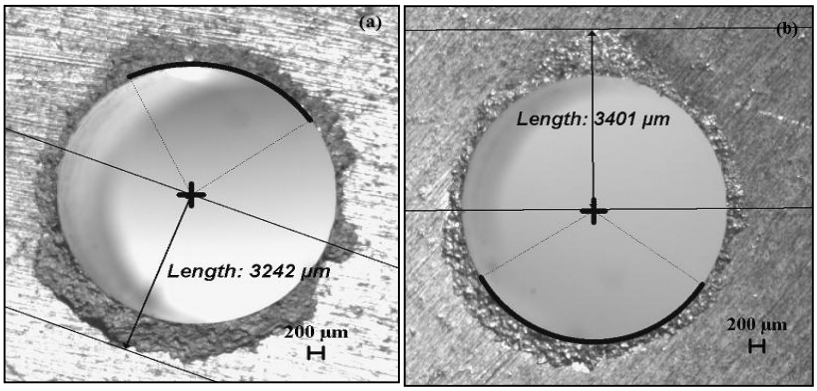

Figure 6.27. Low magnification optical images for the delamination during the employment of the uncoated drills at; (a) V_C=30m/min and f=0.20mm/rev and (b) V_C=40m/min and the f=0.20mm/rev, whilst the drilling of the Mg/GNPs MC.

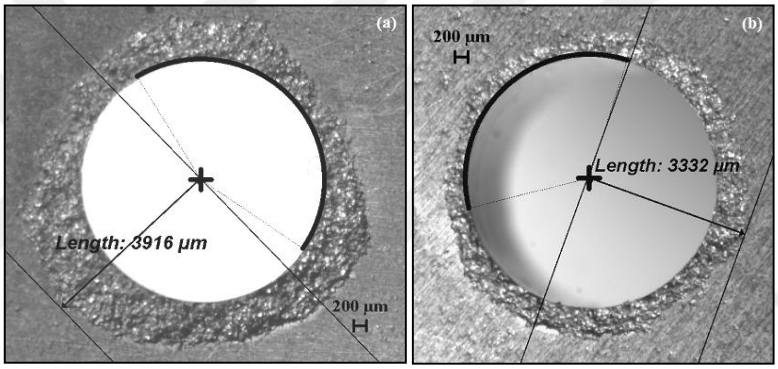

Figure 6.28. Low magnification optical images for the delamination during the employment of the PVD-coated drills at; (a) V_C=50m/min and f=0.15mm/rev and (b) V_C=50m/min and the f=0.20mm/rev, whilst the drilling of the Mg/GNPs MC.

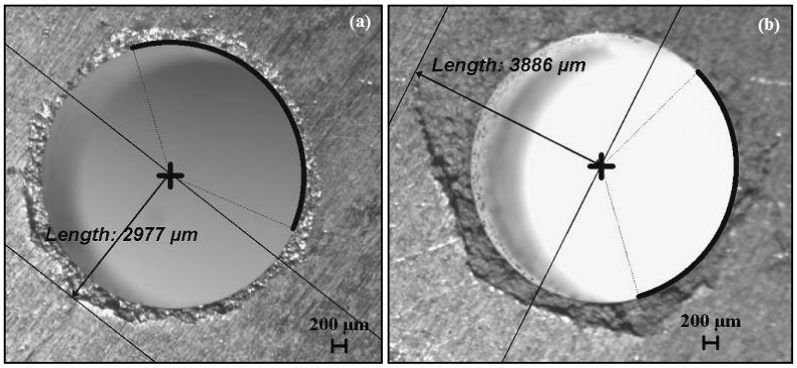

Figure 6.29. Low magnification optical images for the delamination during the employment of the CVD-coated drills at; (a) V_C=30m/min and f=0.20mm/rev and (b) V_C=50m/min and f=0.20mm/rev, whilst the drilling of Mg/GNPs MC.

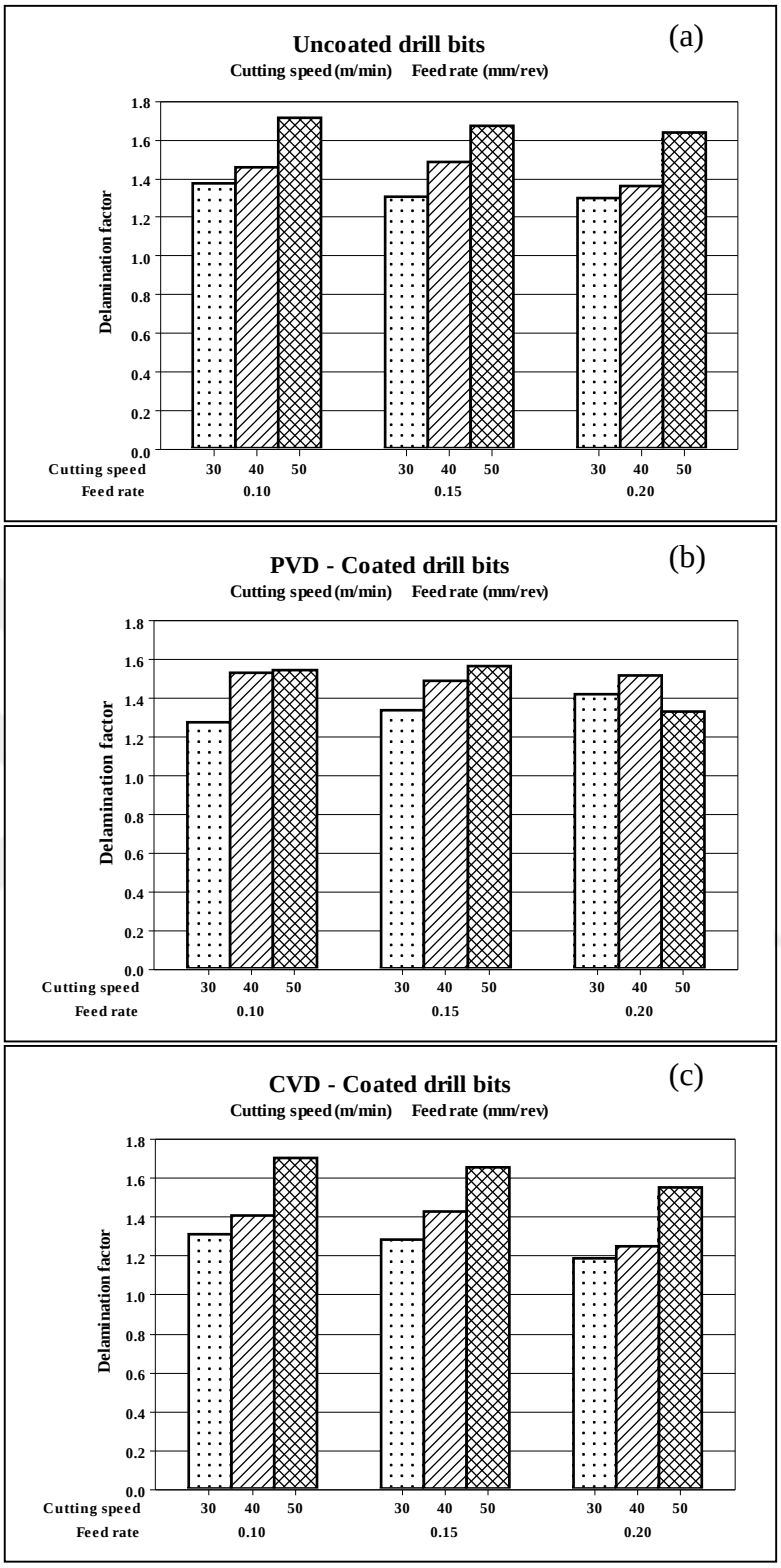

Figure 6.30. Delamination factor vs. the feed rates at the diverse cutting velocities while the employment of; (a) uncoated , (b) PVD-coated drill and (c) CVD-coated drill bits, whilst the drilling of the Mg/GNPs MC.

Foundation on the outcome that is existed in Figure 6.30 (a-c), it is doable to conclude that an increment in the feed rate and the cutting velocity has had a direct effect in the delamination expansion. The locale of the delamination has been enlarged with the rise in the feed rate and the cutting velocity. This is principally recognized to the high crash of the cutting edges, which furthermore directs to the rise in the drilling force. The elevated thrust force, consecutively, guides to a advanced level of the delamination propagation. However, the nominal of the delamination factor was obtained during the employment of the CVD-coated drills at the cutting velocities of 30 m/min and 40 m/min along with the feed rate of 0.20 mm/rev.

Based on the outcome above, it becomes possible to state that the influence of the parameters (the cutting velocity and the feed rate) is greatly further essential than the tool's influence. However, the cutting velocity has to be kept as low down as possible, to diminish the delamination damage extension. The limit on this state is given by the requirement to avoid the unwanted thermal damages that results from the matrix softening.

6.6.1.2. Taguchi's Method Optimization for Delamination Factor While Drilling of Mg/GNPs MC

As observed from Table 6.14 the ranks of the parameters derived from the S/N ratio analysis at the diverse parameter levels for the delamination factor, whilst the drilling of the Mg/GNPs MC. The majority relevant parameter affecting the delamination was the cutting speed, which was tracked by the feed rate and after that the coating type of the drill bit.

Foundation on the plot of the S/N ratio main effects of the delamination factor for the Mg/GNPs MMC that is shown in Figure 6.31 (c). The optimal parameters grouping can get to the lowly value of the delamination factor that are the CVD-coated drills, the cutting velocity of 30 m/min and the feed rate of 0.20 mm/rev.

Table 6.14. The S/N ratio response table (smaller is better) for the delamination factor for Mg/GNPs MC.

	Control factors		
Level	**Cutting speed (m/min)**	**Feed rate (mm/rev)**	**Drill type**
1	**-2.350**	-3.369	-3.003
2	-3.138	-3.316	-3.190
3	-4.051	-2.854	-3.346
Delta	1.701	0.515	0.343
Rank	**1**	2	3

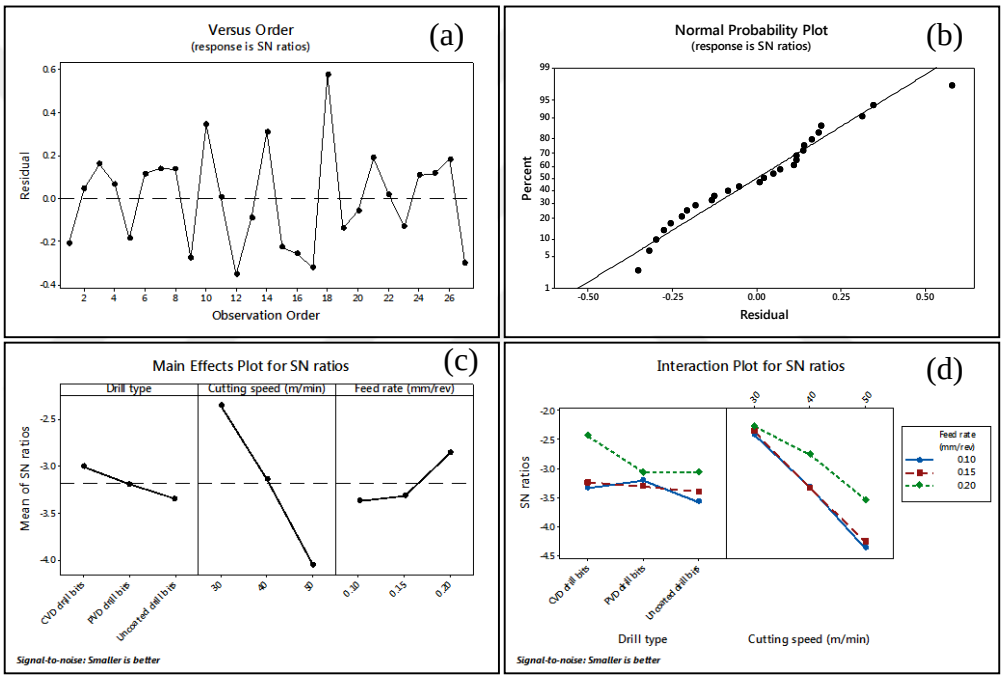

Figure 6.31. (a) Versus order plot for the S/N ratio, (b) normal probability plot for the S/N ratio, (c) main effects plot for the S/N ratio and (d) interaction plot for the S/N ration; for the delamination factor whilst the drilling of the Mg/GNPs MC.

6.6.1.3. ANOVA and Regression Analysis for Delamination Factor Whilst Drilling of Mg/GNPs MC

Found based on the ANOVA analysis outcome for the delamination factor as revealed in the Tables 6.15, the majority powerful factor has affect on the delamination was ascertain to be the cutting velocity factor (V_C) with the contribution

rate of the (63.95%) which was tag along by the feed rate (*f*) (5.65%) and afterward the drill coating category (C_T) (2.30%). The analyses were carried out at a 5% of the significance level and the confidence level of (95%).

The predictive formulas that were formed from the full quadratic regression to the prognostic the delamination factor whilst the drilling of the Mg/GNPs MC were given below in the formulas 6.20, 6.21 and 6.22 for the different coating categories of the drill bits.

Table 6.15. The ANOVA analysis outcome for the delamination factor (Mg/GNPs MC).

Variance source	DF	SS	MS	F-value	P-value	Contribution (%)
V_c	**1**	**0.368654**	**0.368654**	**69.30**	**0.000**	**63.95%**
f	1	0.032598	0.032598	6.13	0.026	5.65%
C_T	2	0.013280	0.006640	1.25	0.315	2.30%
V_c *V_c	1	0.001849	0.001849	0.35	0.564	0.32%
f* f	1	0.006316	0.006316	1.19	0.293	1.10%
V_c *f	1	0.012224	0.012224	2.30	0.150	2.12%
V_c * C_T	2	0.051391	0.025696	4.83	0.024	8.91%
***f* * C_T**	2	0.010385	0.005193	0.98	0.399	1.80%
Error	15	0.079794	0.005320			13.84%
Total	26	0.576492				100%

DF: Degree of freedom, (SS): Sum of squares, MS: Mean square.
V_C: Cutting speed factor, (*f*): Feed rate factor, C_T: Drill type factor. **(R-sq=86.16%)**

- The regression formula for the delamination factor whiles the employment of the uncoated drill bits:

$$f_d = 0.526 + 0.0129V_c + 5.6f + 0.000176V_c^2 - 13f^2 - 0.0638V_cf \quad (6.20)$$

- The regression formula for the delamination factor whiles the employment of the PVD-coated drill bits:

$$f_d = 0.831 + 0.0023V_c + 6.18f + 0.000176V_c^2 - 13f^2 - 0.0638V_cf \quad (6.21)$$

- The regression formula for the delamination factor whiles the employment of the CVD-coated drill bits:

$$f_d = 0.504 + 0.0143V_c + 5f + 0.000176V_c^2 - 13f^2 - 0.0638V_c f \quad (6.22)$$

Where the f_d is the delamination factor, the V_C then becomes the cutting speed and the f is the feed rate. The comparison of the prediction (based on the full quadratic regression was presented and given in the formulas 6.20, 6.21 and 6.22) and the experimental outcome were, however, existed in the Figure 6.32 for the delamination factor (R^2=0.8616) with respect to the experiment order. These results exposed that the regression models could be applied effectively in the predictions of the delamination factor whiles the drilling of the Mg/GNPs MC.

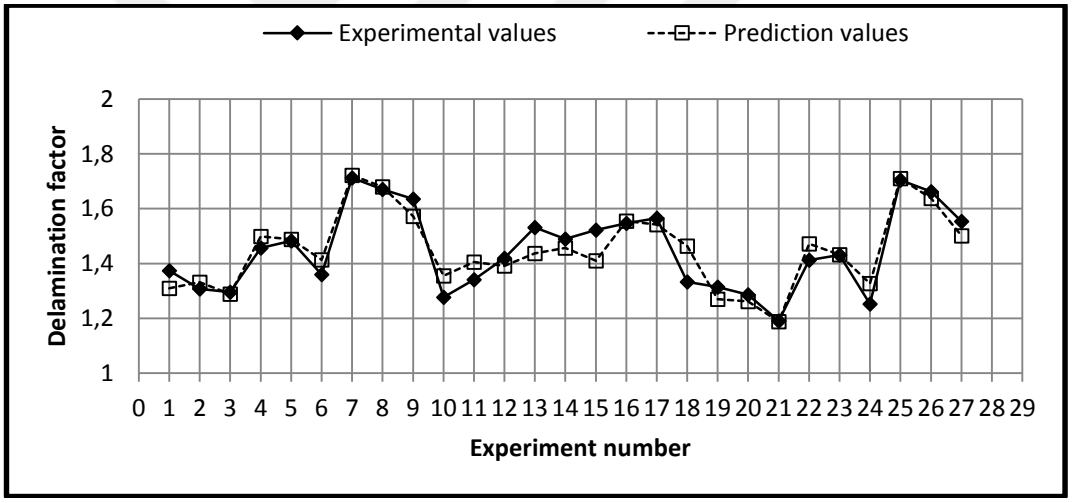

Figure 6.32. Comparison plot of the experimental and predicted outcome for f_d (R^2=0.8616) whilst the drilling of the Mg/GNPs MC.

6.6.2. Delamination While Drilling of Hybrid Mg/SiC/GNPs MC

6.6.2.1. Delamination factor Measured Values While Drilling of Hybrid Mg/SiC/GNPs MC

Figure 6.33 (a-c) illustrates a low magnification optical images for the delamination measurements and its distribution around the holes through the employment of the uncoated, PVD- and CVD-coated drills respectively.

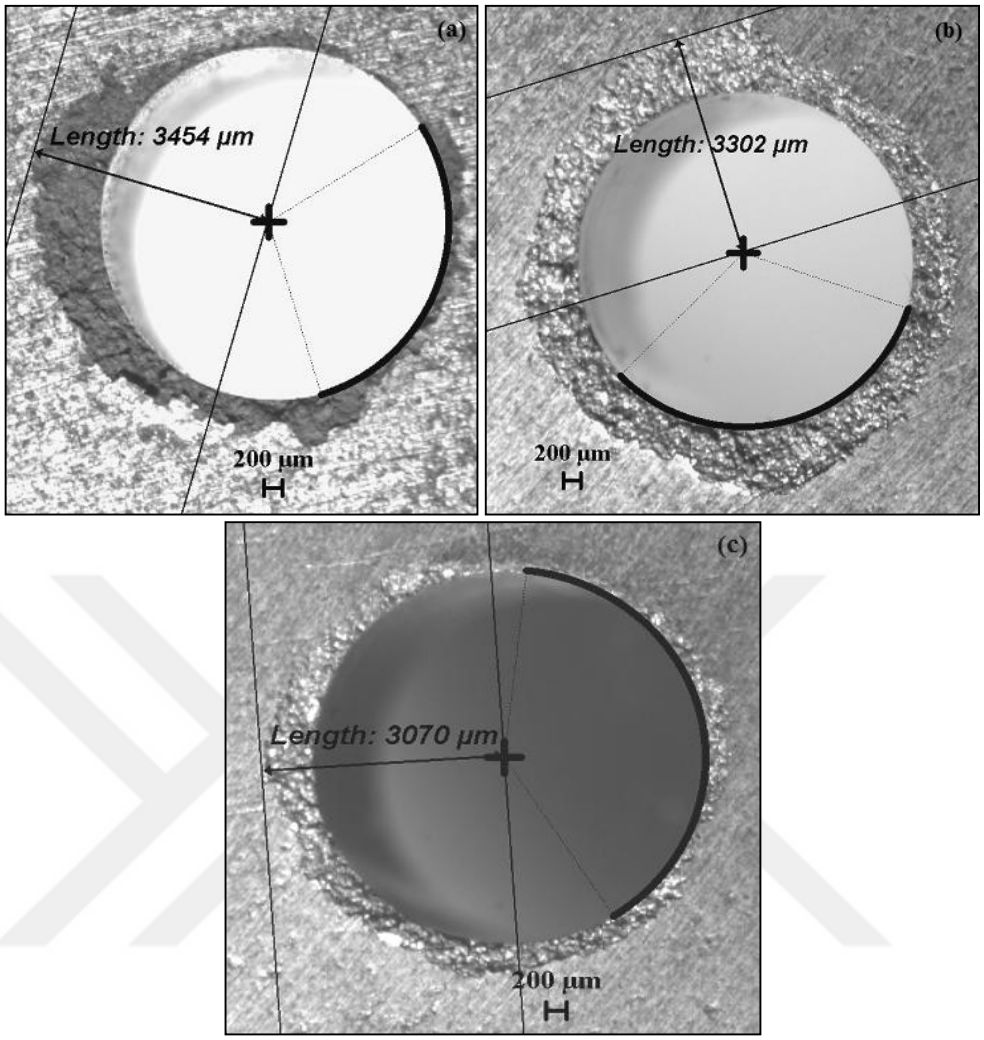

Figure 6.33. Low magnification optical images for the delamination while the utilization of; (a) uncoated drill at V_c=40m/min and f=0.10mm/rev, (b) PVD-coated drill at V_c=30m/min and f=0.15mm/rev and (c) CVD-coated drill at V_c=30m/min and f=0.15mm/rev, while the drilling of hybrid Mg/SiC/GNPs MC.

As revealed in Figure 6.34 (a-c) the delamination factor variant with feed rates at the diverse cutting velocities during the employment of the uncoated, PVD-coated and the CVD-coated drill bits, while the drilling of hybrid Mg/SiC/GNPs MC respectively.

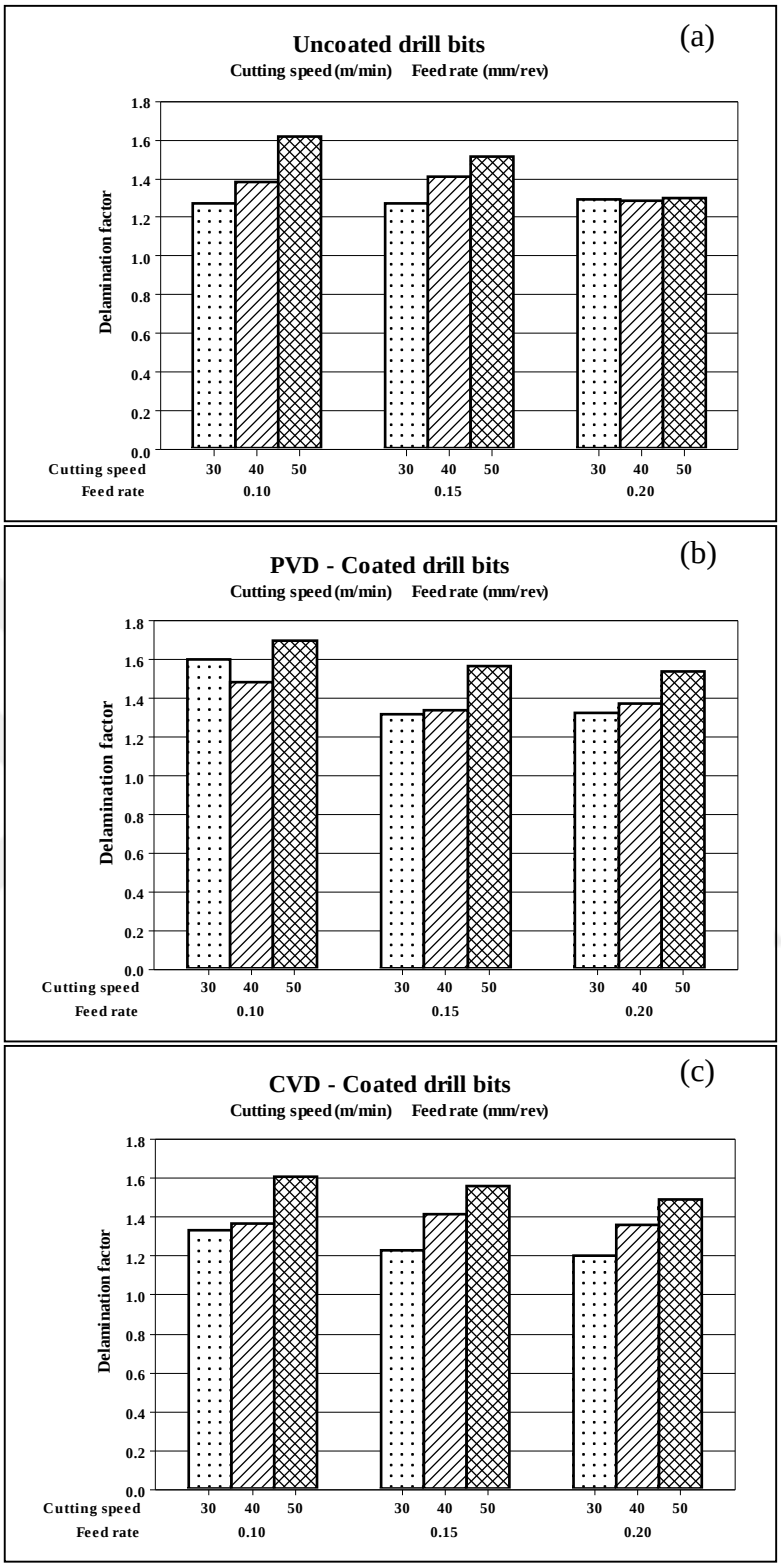

Figure 6.34. Delamination factor vs. the feed rates at the diverse cutting velocities during the employment of; (a) uncoated, (b) PVD-coated and (c) CVD-coated drills, while the drilling of the hybrid Mg/SiC/GNPs MC.

The figure illustrates that the delamination factor amplifies with the rise in the cutting velocity at the diverse levels of the feed rate, and there is no considerable effect by the coating type of the drill bit (uncoated or coated drills). The lowest delamination factor value was reached during the employment of the low cutting velocity (30 m/min) with a combination with 0.20 mm/rev of feed rate. Stand on the above results; it is doable to conclude that, an increase in the feed rate that had a direct effect in the delamination, for the levels of the cutting velocities. In addition, a apparent relationship amid the thrust force outcome and the delamination extension could then be founded. The experimental results derived by C. C. Tsao and H. Hocheng [84] revealed and asserted that though the thrust force is higher with the growing wear, the delamination becomes more probable to take place. L. M. P. Durao et al. [87] stated that the higher feed rate links to higher delamination extension and as the cutting velocity rises; the delamination outcome has a tendency to diminish.

6.6.2.2. Taguchi's Method Optimization of Delamination Factor While Drilling of Hybrid Mg/SiC/GNPs MC

Table 6.16 illustrates the rank positions of the parameters created by S/N ratio analysis for the diverse parameter levels for the delamination factor, throughout the drilling of the hybrid Mg/SiC/GNPs MC. The major parameter has an effect on the delamination factor was the cutting velocity; go after by the feed rate and after that the coating category of drill bits.

Table 6.16. The S/N ratio response table (smaller is better) of the delamination factor for the hybrid Mg/SiC/GNPs MC.

	Control factors		
Level	**Cutting speed (m/min)**	**Feed rate (mm/rev)**	**Drill type**
1	**-2.362**	-3.398	-2.871
2	-2.796	-2.914	-3.327
3	-3.754	-2.601	-2.714
Delta	1.392	0.797	0.613
Rank	**1**	2	3

The plot of the S/N ratio's main effects of the delamination factor for the hybrid Mg/SiC/GNPs MMC is shown in Figure 6.35 (c). Derived from the figure that the optimal parameters grouping to attain the lowly value of the delamination factor which are the CVD-coated drills, the cutting velocity of 30 m/min and the feed rate of 0.20 mm/rev.

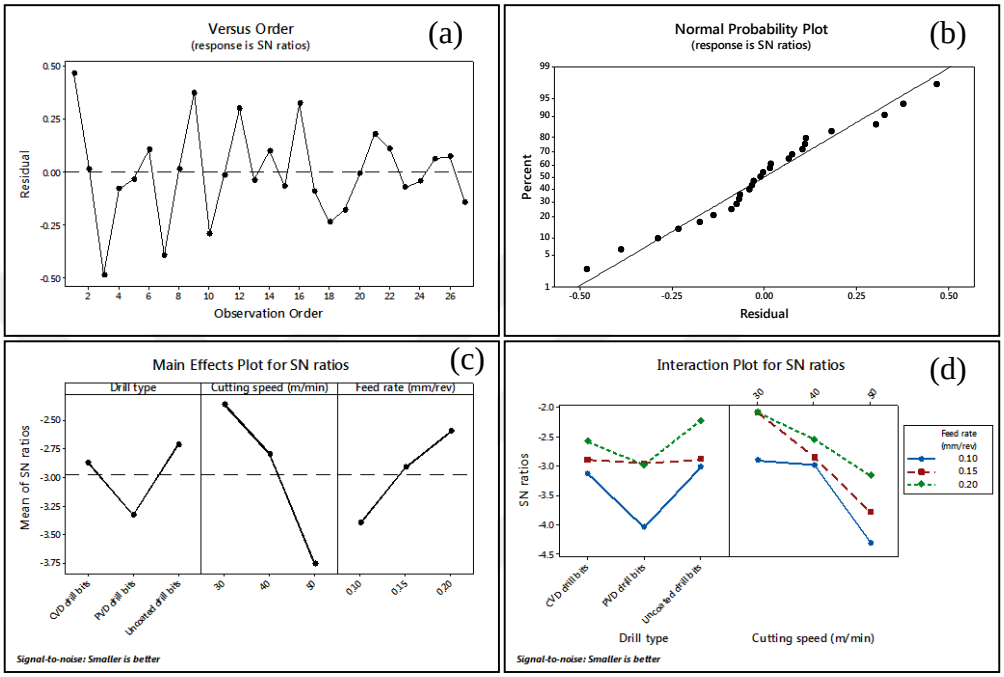

Figure 6.35. (a) Versus order plot for S/N ratio, (b) normal probability plot for S/N ratio, (c) main effects plot for S/N ratio and (d) interaction plot for the S/N ration; for the delamination factor while the drilling of Mg/SiC/GNPs MC.

6.6.2.3. ANOVA and Regression Analysis for Delamination Factor While Drilling of Hybrid Mg/SiC/GNPs MC

Derivative from the ANOVA outcome for the delamination factor whilst the drilling of the hybrid Mg/SiC/GNPs MC are indicated in the Table 6.17. The analyses were done at a 5% significance level and the confidence level of (95%). With according to the Table 6.17, the majority impactful factor on the delamination was the cutting velocity factor (V_C) with the contribution rate of (48.79%), which is tracked by the feed rate (f) (16.63%) and after that the drill coating category (C_T) (10.33%).

Table 6.17. The ANOVA analysis outcome for the delamination factor (hybrid Mg/SiC/GNPs MC).

Variance source	DF	SS	MS	F-value	P-value	Contribution (%)
V_c	**1**	**0.233472**	**0.233472**	**45.34**	**0.000**	**48.79%**
f	1	0.079600	0.079600	15.46	0.001	16.63%
C_T	2	0.49430	0.024715	4.80	0.024	10.33%
V_c *V_c	1	0.014933	0.014933	2.90	0.109	3.12%
***f* f**	1	0.001483	0.001483	0.29	0.599	0.31%
V_c *f	1	0.003468	0.003468	0.67	0.425	0.72%
V_c * C_T	2	0.012259	0.006129	1.19	0.331	2.56%
***f* * C_T**	2	0.006686	0.003343	0.65	0.536	1.40%
Error	15	0.077236	0.005149			16.14%
Total	26	0.478568				100%

DF: Degree of freedom, (SS): Sum of squares, MS: Mean square.
V_C: Cutting speed factor, (*f*): Feed rate factor, C_T: Drill type factor. **(R-sq=83.86%)**

Stand on the predictive formulas that were created for the full quadratic regression models to make a prediction for the delamination factor values while the drilling of the hybrid Mg/SiC/GNPs MC for the different drill bit categories are given and shown below.

- The regression formula for the delamination factor whiles the employment of the uncoated drill bits:

$$f_d = 1.867 - 0.025V_c - 1.83f + 0.000499V_c^2 + 6.3f^2 - 0.034V_cf \quad (6.23)$$

- The regression formula for the delamination factor whiles the employment of the PVD-coated drill bits:

$$f_d = 2.065 - 0.0255V_c - 2.34f + 0.000499V_c^2 + 6.3f^2 - 0.034V_cf \quad (6.24)$$

- The regression formula for the delamination factor whiles the employment of the CVD-coated drill bits:

$$f_d = 1.618 - 0.0197V_c - 1.4f + 0.000499V_c^2 + 6.3f^2 - 0.034V_cf \quad (6.25)$$

Where the f_d is the delamination factor, then the V_C is the cutting velocity and after that the f is the feed rate. The comparison of the predicted (based on the full quadratic regression models is then given in the equations of 6.23, 6.24 and 6.25) and experimental outcome were, then available in Figure 6.36 for the delamination factor (R^2=0.8386) with respect to the experiment order. This outcome exposed that the regression models could be applied technically and successfully in the predictions of the delamination factor through the drilling of hybrid Mg/SiC/GNPs MC.

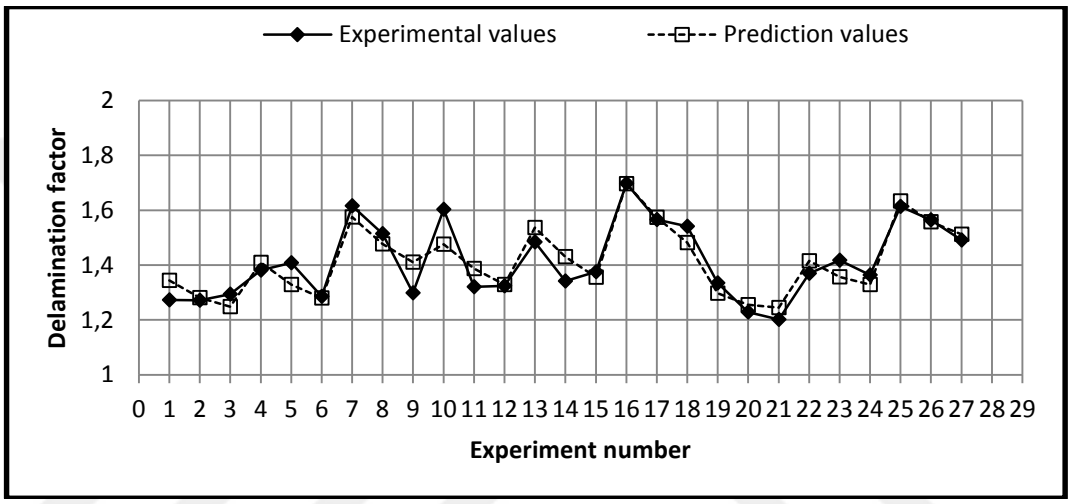

Figure 6.36. Comparison plot of the experimental and predicted outcome for f_d (R^2=0.8386) through the drilling of hybrid Mg/SiC/GNPs MC.

6.7. DRILLED SUBSURFACES AND PRODUCED CHIP MORPHOLOGY

6.7.1. Drilled Surfaces and Produced Chip Morphology While the Drilling of Mg/GNPs MC

Foundation on the Taguchi's analysis of the thrust force, the optimal cases were selected to scrutinize the drilled sub-surfaces and produced chip morphology, and also to monitor and evaluate the delamination formation at the boundaries of the drilled holes.

Based on SEM that had been utilized to monitor and examine the drilled surfaces. The high cutting velocity that causes the inclusive surface damage by reason of the high cutting contact stresses, and also fine grooves cracks were observed, which were attributable to the strain hardening of the Mg matrix.

As seen and further indicated in Figure 6.37 (a) the SEM image of the drilled surface at V_C=50 m/min and f=0.10 mm/rev while the employment of the uncoated drill. The image illustrates the scratches that have been shaped in the vertical pathway of the tool bit during the drilling, the fine grooves, and the BUE, which were by reason of the nature of the matrix (Mg).

Furthermore, for the reason of the heat produced whiles the drilling, a division of oxidation layers had appeared. It could be asserted based on examination that the surfaces created by the uncoated drills were poor with the fine grooves, which have an outcome on the surface excellence in an undesirable manner.

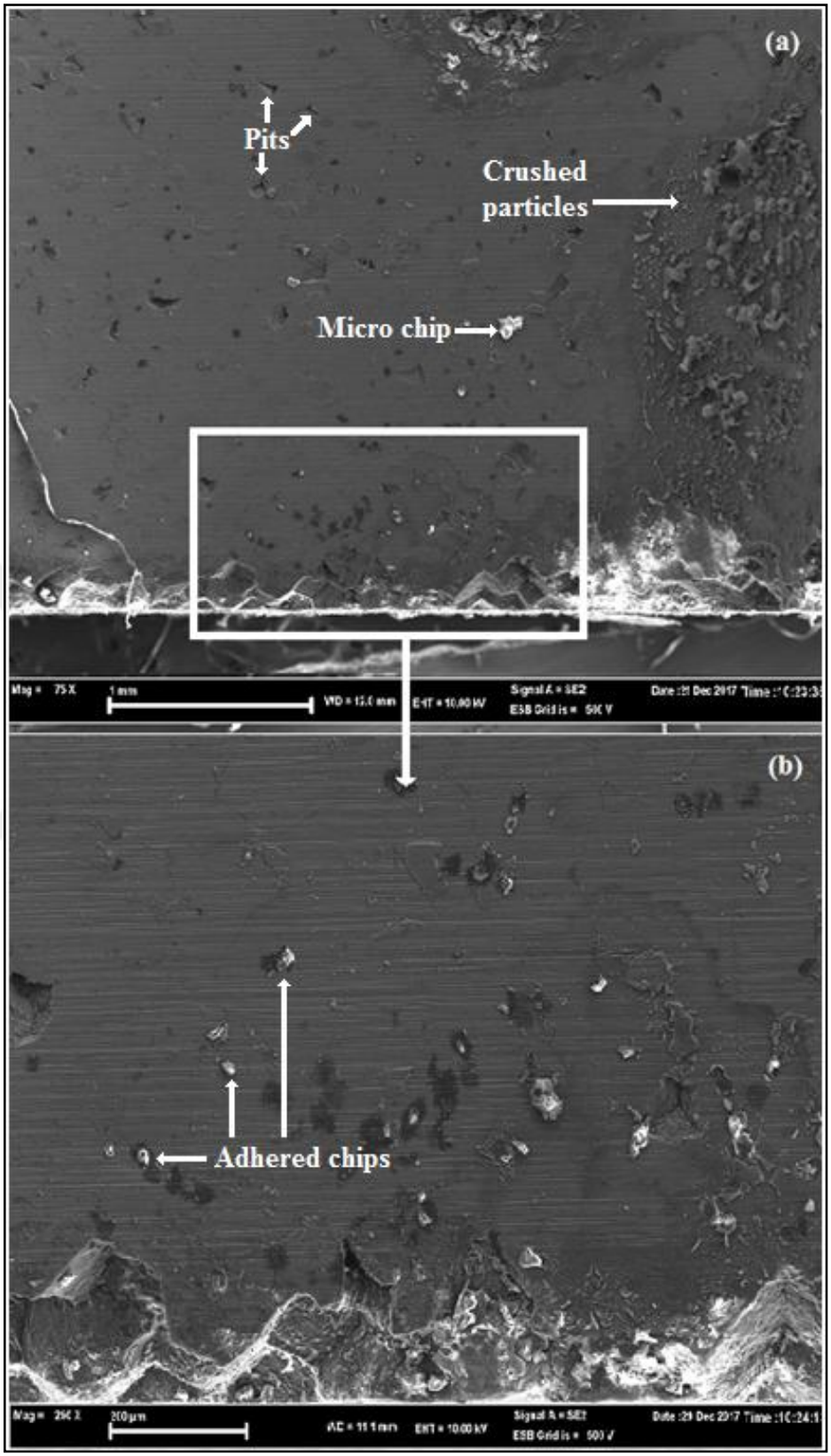

Figure 6.37. The SEM image of the drilled surface while the employment of uncoated drills at V_C=50m/min and f=0.10mm/rev, whilst the drilling of the Mg/GNPs MC.

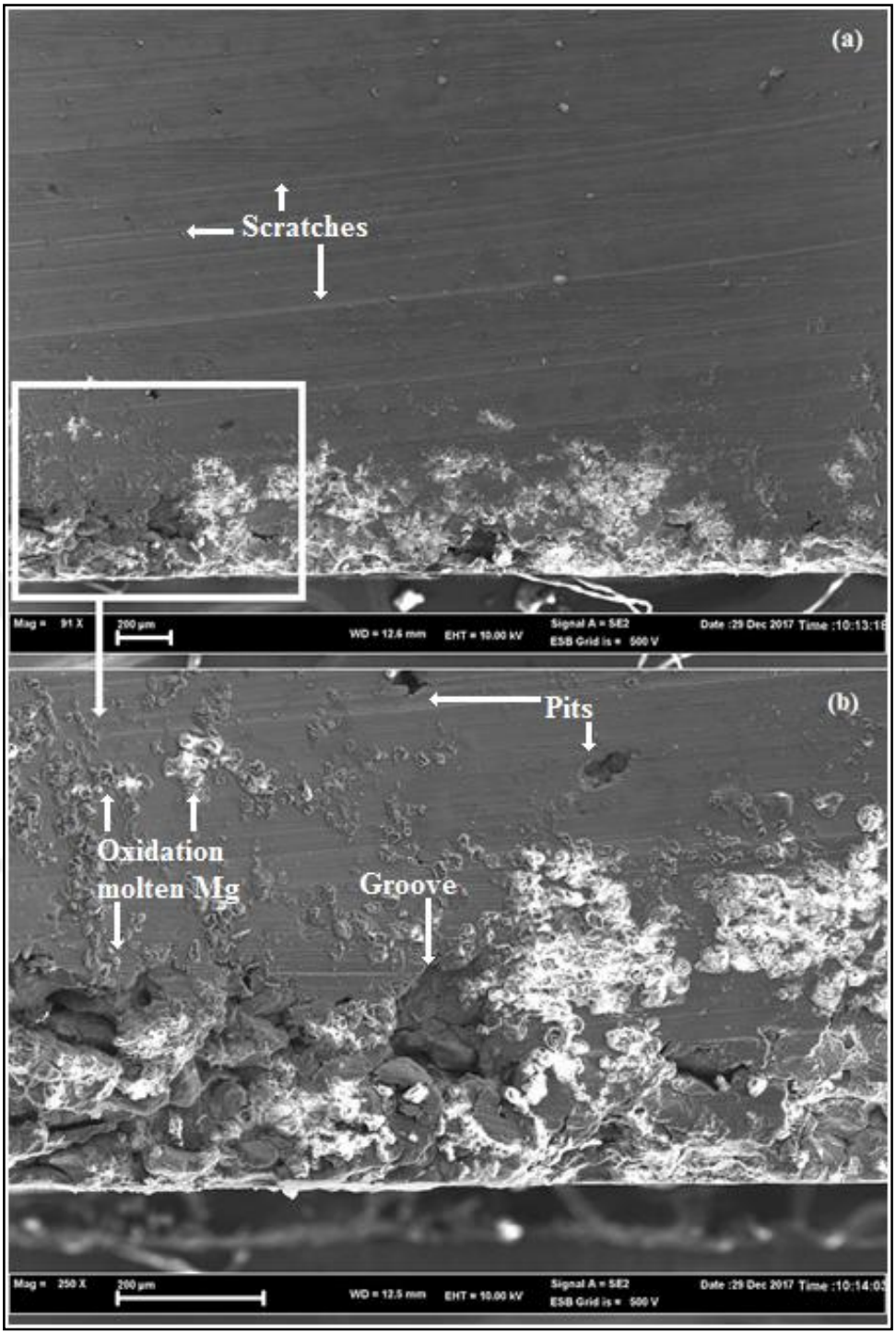

Figure 6.38. SEM image of drilled surface while the employment of the PVD-coated drills at V_C=50 m/min and f=0.10 mm/rev, whilst the drilling of the Mg/GNPs MC.

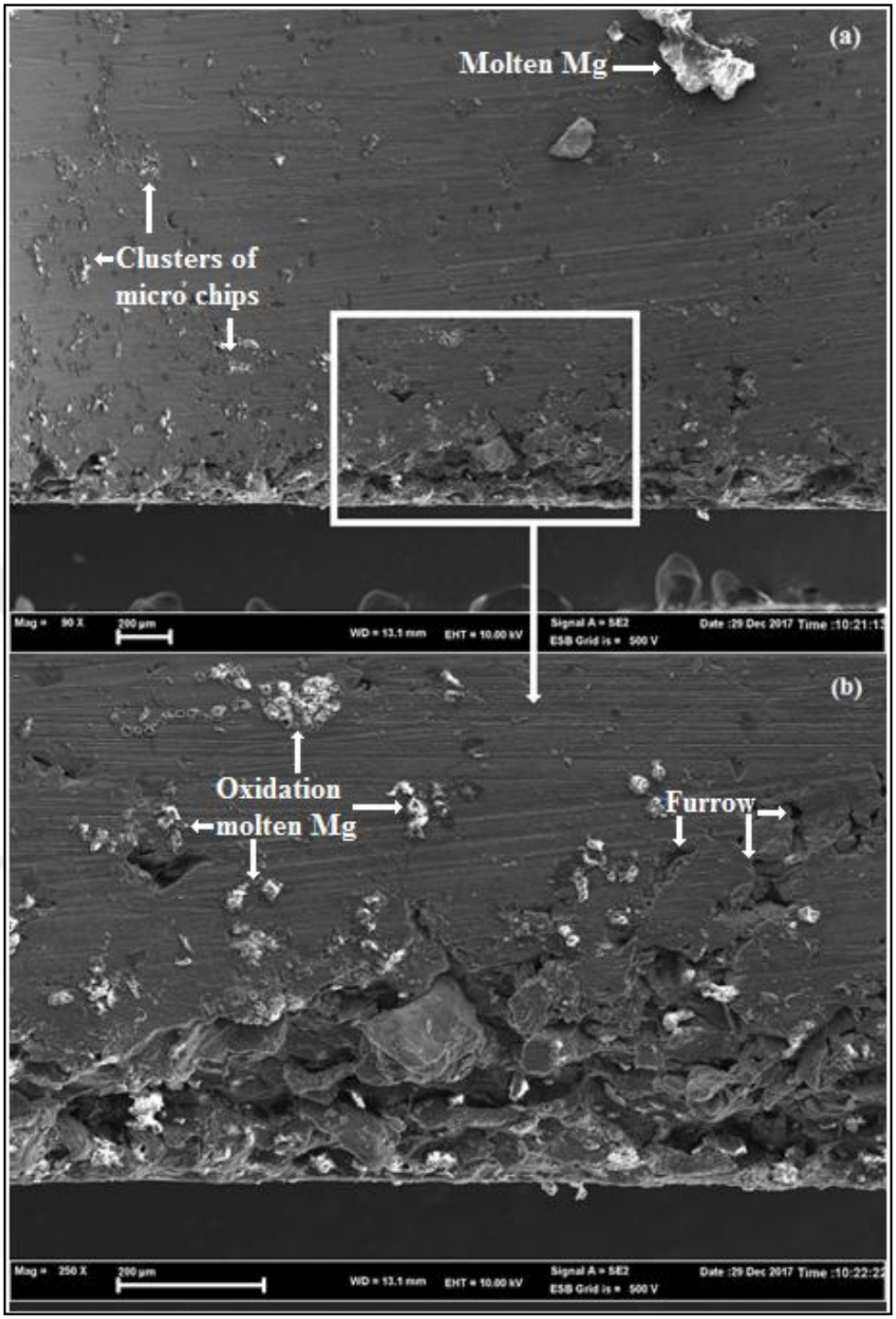

Figure 6.39. SEM image of machined surface while the employment of the CVD-coated drills at V_C=50 m/min and f=0.10 mm/rev, whilst the drilling of the Mg/GNPs MC.

Figure 6.37 (b) reveals push-down category of the delamination at the periphery of the drilled hole. The uncut depth under the drill tends to have the capacity to break the inter-layer bond in the locale in the region of the hole edges. As the drill comes

up to the last division of the uncut depth layer, the uncut depth becomes lesser and the confrontation to the deformation diminishes. Before the last depth is completely break through by the drill, the pressure surpasses the inter-layer bond potency and the delamination then happen.

Accordance to the SEM image of the drilled surface while the appliance of the PVD-coated drill bit at V_C=50 m/min and f=0.10 mm/rev that is revealed in Figure 6.38. The hole drilled surface is then seen as smoother with a little extent of the BUE, this is associated to the tough coating layer (TiN) over the drill bit's surface, which works to diminish the BUE phenomenon.

As noticed from Figure 6.39 that reveals the SEM image of the drilled surface at Vc=50 m/min and f=0.10 mm/rev while employing the CVD-coated drill bit, the feed scratches were visibly clear on the machined surface of the MMC, likewise a tiny quantity of the BUE, fine grooves, and scratches were observed.

The chip configuration whilst machining extremely relies on the process parameters like; the cutting velocity, the feed and the depth of cut. Throughout the drilling, chips were collected by income of the function of examining the characteristics of the chip. The low magnification of the optic images of the chip which were formed throughout the drilling of the Mg/GNPs MC which are been publicized in Figure 6.40(a-c). Commencing from the profile of the chip that could be confidential as the saw-toothed chips short category [8,26,73]. The chip configuration whiles the drilling that is gone along with a very harsh plastic deformation at the shear region and this owes to the lack of the adequate ductility of the workpiece material, then the crack initiation limits the deformation. As well, the adding of the GNPs increase the brittleness of the MMC, and by this reason the formed chip was short.

The hasty tool wear consequence in changing the tool geometry all the way through the machining, which directly influence the environment in the deformation sector that in turn, had been affecting whether continuous, or semi-continuous chip that were created.

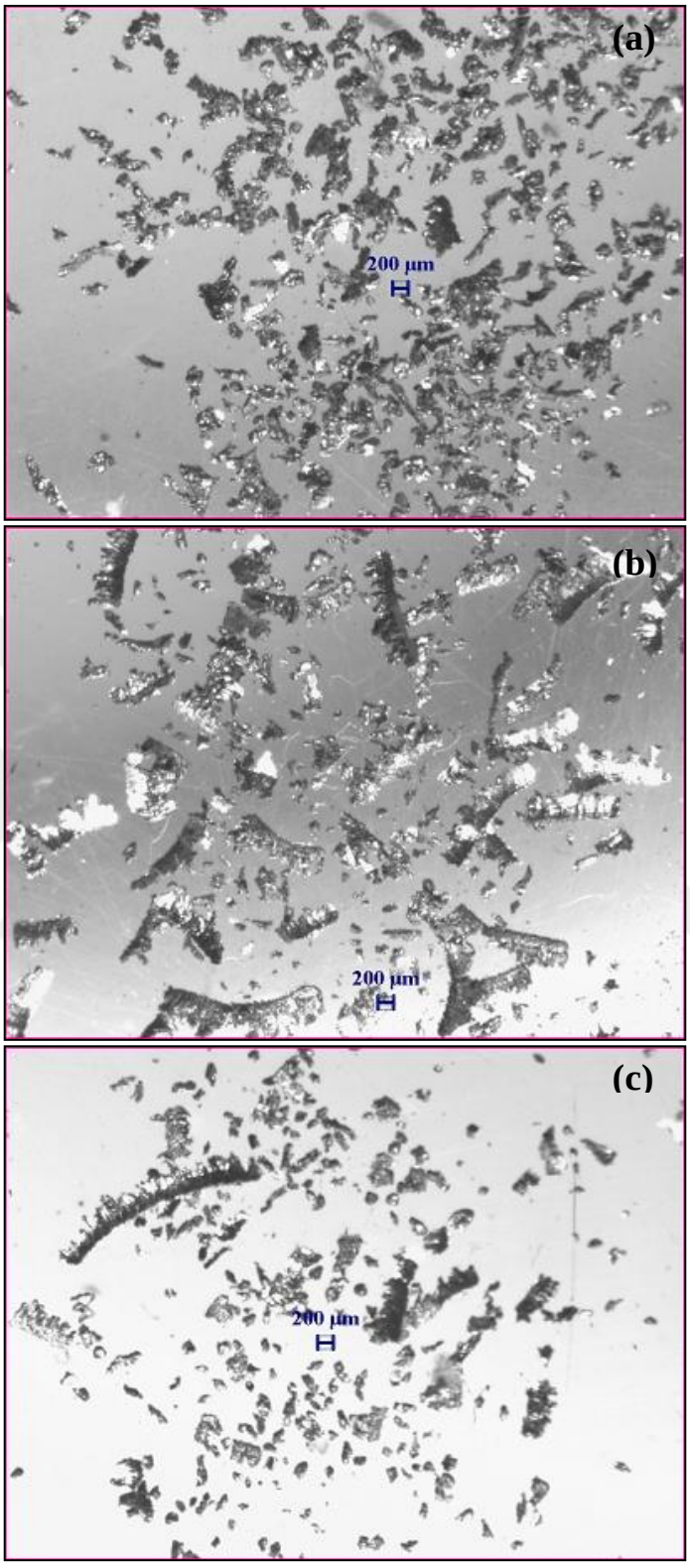

Figure 6.40. Low magnification optic image for the formed chip while the utilization of: (a) uncoated, (b) PVD-coated, and (c) CVD-coated drills at V_C=50 m/min and f=0.10 mm/rev, whilst the drilling of the Mg/GNPs MC.

6.7.2. Drilled Surfaces and the Produced Chip Morphology While the Drilling of Hybrid Mg/SiC/GNPs MC

Precisely with a careful observation of the drilled surface that demonstrates the removed SiC particles which were rubbed on the drilled surface caused scratches, as revealed in Figures 6.41, 6.42 and 6.43 for the drilled surfaces whilst the drilling of the hybrid Mg/SiC/GNPs MC. In addition, the micro-cracks were created by reason of the strain harden of the Mg matrix.

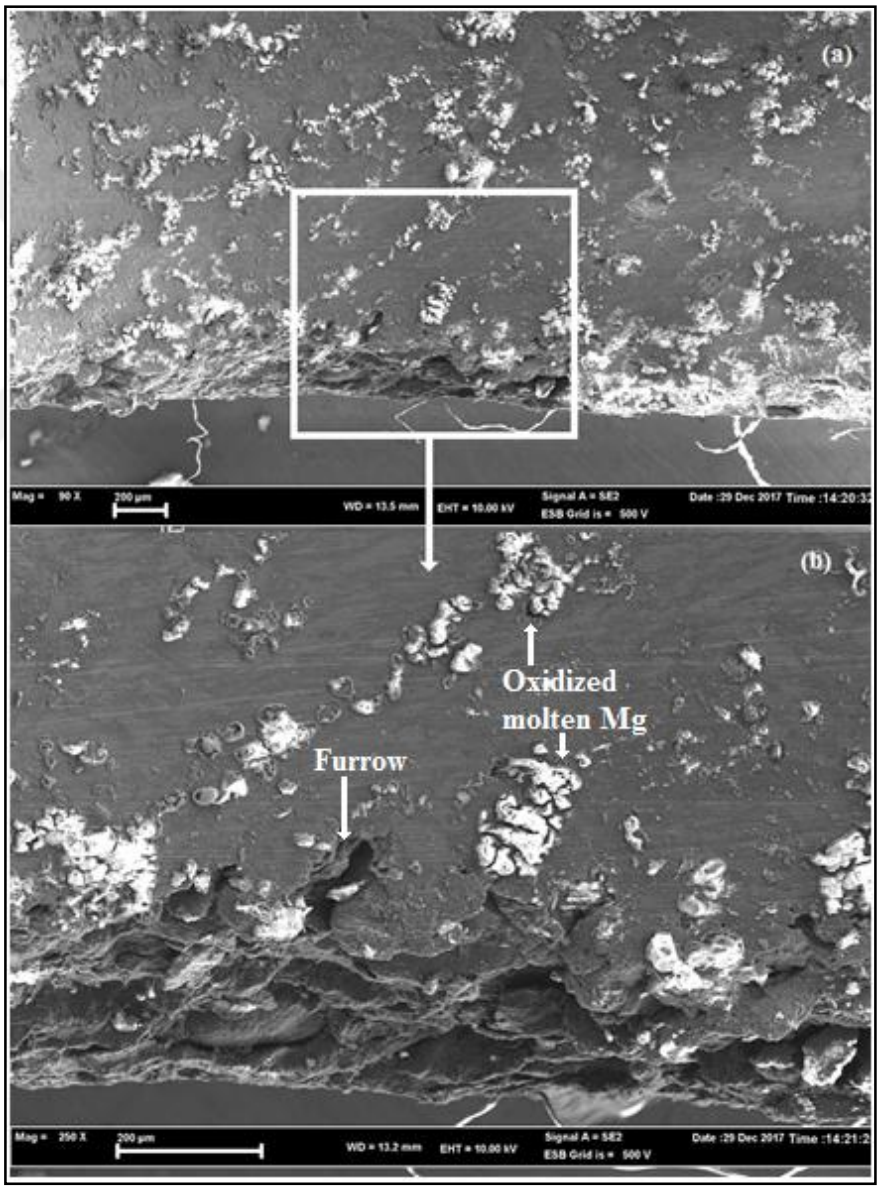

Figure 6.41. SEM image of drilled surface when using uncoated drill bit at V_C=50 m/min and f=0.10 mm/rev, whilst the drilling of hybrid Mg/SiC/GNPs MC.

The cracks, which were observed in the SEM images were obtained in the Figure 6.42 are for the reason of the strain hardening outcome of the matrix material. Whilst a numeral of micro-cracks gather simultaneously close up to the SiC particle, it therefore created a void around where the SiC particle placed, and at that time the grooves were formed.

It suggested that the grooves are attributable to the SiC particles being pulled away from the composite and dragged over the machined surface, which causes the scratches. The dislodged abrasive particles have created grooves on the surface of the composite just about when the tool edge is attached the hard and the coarse particles. The happening of the pulling-out in such way, bring into being to have increased as the contact load increased [28].

Once the SiC particles are pulling-out while the drilling procedure, the cracks and the pits are shaped on the surface and cause a decline in the surface finishing. According to A. R. Ahamed et al. [41], they reported that the hard SiC and the B_4C particles were broken away from each other from the surface cased in a quantity of cavities on the drilled surface while the drilling procedure of the hybrid MMCs was carried-out.

The observation of the damaged surface in Figure 6.42 reveals that an elevated cutting velocity causes an extensive surface damage in the composites by reason of the high contact load [36]. Although drilling research on the machinability of the hybrid Al/SiC/Gr MMC that was conducted by Y. Altunpak et al. [39], they stated that the micro-cracks and pits were observed on the drilled composite. Figure 6.42 (b) specified the severe and the thick micro-cracks, which has resulted to the exposure of the SiC particles.

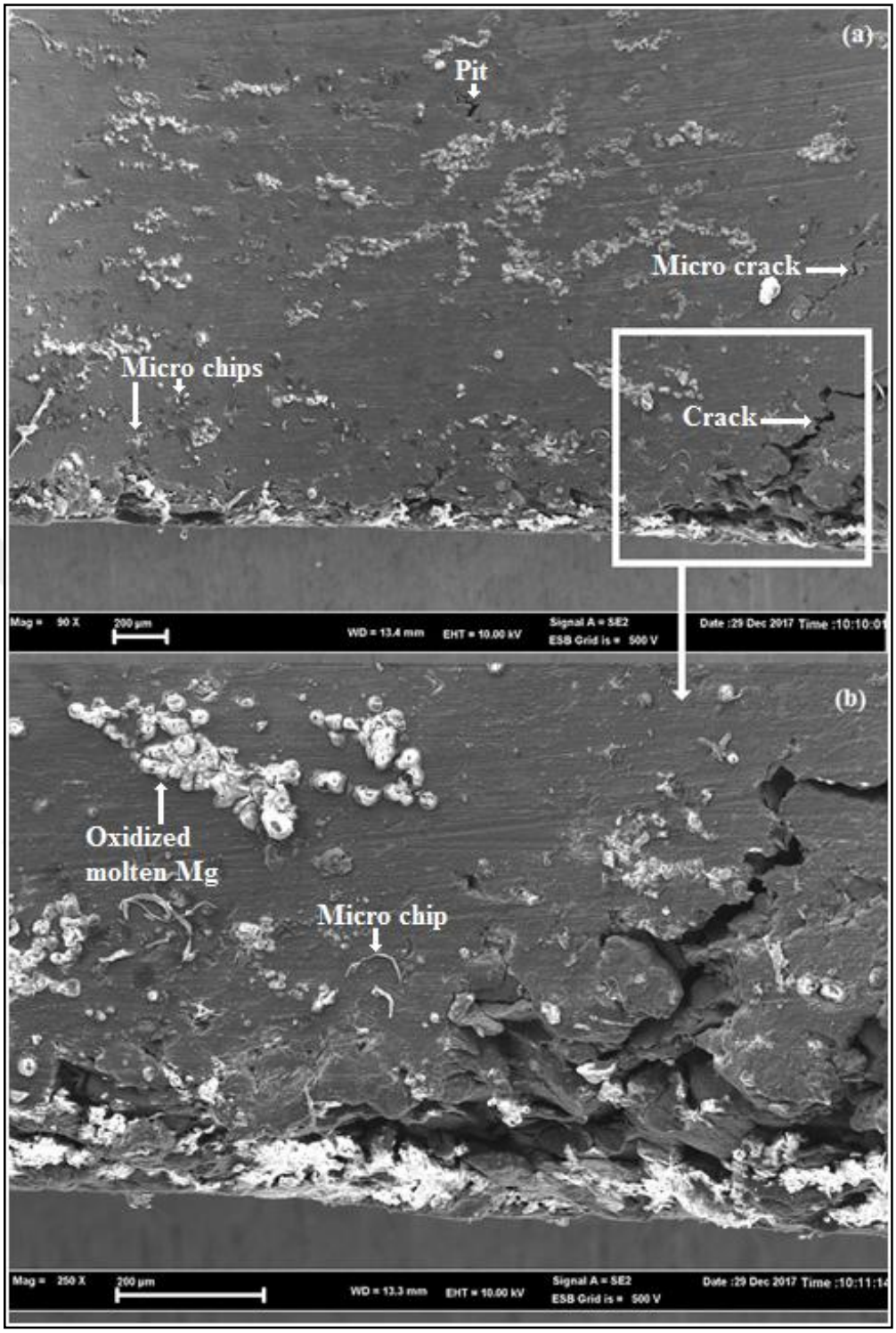

Figure 6.42. SEM image of drilled surface while the employment of PVD-coated drill at V_C=50 m/min and f=0.10 mm/rev, while drilling of hybrid Mg/SiC/GNPs MC.

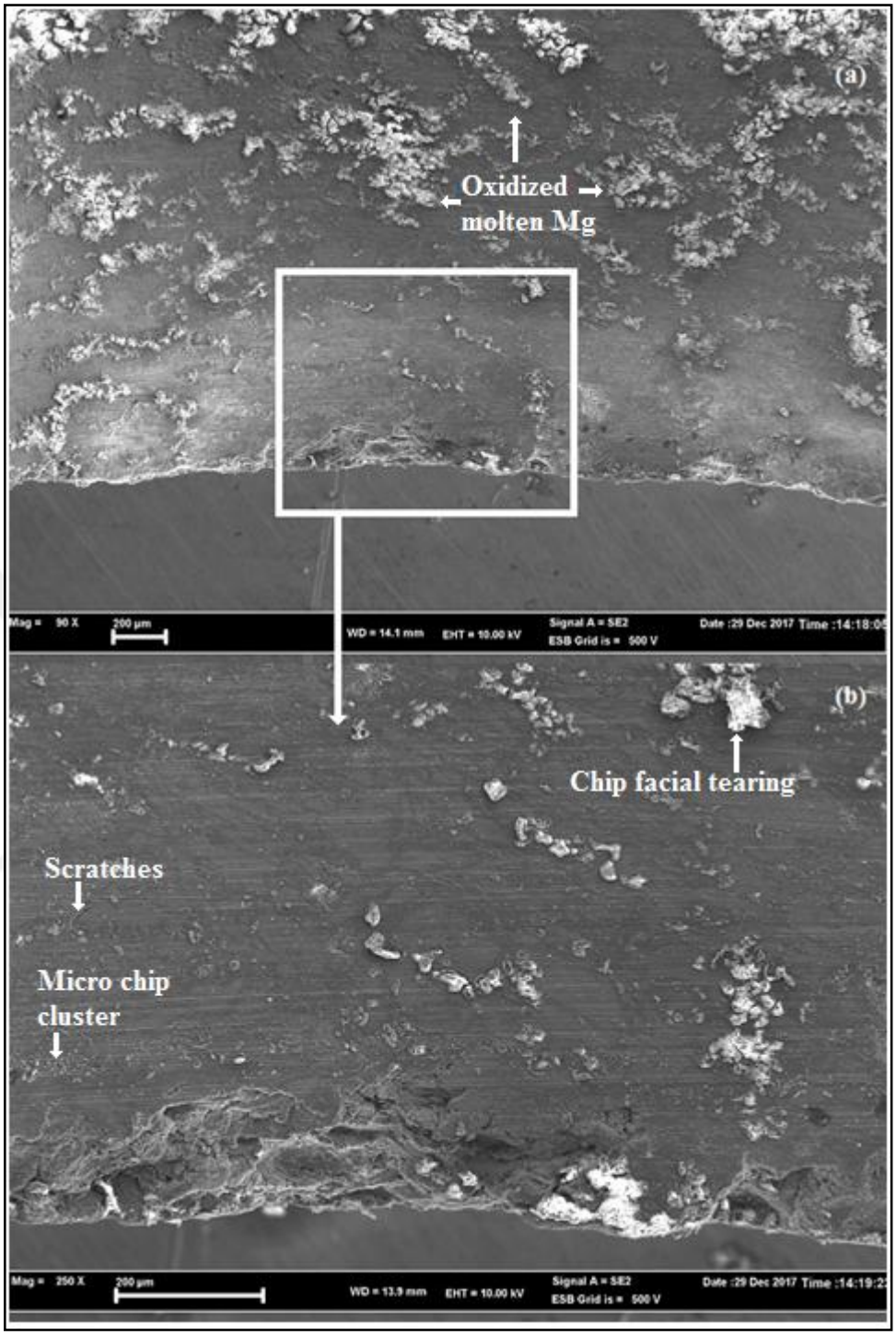

Figure 6.43. SEM image of the drilled surface during the employment of the CVD-coated drill at V_C=50 m/min and f=0.10 mm/rev, while the drilling of the hybrid Mg/SiC/GNPs MC.

Generally, the performing of coated drills is better whilst compared to the uncoated drills at the diverse feed rate and the cutting velocity levels which are applied in this research study, the similar result was achieved by A. Muniaraj et al. [71].

Furthermore, the coated drills showed the smoother machined surfaces as publicized in Figures 6.42 and 6.43, and the uncoated drills presented an additional BUE amount more than the coated drills, which enabled the participation of the coarsely drilled surfaces.

Commencing the drilling of Mg-MCs reinforced with the SiC particles, the chip shaped were the saw tooth and the segmental chip as publicized in Figure 6.44 (a-c). The adding of the SiC particle into the Mg matrix has caused a decline in the ductility and this formulates a composite superlative for forming of such segmental chip, which easily discarded once the drilling procedure is going on. This could be valuable to the machinability characteristics. Typically, the short chip that was produced in this research study by reason of the pullout of the SiC particles and the crack propagation along the SiC and matrix interface [70].

Through the findings, it becomes visible from the images in Figure 6.44 that the chatter of the SiC particles is uniform among the chip, which can perform as the stress raisers to assist the crack transmission. It can be asserted that the explanation for the formation of the segmental chip category whiles the drilling of the Mg/SiC/GNPs is the abrasive SiC particles that work as the obstacles on the pathway of the plastic deformation of the Mg matrix. G. S. Samy and S. T. Kumaran [36] stated that the high temperature generated in the drilling of the MMCs explicitly has an effect on the chip formation characteristics. The raise in the heat in the cutting locale guides to the foundation of the short chip. A. Muniaraj et al. [71] found that the chip shaped within the drilling of the hybrid composite through utilization of the coated carbide drills are shorter by the length, discontinuous and the chain of the chips segments that are attached to each other. Foundation on the findings by J. T. Lin et al. [7], they concluded that the decline in the ductility of the composite by the adding of the SiC particles assists to diminish the configuration of semi-continuous category of the chip; this reaches the better chip control.

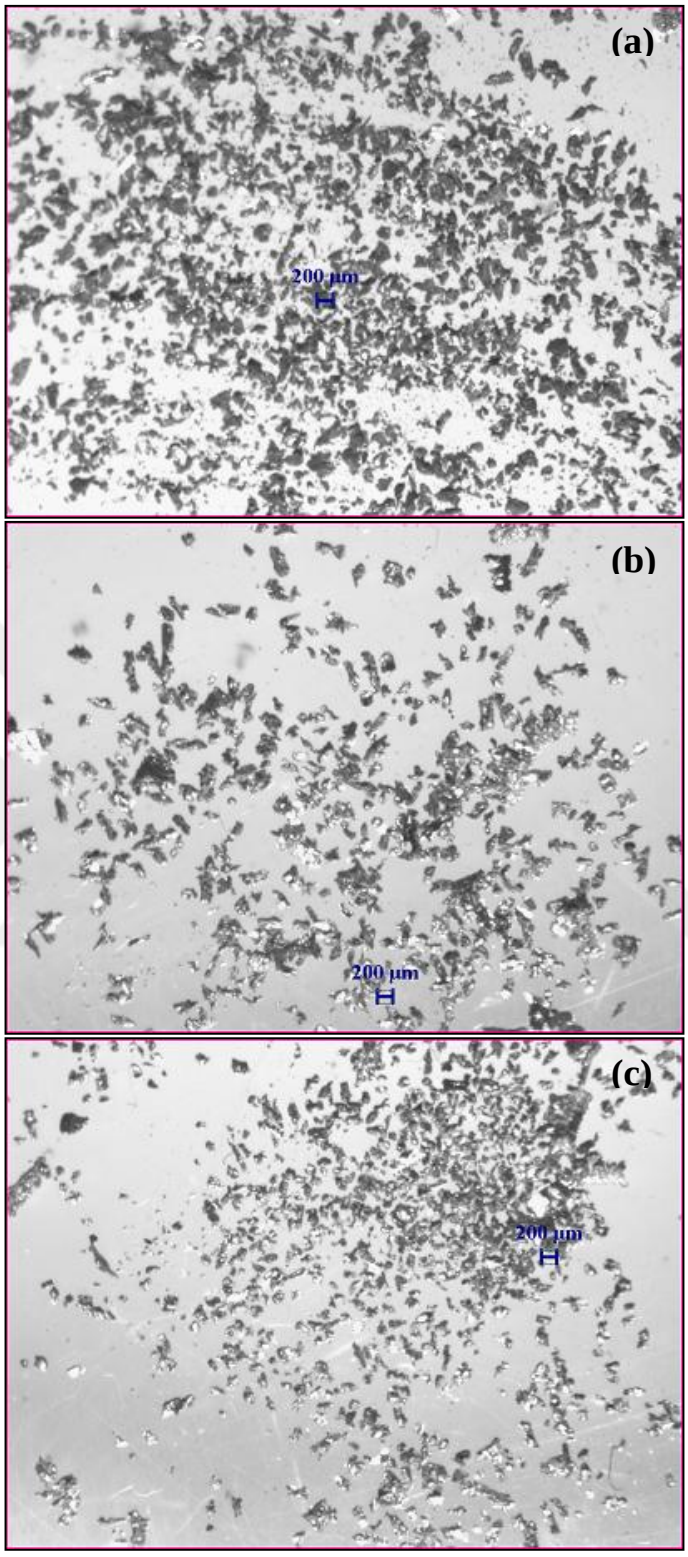

Figure 6.44. The low magnification optic image for the formed chip while the employment of; (a) uncoated, (b) PVD-coated, and (c) CVD-coated drill bits at V_C=50 m/min and f=0.10 mm/rev, whilst the drilling of the hybrid Mg/SiC/GNPs MC.

As experiential in Figure 6.44, an importance amount of the powdery chips were formed; this state could be credited to the rise in the brittleness of the composite that was based on the adding up of the SiC_P and the GNPs, and to the rubbing amid the tool cutting edge and the drilled surface. In addition, we could propose that the SiC particles into the composites performing as the chip breakers and that are why the short and powdery chips were formed.

6.8. WORN DRILL BITS OPTICAL INVESTIGATION

Certain to the Taguchi's analysis for the thrust force, the optimal and the worse belongings were selected to scrutinize the tool wear through the low magnification optical examination.

6.8.1. Worn Drill Bits Optical Investigation While Drilling of Mg/GNPs MC

Providing of the effect of the harsh conditions of the pressure and the temperature at the drill cutting edges get in contact with the composite and formed chip, the wear of the cutting tool whilst the machining is by all means unavoidable. The damage to the tool edge may take place prematurely and on a large level, or progressively, leading to the finale of the tool life. The tool wear brings undesirable consequences, for instance, the diminution in the tool edge strength, increment in tool load and the power utilization, increased cutting temperature, the drawbacks in the surface finishing, reduced dimensional precision, and finally the deprivation of the productivity efficiency.

The wear mechanisms of the carbide drills were employed in this research study can be categorized into the abrasive wear, the adhesion wear, and the BUE layer that is covered the chisel edge for the uncoated drill bits as publicized in Figure 6.45. X. Wei et al. [40] reported that the wear modes of the carbide tool through the drilling of MMC were classified to the abrasive, adhesion wears and the micro-breakage on the tool surface. The soften Mg while the dry drilling spontaneously transmitted to the bit, and adhered on the drill chisel edge as publicized in Figure 6.45 (b). The adhered Mg layers roofed the chisel edge of the drill, thus, a prominent BUE was

seen to have been formed, which altered the geometry of the drill by increasing its diameter, prompting the feed rate to increase.

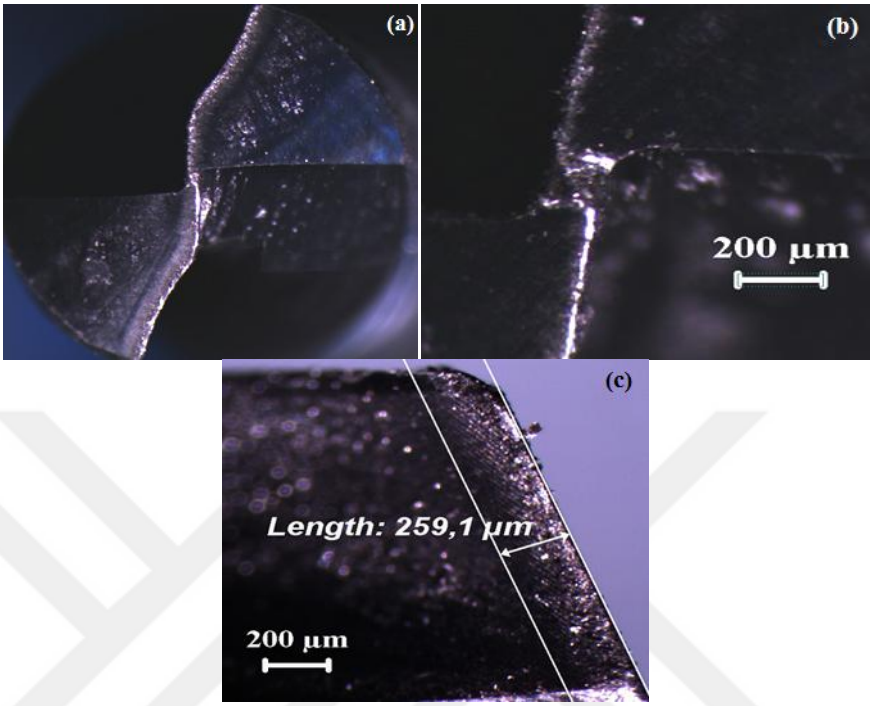

Figure 6.45. Low magnification optical image: (a) top view, (b) chisel edge, and (c) flank face for the worn uncoated drill bit at V_C=30 m/min and f=0.20 mm/rev, while the drilling of Mg/GNPs MC.

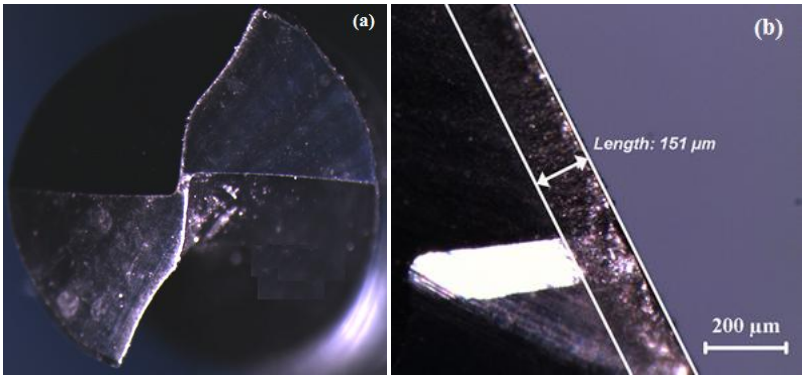

Figure 6.46. Low magnification optical image: (a) top view, and (b) flank face for the worn uncoated drill bit at V_C=50 m/min and f=0.10 mm/rev, while the drilling of the Mg/GNPs MC.

Furthermore, when utilization the higher cutting velocity with the low feed rate, the BUE configuration in the chisel edge is reduced which as publicized in Figure 6.46, also the flank wear width is reduced to 151µm. According to the outcome achieved

by A. Taskesen and K. Kutukde [72], the abrasive wear and the BUE were observed on the drills cutting edges, and the uncoated carbide drills were suffered from the BUE more than the coated (TiAlN) carbide drills.

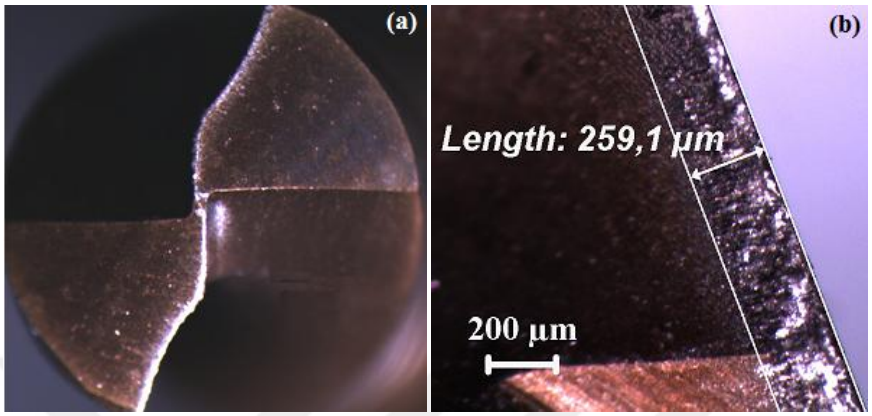

Figure 6.47. Low magnification optical image: (a) top view, and (b) flank face, for the worn PVD-coated drill bit at V_C=40 m/min and f=0.20 mm/rev, while the drilling of the Mg/GNPs MC.

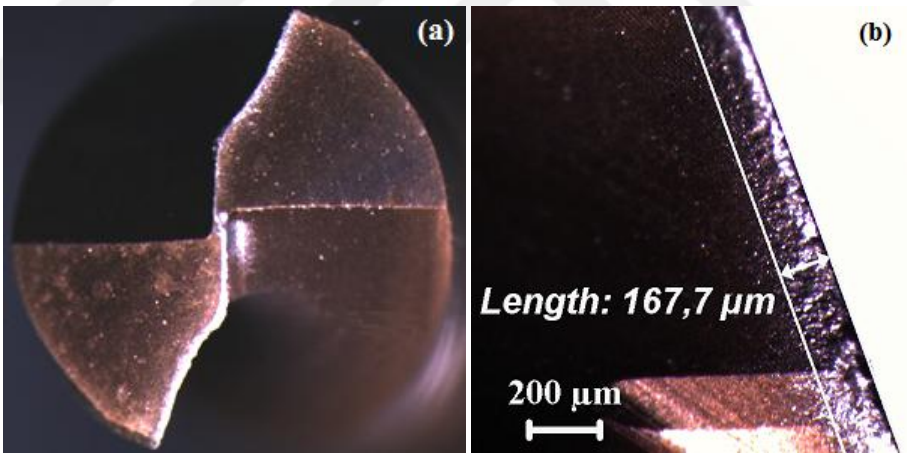

Figure 6.48. Low magnification optical image: (a) top view and (b) flank face, for the worn PVD-coated drill bit at V_C=50 m/min and f=0.10 mm/rev, while the drilling of the Mg/GNPs MC.

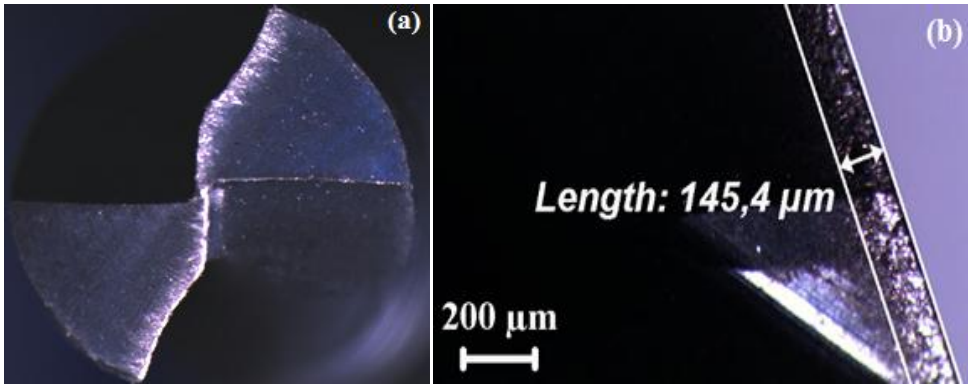

Figure 6.49. Low magnification optical image: (a) top view and (b) flank face, for the worn CVD-coated drill bit at V_C=30 m/min and f=0.20 mm/rev, while the drilling of the Mg/GNPs MC.

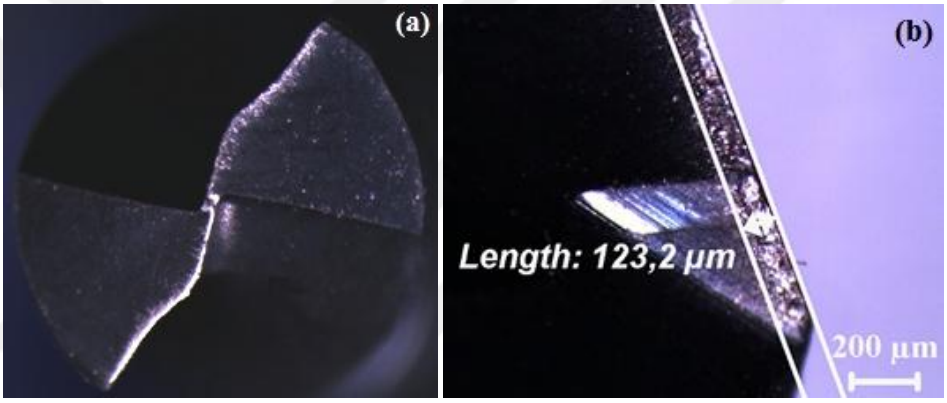

Figure 6.50. Low magnification optical image: (a) top view and (b) flank face, for the worn CVD-coated drill bit at V_C=50 m/min and f=0.10 mm/rev, while the drilling of the Mg/GNPs MC.

6.8.2. Worn Drill Bits Optical Investigation While Drilling of Hybrid Mg/SiC/GNPs MC

Essentially, the hardness of the reinforcement becomes a main parameter affecting the tool wear [64]. The figures 6.51-6.56 are presented the low magnification optical images for the worn drills were utilized for the drilling procedure of the hybrid Mg/SiC/GNPs MC.

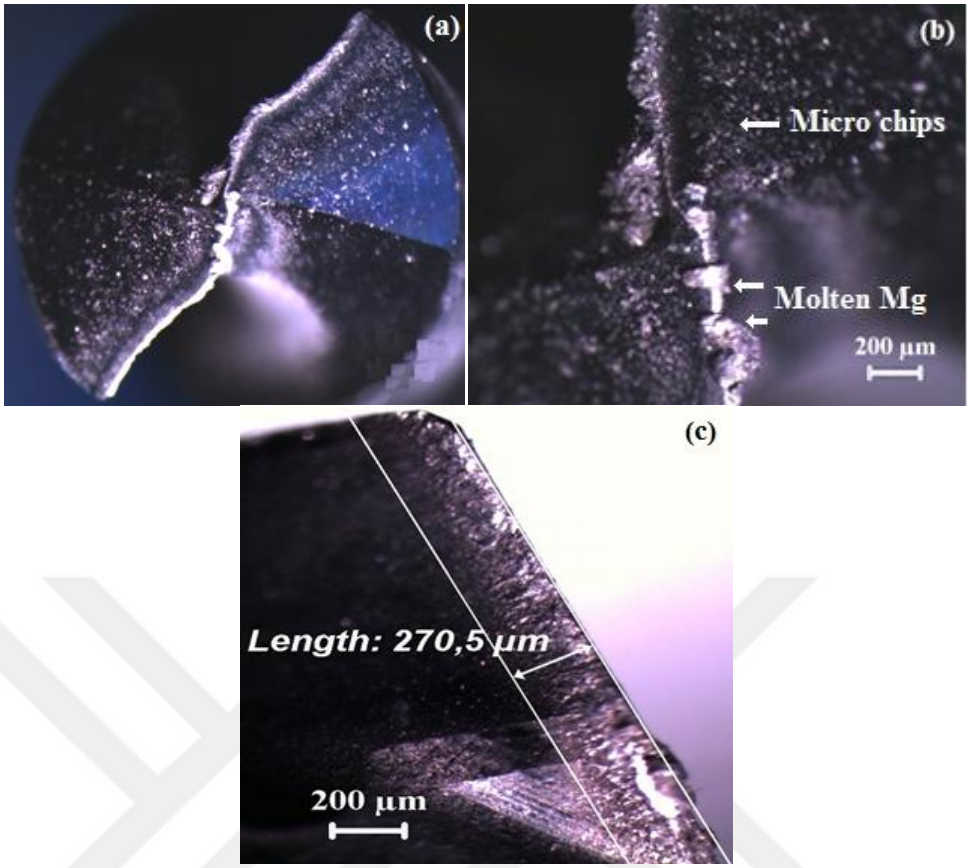

Figure 6.51. Low magnification optical image: (a) top view, (b) chisel edge, and (c) flank face for the worn uncoated drill bit at V_C=30 m/min and f=0.20 mm/rev, while drilling of the hybrid Mg/SiC/GNPs MC.

In Figure 6.51, the majority mechanism of wear is the abrasion on the flank face, and the trace of reinforcing particles is visibly clear in succession parallel to the cutting pathway, [41] obtained the similar result. The figure evidently shows the adhesion of Mg matrix on the flank face of the drill. It could be observed that the abrasive character of the SiC particles finds the flank wear. For the basis that the high load created at the tool and composite interface, the worn flank encourages the adhesion of the composite [12]. Along with this, another category of the chip configuration was observed, the stick-slip rubbing of the chip segment on the drill edge and the chisel that is clear visible in Figure 6.51 (b). This sort of rubbing causes a variant in the thrust force, and somewhat influences the mechanism of wear. Moreover, the reduction in the ductility of the composite composes the stick section of rubbing lesser than that of the slipping section through the chip formation progression.

Meanwhile, it as well found an extra significant abrasive wear than adhesive wear on the tool surfaces.

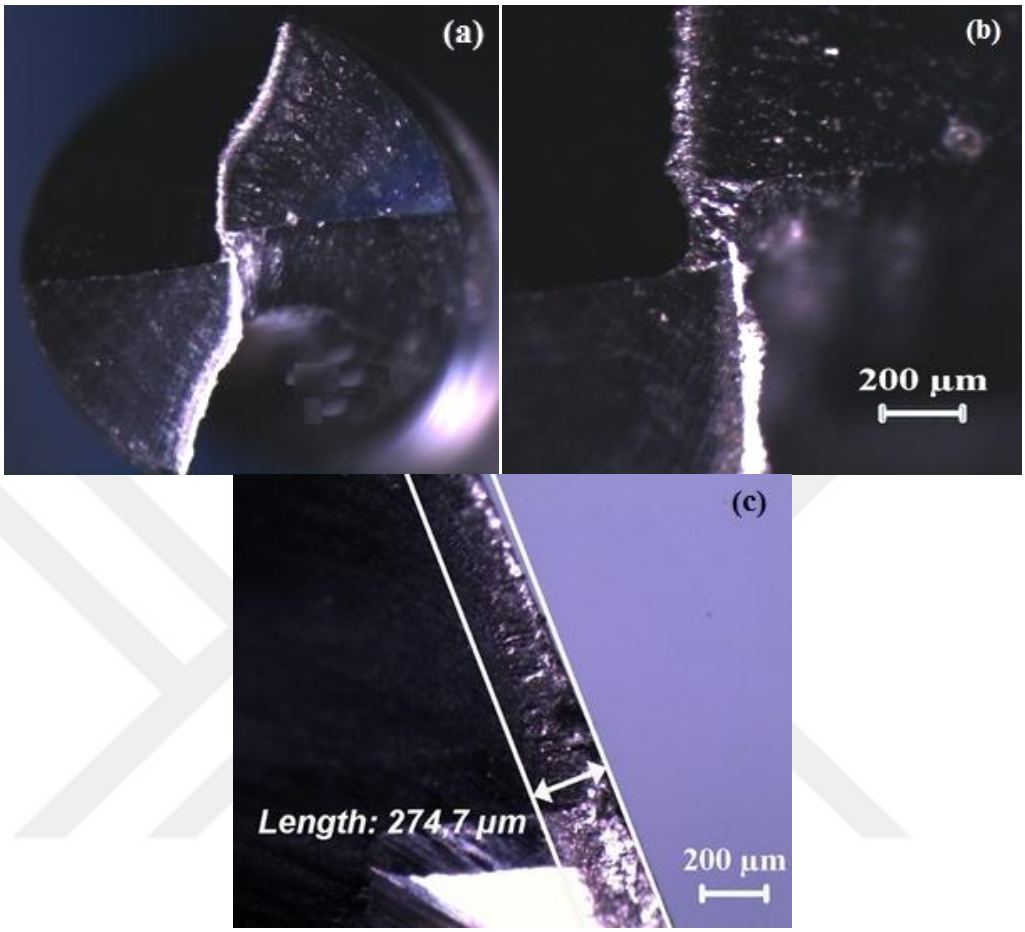

Figure 6.52. Low magnification optical image for: (a) top view, (b) chisel edge, and (c) flank face, for the worn uncoated drill bit at V_C=50 m/min and f=0.10 mm/rev, whilst the drilling of the hybrid Mg/SiC/GNPs MC.

Assertively, it could be seen from Figures 6.51 (c) and 6.52 (c) that the flank wear was created by the abrasive nature of the SiC particles [6,63]. We can advocate that the tool wear in the flank be caused by both the abrasive and adhesive wear mechanisms.

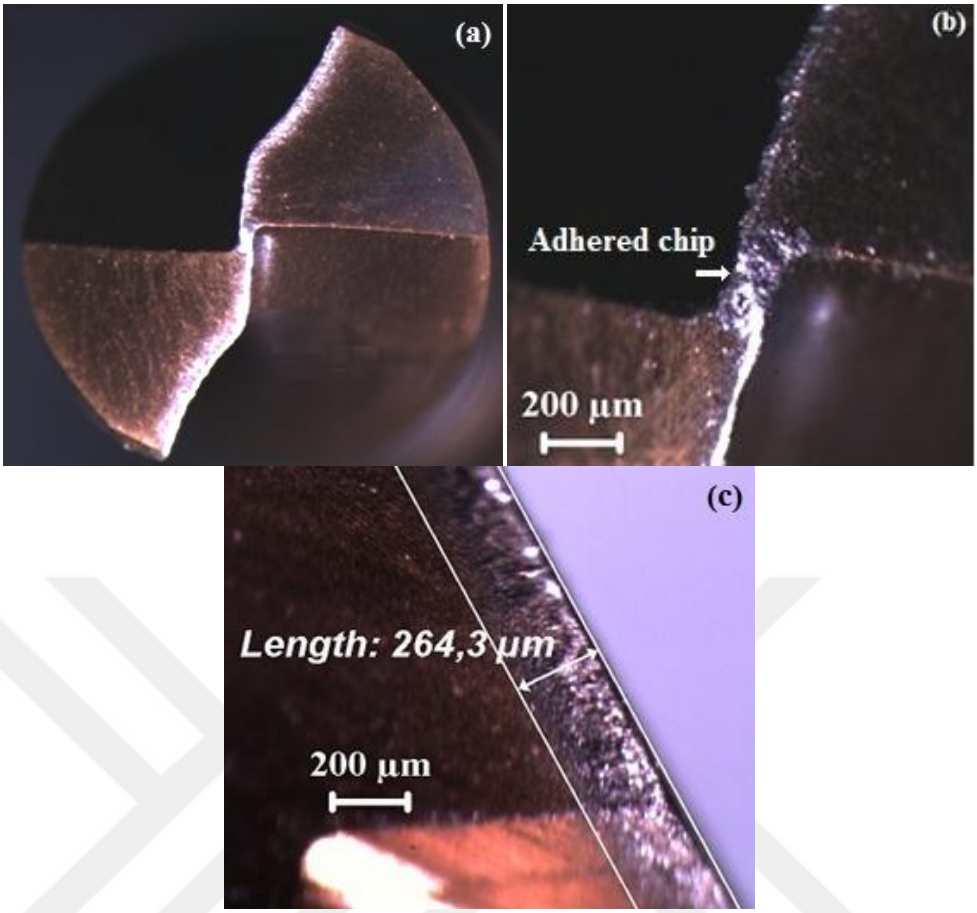

Figure 6.53. Low magnification optical image: (a) top view, (b) chisel edge, and (c) flank face, for the worn PVD-coated drill bit at V_C=30 m/min and f=0.20 mm/rev, whilst the drilling of the hybrid Mg/SiC/GNPs MC.

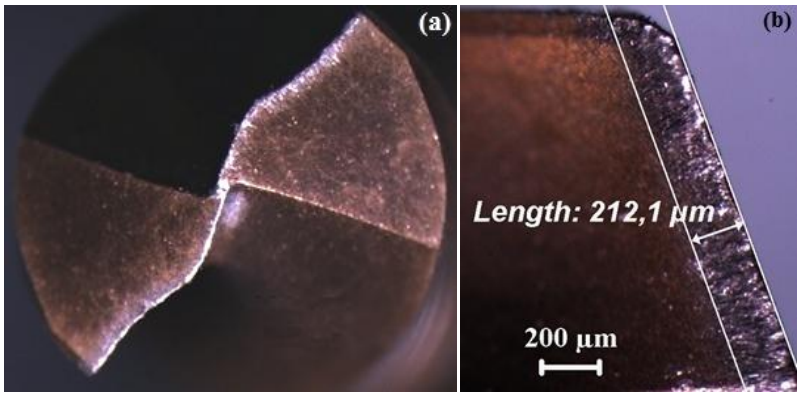

Figure 6.54. Low magnification optical image: (a) top view, and (b) flank face, for the worn PVD-coated drill bit at V_C=50 m/min and f=0.10 mm/rev, whilst the drilling of the hybrid Mg/SiC/GNPs MC.

As resulting from the Figures 6.53 and 6.54, be able to monitor that the BUE was formed typically on the tool's flank face and chisel edge. However, the image exists

in the Figure 6.54 (b) signifies that the prime wear mechanism was the abrasive, which created analogous to the cutting pathway by reason of the abrasive SiC particles action. However, with the PVD- and the CVD-coated carbide drill bits, considerably the less BUE formation that was observed than the uncoated drills, as observed in the Figures 6.51-6.56. The clarification is that the coated drills were disallowed the diffusion and the adhering activity through the making of the thermal barrier, the comparable results were reported by [72].

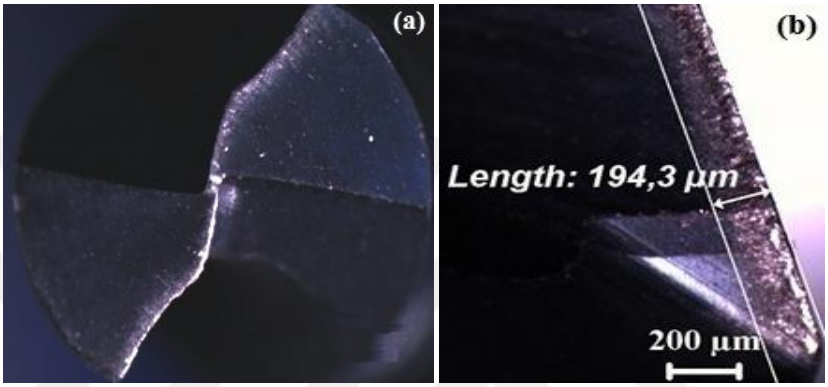

Figure 6.55. Low magnification optical image: (a) top view, and (b) flank face, for the worn CVD-coated drill bit at V_C=40 m/min and f=0.20 mm/rev, whilst the drilling of the hybrid Mg/SiC/GNPs MC.

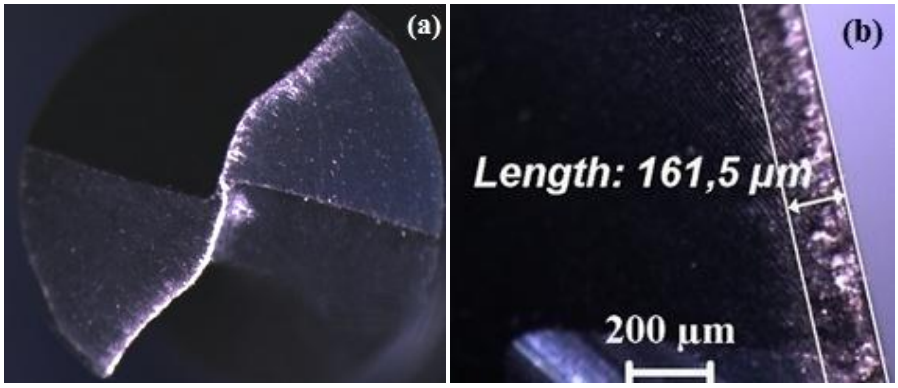

Figure 6.56. Low magnification optical image: (a) top view, and (b) flank face, for the worn CVD-coated drill bit at V_C=50m/min and f=0.10mm/rev, whilst the drilling of the hybrid Mg/SiC/GNPs MC.

Generally, the tool wear mechanisms that could be observed in the worn uncoated and coated carbide drills, which were utilized whist the drilling of the hybrid

Mg/SiC/GNPs MC, which are publicized in the Figures 6.51-6.56, the prime tool wear mechanisms are detailed and listed as follows:

1. Abrasive wear: the mechanical perform amid the composite, the shaped chip and the drill bit which was the mechanism that generated the abrasive wear. The obvious abrasive wear, which was created as a result of the sliding rubbing in the existence of rough reinforcement (SiC particles) that embedded into the Mg matrix and existed on the drill bit surfaces, so the tool material removed away by the mechanical perform of the harsh reinforcement particles in the contact interface moving above the tool face's surfaces.

2. Adhesion wear: the adhesion is referred to the combination occurrence in the action part amid the tool and the hybrid Mg/SiC/GNPs MC. The adhesive wear is caused by way of the cracking of the asperity intersections linking the cutting drill bit and the composite. In the drilling procedure, the rubbing amid the drill and the composite created masses of heat, which has soften the Mg, thus this raises the cutting resistance. The pieces of the composite that were taken away by the fracture in the contact part, then these pieces were consolidated on the drill edges, so the adhesive wear occurs. According to N. Muthukrishnan and J. P. Davim [75] they accomplished that the prime mechanism of the wear is the abrasion among the SiC reinforcing particles and the cutting tool material whilst the drilling of MMCs.

3. Built-up-edge (BUE): with the employment of coated drills, significantly less BUE configuration was observed once compared to the uncoated drills, as publicized in Figures 6.51-6.56. The rationalization for this is that the coated tools had disallowed the diffusion and the adhering doings through creation a thermal barrier.

4. Chisel edge wear: This was observed during the employment of the uncoated and coated drill tools, and the chisel edge was covered through the significance of BUE layers as publicized in Figures 6.51 (b), 6.52 (b) and 6.53(b), B. Mubaraki et al. [37] reported the same result.

CHAPTER 7

CONCLUSIONS AND RECOMMENDATIONS

In this chapter, foundation on the present thesis research the main conclusions are summarized, and furthermore followed by detailed recommendations for the future work.

7.1. CONCLUSIONS

This thesis research was presented analysis and evaluation assessments study of the drilling of Mg-MMCs. The presented examination and optimization succeeded effectively in the provision of an inclusive understanding to the Mg-MMCs drilling procedure machinability aspects. The comprehensive understanding have been achieved throughout systematic experimental investigations on the machinability of hybrid Mg-MMCs reinforced with the nano-sized of GNPs and the micro-sized of SiC particles. The parameters were taken into account in the experimental tests are the cutting velocity, feed rate and the coating category of carbide drills. foundation on the analyses and optimization of the microstructure, thrust force, torque, drilled surface roughness, delamination factor, drilled surface morphology, the chip formed morphology and ultimately the worn drills bits optical investigation: the conclusions could be analyzed as follow;

1. The Mg/0.25wt%GNPs and hybrid Mg/10wt%SiC/0.25wt%GNPs MMCs has been execellently fabricated through the employment of the powder metallurgy method, and the homogenous uniformity distribution of the SiC_P and GNPs into the Mg matrix was recognized and confirmed through the SEM examination, and the microstructure was without of the macro defects.

2. The Drilling of the Mg/GNPs MMCs:

- The thrust forces as well as the surface roughness were extremely reliant on the feed rate and the cutting velocity parameters whist the employment of uncoated and coated carbide bits.

- Based on the results outcome, the thrust forces significantly amplified with the increment in the feed rate, and decreased along with a raise in the cutting velocity. The uncoated carbide bits produced a high thrust forces much more than the coated carbide bits.

- An increment in the feed rate and the cutting velocity has had a direct effect in the delamination expansion. The locale of the delamination has been enlarged with the rise in the feed rate and the cutting velocity.

- The Taguchi and ANOVA analysis obtained that the majority relevant parameters that have an effect on the thrust forces and surface roughness were found to be the feed rate, which was tracked by the cutting velocity with the percent contribution of 56.51% and 14.17% for the thrust forces; and 35.53% and 17.06% for the surface roughness respectively.

- The optimal control parameters levels for minimizing the thrust forces were V_C= 50 m/min and f= 0.10 mm/rev while the employment of PVD-coated drills. Whilst for the surface roughness were V_C= 30 m/min and f= 0.10 mm/rev while the employment of CVD-coated drills, and for the delamination factor were V_C= 30 m/min and f= 0.20 mm/rev during the employment of CVD-coated drills.

3. The drilling of the hybrid Mg/SiC/GNPs MMCs:

- The thrust forces were increased by the increase of the feed rate, whilst it declined with the increase of the cutting velocity. The highest thrust forces were achieved at lower cutting speed during the utilized of uncoated bits. However, with PVD-coated bits, the lowest thrust forces were at the cutting velocity of 50 m/min alongside with the all levels of feed rate parameter.

- The Taguchi and ANOVA statistical analysis exposed that the majority significant parameters that had control on the thrust forces were the coating category of the drill, which go after by the cutting velocity parameter and subsequently the feed rate. The optimal parameters grouping to attain the minimum values of the thrust forces were the PVD coated bit, the cutting velocity of 50 m/min, and feed rate of 0.10 mm/rev.

- The surface roughness (R_a) values of the drilled surfaces were lesser all through the employment of the coated bits. The higher value was obtained during the usage of the uncoated bits at a cutting velocity of 40 m/min and a

0.15 mm/rev of feed rate. The results specified that the lowly feed rate was much more preferred in the drilling of the hybrid Mg/SiC/GNPs MMC. The increase in the feed rate was seen to make a raise on the thrust forces and this affected the surface finishing.

- The Taguchi statistical analysis exemplified the majority significant parameters that had affected the surface roughness (R_a) which were the coating category of drill, which then tag along by the cutting velocity and then come the feed rate parameter.

- The delamination factor amplifies with the rise in the cutting speed at the diverse levels of the feed rate, and there is no substantial effect by the coating type of the drills. The lowest delamination factor value was reached during the employment of the low cutting velocity (30 m/min) with 0.20 mm/rev of feed rate.

- The majority relevant parameter affecting the delamination factor was the cutting speed, which was tracked by the feed rate and after that the coating type of the drill bit.

Table 7.1. The optimization results based on the Taguchi and ANOVA analysis.

Composite	Control parameter	Contribution (%)	The optimal parameters combination
Thrust force analysis (F_{th})			
Mg/GNPs	f	56.51%	PVD-coated, V_C =50 m/min, f = 0.10 mm/rev
Mg/SiC/GNPs	C_T	40.01%	PVD-coated, V_C =50 m/min, f = 0.10 mm/rev
Torque analysis (T)			
Mg/GNPs	f	40.65%	PVD-coated, V_C =40 m/min, f = 0.10 mm/rev
Mg/SiC/GNPs	f	20.65%	PVD-coated, V_C =50 m/min, f = 0.10 mm/rev
Surface roughness analysis (R_a)			
Mg/GNPs	f	35.53%	CVD-coated, V_C =30 m/min, f = 0.10 mm/rev
Mg/SiC/GNPs	C_T	11.33%	PVD-coated, V_C =50 m/min, f = 0.10 mm/rev
Delamination factor analysis (f_d)			
Mg/GNPs	V_C	63.95%	CVD-coated, V_C =30 m/min, f = 0.20 mm/rev
Mg/SiC/GNPs	V_C	48.79%	CVD-coated, V_C =30 m/min, f = 0.20 mm/rev

4. The surfaces were shaped through the employment of the uncoated bits were poor in the quality, with fine grooves have an effect on the surface finishing, and the performance of the coated bits was better when compared to the uncoated bits at the diverse feed rates and cutting velocities were employed in this research study. The hole drilled surface was much more smoother and flatter with the existence of some collection of the BUE during the employment of the PVD- and the CVD-coated bits, this was consequently of the tough coating layer (TiN and AlTiN) which reduced the BUE phenomenon.

5. The predictive experimental models were derived through the full quadratic regression could have been employed to predict the thrust forces, the surface roughness and the delamination factor with assorted drilling parameters. Table 7.1 presents the outlines of the Taguchi and ANOVA analysis results during the optimization procedure for thrust force, torque, surface roughness and the delamination factor.

6. The tool wear mechanisms of the carbide drills were employed in this research study can be categorized into the abrasive wear, the adhesion wear, and the BUE layer that is covered the chisel edge for the uncoated drills.

7.2. RECOMMENDATIONS

Even though this study has provided a primary investigation on the machinability of a novel Mg-MMCs, more work is still requisite to accomplish further sympathetic of the underlying phenomenon and to further improve the operation conditions. The enhanced strength and the abrasive and harsh nature of the reinforcement brought the great challenges for the ensuing inevitable machining procedure for the Mg-MMCs. The consequence of the particles size and the fraction volume, cutting conditions and the tool geometry and the coating ought to have been systematically analyzed. However, the machined facade quality, instantaneous cutting forces, generated temperature and tool wear should be coupled with the diverse tools materials, geometries and the coating through the employment of advanced rank of signal handing out procedures and techniques.

REFERENCES

1. Parsian, A., Magnevall, M., Beno, T. and Eynian, M., "A mechanistic approach to model cutting forces in drilling with indexable inserts", ***Procedia CIRP***, 25: 74-79 (2014).

2. Anand, R. S. and Patra, K., "Mechanistic cutting force modeling for micro-drilling of CFRP composite laminates", ***CIRP Journal of Manufacturing Science and Technology***, 16: 55-63 (2017).

3. Satoshi E., "Effects of twist drill point geometry on torque and thrust", ***Sci. Rep. Fac. Edu. Gifu Univ.***, 36: 165-174 (2012).

4. Sekulic, M., Kovac, P., Gostimirovic, M. and Hadzistevic, M., "Prediction of the main cutting force in drilling by Kienzle equation", ***Journal of Trends in the Development of Machinery and Associated Technology***, 18(1): 27-30 (2014).

5. Thakre, A. A. and Soni, S., "Modeling of burr size in drilling of aluminum silicon carbide composites using response surface methodology", ***Engineering Science and Technology***, 19: 1199-1205 (2016).

6. Davim, J. P. and Antonio, C. A. C., "Optimal drilling of particulate metal matrix composites based on experimental and numerical procedures", ***International Journal of Machine Tools and Manufacture***, 41: 21-31 (2001).

7. Lin, J. T., Bhattacharyya, D. and Ferguson, W. G., "Chip formation in the machining of SiC-particle-reinforced aluminium-matrix composites", ***Composites Science and Technology***, 58: 285-291 (1998).

8. Pedersen, W. and Ramulu, M., "Facing SiC_P/Mg metal matrix composites with carbide tools", ***Journal of Materials Processing Technology***, 172: 417-423 (2006).

9. Nicholls, C. J., Boswell, B., Davies, I. J. and Islam, M. N., "Review of machining metal matrix composites", ***International Journal of Advanced Manufacturing Technology***, 90: 2429-2441 (2016).

10. Palanikumar, K. and Muniaraj, A., "Experimental investigation and analysis of thrust force in drilling cast hybrid metal matrix (Al-15%SiC-4%graphite) composites", ***Measurement***, 53: 240-250 (2014).

11. Sahin, Y. and Sur, G., "The effect of Al2O3, TiN and Ti (C,N) based CVD coatings on tool wear in machining metal matrix composites", ***Surface and Coatings Technology***, 179: 349-355 (2004).

12. Rajmohan, T., Palanikumar, K. and Kathirvel, M., "Optimization of machining parameters in drilling hybrid aluminium metal matrix composites", ***Trans. Nonferrous Met. Soc. China***, 22: 1286-1297 (2012).

13. Teti, R., "Machining of composite materials", ***CIRP Annals***, 51(2): 611-634 (2002).

14. Weinert, K. and Lange, M., "Machining of magnesium matrix composites", ***Advanced Engineering Materials***, 3: 975-979 (2001).

15. Gupta, M. and Wong, W. L. E., "Magnesium-based nanocomposites: lightweight materials of the future", ***Materials Characterization***, 105: 30-46 (2015).

16. Rashad, M., Pan, F. and Asif, M., "Magnesium matrix composites reinforced with graphene nanoplatelets", ***Graphene Materials: Fundamentals and Emerging Applications***; John Wiley & Sons: Hoboken, NJ, USA, 151–189 (2015).

17. Rashad, M., Pan, F., Tang, A., Asif, M., Hussain, S., Gou, J. and Mao, J., "Improved strength and ductility of magnesium with addition of aluminum and graphene nanoplatelets (Al+GNPs) using semi powder metallurgy method", ***Journal of Industrial and Engineering Chemistry***, 23: 243-250 (2015).

18. Rashad, M., Pan, F., Tang, A., Asif, M., She, J., Gou, J., Mao, J. and Hu, H., "Development of magnesium-graphene nanoplatelets composite", ***Journal of Composite Materials***, 49(3): 285-293 (2015).

19. Rashad, M., Pan, F., Tang, A., Lu, Y., Asif, M., Hussain, S., She, J., Gou, J. and Mao, J., "Effect of graphene nanoplatelets (GNPs) addition on strength and ductility of magnesium-titanium alloys", ***Journal of Magnesium and Alloys***, 1: 242-248 (2013).

20. Rzychon, T., Dybowski, B., Grye, A. and Dudek, M.,"Mechanical properties and microstructure of WE43 magnesium matrix composite reinforced SiC particles", ***Archives of Foundry Engineering***, 15(1): 99-102 (2015).

21. Subramanian, J., Loh, Z., Seetharaman, S., Hamouda, A. S. and Gupta, M., "Microstructure and mechanical properties of Mg-5Nb metal-metal composite reinforced with nano SiC ceramic particles", ***Metals***, 2: 178-194 (2012).

22. Rashad, M., Pan, F., Tang, A., Asif, M. and Aamir, M., "Synergetic effect of graphene nanoplatelets (GNPs) and multi-walled carbon nanotube (MW-CNTs) on mechanical properties of pure magnesium", ***Journal of Alloys and Compounds***, 603: 111-118 (2014).

23. Jiang, Q. C., Li, X. L. and Wang, H. Y., "Fabrication of TiC particulate reinforced magnesium matrix composites", ***Scripta Materialia***, 48: 713-717 (2003).

24. Reddy, S. U., Srikanth, N., Gupta, M. and Sinha, S. K., "Enhancing the properties of magnesium using SiC particulates in sub-micron length scale", ***Advanced Engineering Materials***, 6: 957-964 (2004).

25. Rashad, M., Pan, F., Asif, M. and Tang, A., "Powder metallurgy of Mg-1%Al-1%Sn alloy reinforced with low content of graphene nanoplatelets (GNPs)", ***Journal of Industrial and Engineering Chemistry***, 20: 4250-4255 (2014).

26. Taskesen, A. and Kutukde, K., "Experimental investigation and multi-objective analysis on drilling of boron carbide reinforced metal matrix composites using grey relational analysis", ***Measurement***, 47: 321-330 (2013).

27. Davim, J. P., "Study of drilling metal-matrix composites based on the Taguchi techniques", ***Journal of Materials Processing Technology***, 132: 250-254 (2003).

28. Rajmohan, T., Palanikumar, K. and Davim, J. P., "Analysis of surface integrity in drilling metal matrix and hybrid metal matrix composites", ***J. Mater. Sci. Technol.***, 28(8): 761-768 (2012).

29. Altintas, Y., "Manufacturing Automation: metal cutting mechanics, machine tool vibrations, and CNC design 2nd ed.", ***Cambridge University Press***, 4-52 (2012).

30. Boothroyd, G. and Knight, W. A., "Fundamentals of machining and machine tools 2nd ed.", ***Marcel Dekker, INC., 270 Madison Avenue, New York***, (1989).

31. Internet: Kennametal Inc., "Master Catalogue, Kennametal twist drills, KHSS drill dictionary", **https://www1.mscdirect.com/images/solutions/kennametal/hss_tech_data.pdf**, (2018).

32. Internet: Millwright, "Drilling, Machining, First Period", **http://www.oldshig-h.ca/documents/drilling.pdf**, (2013).

33. Khan, Z. M., "A study of the drilling of advanced carbon fibre composites", PhD Thesis, ***University of Salford, Department of Aeronautical and Mechanical Engineering***, England, 49-51 (1991).

34. Chandrasekharan, V., Kapoor, S. G. and Devor, R. E., "A mechanistic approach to predicting the cutting forces in drilling: with application to fiber-reinforced composite materials", ***Journal of Engineering for Industry***, 117: 559-570 (1995).

35. Ekici, E., Motorcu, A. R. and Uzun, G., "An investigation of the effects of cutting parameters and graphite reinforcement on quality characteristics during the drilling of Al/10B_4C composites", ***Measurement***, 95: 395-404 (2017).

36. Samy, G. S. and Kumaran, S. T., "Measurement and analysis of temperature, thrust force and surface roughness in drilling of AA (6351)-B_4C composite", ***Measurement***, 103: 1-9 (2017).

37. Mubaraki, B., Bandyopadhyay, S., Fowle, R., Mathew, P. and Heath, P. J., "Drilling studies of an Al_2O_3-Al metal matrix composite", ***Journal of Materials Science***, 30: 6273-6280 (1995).

38. Morin, E., Masounave, J. and Laufer, E. E., "Effect of drill wear on cutting forces in the drilling of metal-matrix composites", ***Wear***, 184: 11-16 (1995).

39. Altunpak, Y., Ay, M. and Aslan, S., "Drilling of a hybrid Al/SiC/Gr metal matrix composites", ***International Journal of Advanced Manufacturing Technology***, 60: 513-517 (2012).

40. Wei, X., Qi, L., Zhou, J., Ju, L. and Tian, W., "Tool wear morphologies and mechanisms for cutting Cf/Mg composites", ***International Journal of Advanced Manufacturing Technology***, 86: 613-619 (2016).

41. Ahamed, A. R., Asokan, P., Aravindan, S. and Prakash, M. K., "Drilling of hybrid Al-5%SiC_P-5%B_4C_P metal matrix composites", ***International Journal of Advanced Manufacturing Technology***, 49: 871-877 (2010).

42. Dhavamani, C. and Alwarsamy, T., "Optimization of machining parameters for aluminum and silicon carbide composite using genetic algorithm", ***Procedia Engineering***, 38: 1994-2004 (2012).

43. Ghandeharium, A., "Mechanics of machining metal matrix composites: analytical modeling and finite element simulation", PhD Thesis, ***University of Ontario Institute of Technology, Faculty of Engineering and Applied Science***, Ontario, 55-56 (2015).

44. Gupta, N., Luong, D. D., and Cho, K., "Magnesium matrix composite foams density, mechanical properties and applications", ***Metals***, 2: 238-252 (2012).

45. Das, A. and Harimkar, S. P., "Effect of graphene nanoplate and silicon carbide nanoparticle reinforcement on mechanical and tribological properties of spark plasma sintered magnesium matrix composites", ***J. Mater. Sci. Technol.***, 30(11): 1059-1070 (2014).

46. Sohn, K., Euh, K., Lee, S. and Park, I., "Mechanical property and fracture behavior of squeeze cast Mg matrix composites", ***Metallurgical and Materials Transactions***, 29A: 2543-2554 (1998).

47. Lianxi, H. and Erde, W., "Fabrication and mechanical properties of SiC_W/ZK51A magnesium matrix composite by two step squeeze casting", ***Materials Science and Engineering A***, 278: 267-271 (2000).

48. Gorji, R. R., Alizadeh, A. and Jafari, H., "Microstructure and mechanical properties of stir cast ZX51/Al_2O_{3P} magnesium matrix composites", ***Materials Science and Engineering A***, 674: 413-418 (2016).

49. Karabulut, S., Gokman, U. and Cinici, H., "Study on the mechanical and drilling properties of AA7039 composites reinforced with $Al_2O_3/B_4C/SiC$ particles", ***Composites Part B***, 93: 43-55 (2016).

50. Zhu, Y. P., Jin, P. P., Fei, W. D., XU, S. C. and Wang, J. H., "Effects of Mg2B2O5 whiskers on microstructure and mechanical properties of AZ31B magnesium matrix composites", ***Materials Science and Engineering A***, 684: 205-212 (2017).

51. Kandil, A., "Microstructure and mechanical properties of SiC_P/AZ91 magnesium mayrix composites processed by stir casting", ***Journal of Engineering Sciences, Assiut University***, 40(1): 255-270 (2012).

52. Luo, A., "Processing, microstructure, and mechanical behavior of cast magnesium metal matrix composites", ***Metallurgical and Materials Transactions A***, 26: 2445-2455 (1995).

53. Ezatpour, H. R., Sajjadi, S. A., Sabzevar, M. H. and Huang, Y., "Investigation of microstructure and mechanical properties of Al6061-nanocomposite fabricated by stir casting", ***Materials and Design***, 55: 921-928 (2014).

54. Zhang, Q., "Development of hybrid Mg-based composites", Master Degree Thesis, ***University of Windsor, Faculty of Graduate Studies and Research***, Ontario, 85-88 (2009).

55. Fukuda, H., Kondoh, K., Umeda, J. and Fugetsu, B., "Interfacial analysis between Mg matrix and carbon nanotubes in Mg-6wt%Al alloy matrix composites reinforced with carbon nanotubes", ***Composites Science and Technology***, 71: 705-709 (2011).

56. Yuan, Q., Zeng, X., Liu, Y., Luo, L., Wu, J. and Wang, Y., "Microstructure and mechanical properties of AZ91 aaloy reinforced by carbon nanotubes coated with MgO", ***Carbon***, 96: 843-855 (2016).

57. Shin, D., "Microstructural characteristics of magnesium metal matrix composites", Master Degree Thesis, ***University of Central Florida, Department of Mechanical Materials and Aerospace Engineering***, Florida, 15-16 (2012).

58. Ye, J., He, J. and Schoenung, J. M., "Cryomilling for the fabrication of a particulate B4C reinforced Al nanocomposite: part I. effects of process conditions on structure", ***Metallurgical and Materials Transactions A***, 37: 3099-3109 (2006).

59. Suryanarayana, C. and Al-Aqeeli, N., "Mechanically alloyed nanocomposites", ***Progress in Materials Science***, 58: 383-502 (2013).

60. Kaneda, H. and Choh, T., "Fabrication of particulate reinforced magnesium composites by applying a spontaneous infiltration phenomenon", ***Journal of Materials Science***, 32: 47-56 (1997).

61. Elbert, T., Moll, F. and Kainer, K. U., “Spray forming of magnesium alloys and composites”, Powder Metallurgy, 40(2): 126-130 (1997).

62. Sklenicka, V., Pahutova, M., Kucharova, K., Svoboda, M. and Langdon, T. G., “Creep processes in magnesium alloys and their composites”, ***Metallurgical and Materials Transactions A***, 33: 883-889 (2002).

63. Li, X. P. and Lu, L., “Study of the reinforcement percentage of Mg-Al-SiC MMC in relation to the mechanical properties and machinability”, ***Materials Science Forum***, 437: 185-188 (2003).

64. Weinert, K., “A consideration of tool wear mechanism when machining metal matrix composites (MMC)”, ***Annals of the CIRP***, 42(1): 95-98 (1993).

65. Zhaohui, W., Yonglin, K., Wenchao, D., Hongjin, Z., Jinwei, L. and Yue, X., “Study of grain refinement and SiC nanoparticle reinforced magnesium alloys”, ***Materials Science Forum***, 488: 889-892 (2005).

66. Mordike, B. L. and Ebert, T., “Magnesium properties-applications-potential”, ***Materials Science and Engineering A***, 302: 37-45 (2001).

67. Prathap, P. S., Vengatachalapathy, V. S. K. and Palaniradja, K., “Machining of hybrid metal matrix composites and its further improvement- a review”, ***International Journal of Engineering and Advanced Technology***, 4(1): 11-15 (2014).

68. Sekhar, R. and Singh, T. P., “Mechanisms in turning of metal matrix composites: a review”, ***Journal of Materials Research and Technology***, 4(2) 197-207 (2015).

69. Jadhav, S., Sankpal, J., Chaudhari, M. and Patil, N., “A review on drilling of metal matrix composites”, ***International Journal of Current Engineering and Technology***, 6: 82-88 (2016).

70. Saravanakumar, M., Natarajan, N. and Krishnaraj, V., “Study of cutting forces in machining of magnesium composite by response surface methodology”, ***Carbon-Science and Technology***, 7(1) 36-58 (2015).

71. Muniaraj, A., Das, S. L. and Palanikumar, K., “Evaluation of thrust force and surface roughness in drilling of Al/SiC/Gr hybrid metal matrix composite”, ***International Journal of Latest Research in Science and Technolog***y, 2(4): 4-8 (2013).

72. Taskesen, A. and Kutukde, K., “Analysis and optimization of drilling parameters for tool wear and hole dimensional accuracy in B_4C reinforced Al-alloy”, ***Transactions of Nonferrous Metals Society of China***, 23: 2524-2536 (2013).

73. Davim, J. P. and Baptista, A. M., "Cutting force, tool wear and surface finish in drilling metal matrix composites", Proc. Instn. Mech. Engrs., 215(part E) 177-183 (2001).

74. Teng, X., Huo, D., Wong, E., Meenashisundaram, G. and Gupta, M., "Micro-machinability of nanoparticle-reinforced Mg-based MMCs: an experimental investigation", ***International Journal of Advanced Manufacturing Technology***, 87(5): 2165-2178 (2016).

75. Muthukrishnan, N. and Davim, J. P., "An investigation of the effect of work piece reinforcing percentage on the machinability of Al-SiC metal matrix composites", ***Journal of Mechanical Engineering Research***, 3(1): 15-24 (2011).

76. Basavarajappa, S., "Tool wear in turning of graphitic hybrid metal matrix composites", ***Materials and Manufacturing Processes***, 24: 484-487 (2009).

77. Ay, M., "Optimization of cutting parameters and graphite rate in drilling of a hybrid aluminium matrix composites", ***Journal of Engineering and Fundamentals***, 2(2): 42-50 (2015).

78. Doomra, V. K., Debnath, K. and Singh, I., "Drilling of metal matrix composites: experimental and finite element analysis", ***Journal of Engineering Manufacture***, Proc. IMechE Part B: 1-5 (2014).

79. Ay, M., Altunpak, Y. and Hartomacioglu, S., "The grey-based Taguchi method: optimization of drilling of hybrid aluminum matrix composites", ***Acta Physica Polonica A***, 131: 551-554 (2017).

80. Fathipour, M., Zoghipour, P., Tarighi, J. and Yousefi, R., "Investigation of reinforced SiC particles percentage on machining force of metal matrix composite", ***Modern Applied Science***, 6(8): 9-20 (2012).

81. Anthony, X. M. and Ajith, K. J. P., "Machinability of hybrid metal matrix composite- a review", ***Procedia Engineering***, 174: 1110-1118 (2017).

82. Hung, N. P., Loh, N. L. and Xu, Z. M., "Cumulative tool wear in machining metal matrix composites partII: machinability", ***Journal of Materials Processing Technology***, 58: 114-120 (1996).

83. Said, M. S., Ghani, J. A., Syed, A., Azlan, M. F., Latiff, Z. A. and Zubir, B., "Tool wears on drill metal matrix composites (MMC) Al-Si/10%AlN material", ***ARPN Journal of Engineering and Applied Science***, 11(12): 7677-7682 (2016).

84. Tsao, C. C. and Hocheng, H., "Effect of tool wear on delamination in drilling composite materials", ***International Journal of Mechanical Sciences***, 49: 983-988 (2007).

85. Shunmugesh, K., Rajasekar, R., Moganapriya, C. and Karthik, V., "Optimization of machining force and delamination factor of GFRP in dry drilling process using Taguchi method", ***Advances in Natural and Applied Sciences***, 11(8): 220-230 (2017).

86. Karimi, N. Z., Heidary, H., Yousefi, J., Sadeghi, S. and Minak, G., "Experimental investigation on delamination in nanocomposite drilling", ***FME Transactions***, 46: 62-69 (2018).

87. Durao, L. M. P., Tavares, J. M. R. S., Albuquerque, V. H. C., Marques, J. F. S. and Andrade, O. N. G., "Drilling damage in composite material", ***Materials***, 7: 3802-3819 (2014).

88. Wei, J., Atif, R., Vo, T. and Inam, F., "Graphene nanoplatelets in epoxy system:dispersion, reaggregation, and mechanical properties of nanocomposites", ***Journal of Nanomaterials***, 2105: 1-12 (2015).

89. Internet: Strem Chemicals Inc., "Graphene Nanoplatelets", **https://www.strem.com/uploads/resources/documents/graphene_nanplatelets_copy1.pdf** (2018).

90. Rashed, A. H., "Properties and characteristics of silicon carbide", ***POCO Graphite Inc., 300 Old Greenwood Rd***, Decatur, 11-15 (2002).

91. Stoldt, C. R., Fritz, M. C., Carraro, C. and Maboudian, R., "Micromechanical properties of silicon carbide thin films deposited using single-source chemical-vapor deposition", ***Applied Physics Letters***, 79(3): 347-349 (2001).

92. Jayakumar, J., Raghunath, B. K. and Rao, T. H., "Recent development and challenges in synthesis of magnesium matrix nano composites- a review", ***International Journal of Latest Research in Science and Technology***, 1(2): 164-171 (2012).

93. Chen, W., "Some experimental investigations in the drilling of carbon fiber reinforced plastic (CFRP) composite laminates", ***International Journal of Machine Tools and Manufacture***, 37(8): 1097-1108 (1997).

94. Fernandes, M. and Cook, C., "Drilling of carbon composites using a one shot drill bit, Part I: five stage representation of drilling and factors affecting maximum force and torque", ***International Journal of Machine Tools and Manufacture***, 46: 70-75 (2006).

RESUME

Mustafa M. ABDULGADIR was born in Elgubba/Libya in 1971. He completed high school education in Omar Elmukhtar High School in Elgubba city, after that, he completed undergraduate program at Faculty of Engineering/Garyounes University/Department of Industrial Engineering and Manufacturing Systems in 1994. Then in 2001, he started his Master of Science (M.Sc.) study at Mechanical Faculty/University of West Bohemia/Czech Republic, and he got his certificate in 2004 (Manufacturing Processes - Technology of Metal Cutting). He completed his PhD degree study at Karabük University/Institute of Natural and Applied Sciences/Department of Manufacturing Engineering in 2018.

CONTACT INFORMATION

Address in Turkey: Karabük University-Graduate School of Natural & Applied Sciences-Demir/Çelik Campus/KARABUK

Address in Libya : Higher Technical Institute of engineering professions/Elgubba-Libya

E-mail : elgubba2008@yahoo.com